NONCANONICAL NF-κB SIGNALING DRIVES GLIOMA INVASION BY PROMOTING MT1-MMP ACTIVATION, PSEUDOPODIA FORMATION, AND ITGA11 EXPRESSION

A Dissertation

by

CAMILLE L. DURAN

Submitted to the Office of Graduate and Professional Studies of
Texas A&M University
in partial fulfillment of the requirements for the degree of

DOCTOR OF PHILOSOPHY

Chair of Committee,	Kayla J. Bayless
Committee Members,	Robert C. Burghardt
	Raquel Sitcheran
	David W. Threadgill
Interdisciplinary Faculty Chair,	Dorothy E. Shippen

May 2017

Major Subject: Genetics

ABSTRACT

A hallmark of high grade glioma is highly aggressive, diffuse invasion into normal brain tissue, contributing to a 100% recurrence rate and resistance to current therapies. Recent efforts to determine molecular differences in high grade glioma and define tumor subtypes have revealed that the noncanonical NF-κB transcription factor RelB is upregulated in the highly aggressive mesenchymal subtype, as well as in recurrent tumors. The studies presented here seek to better understand how noncanonical NF-κB signaling drives glioma cell invasion in a three-dimensional (3D) environment. Stabilization of NF-κB-inducing kinase (NIK), a critical driver of noncanonical NF-κB signaling, promoted glioma cell adhesion, spreading, and pseudopodia formation on collagen, which is expressed at low levels in normal brain tissue but highly upregulated within the stroma and surrounding tissue of glioma. As NIK expression appeared to regulate glioma cell behavior on collagen, we investigated whether NIK controls the expression of integrins known to bind collagen. We found NIK expression upregulated the integrin alpha 11 subunit (ITGA11), while it did not significantly affect the expression of ITGA1, ITGA2, or ITGA10. Analysis of human tumor samples revealed that ITGA11 expression was increased in glioma tissue compared to normal brain tissue. Furthermore, when testing multiple glioma lines, ITGA11 expression positively correlated with invasiveness into 3D collagen matrices. Investigation of a key transmembrane metalloproteinase revealed that NIK expression enhanced the localization of active, phosphorylated membrane-type 1 matrix metalloproteinase (MT1-MMP) to pseudopodial structures. In a heterologous

system, ITGA11 and MT1-MMP formed a complex, suggesting these transmembrane proteins could interact in glioma cells to facilitate coordinated recognition and degradation of collagen during invasion. Finally, silencing of ITGA11 in an invasive glioma line attenuated invasion into 3D collagen matrices. Collectively, these data reveal an ability of NIK to promote directed glioma cell invasion, pseudopodia formation, ITGA11 expression, and activated MT1-MMP localization to pseudopodia. These data suggest ITGA11 could serve as a novel marker for more invasive glioma and a potential therapeutic target in glioma.

DEDICATION

This dissertation is dedicated to the three most influential people in my life: my mom, Jeff, and Alex. My mom has taught me strength and perseverance, Jeff taught me passion and kindness, and Alex has taught me humor and friendship.

ACKNOWLEDGMENTS

I would like to sincerely thank my advisor, Dr. Kayla Bayless, for her guidance and support during my time at Texas A&M University. I will forever be grateful for the opportunities she has provided me and the generosity she has shown me. Her office door was always open to me to talk about science, life, and sports. Her mentorship, encouragement, and friendship were instrumental to my success in graduate school. She has always had confidence in me even when I wasn't sure of myself.

I would also like to thank my committee member, Dr. Raquel Sitcheran, for her advice and encouragement. I am grateful for the opportunity she gave me to collaborate with her lab working on my dissertation project. I also want to thank my committee members, Drs. Robert Burghardt, and David Threadgill, for their guidance and advice during my studies. I thank the faculty and staff of the Interdisciplinary Program of Genetics and the Department of Molecular and Cellular Medicine for their support and opportunities to present my research.

I want to thank all of my friends and colleagues in the Bayless lab: Colette Abbey, Dr. Hojin Kang, Dr. Jui Dave, Rebecca Smith, Dr. David Howell, and Connor Pogue. I appreciate all of their support and training in the lab and I am grateful for the fun work environment they created. In particular, I would like to thank Colette Abbey for her friendship, kindness, and for always being there for me. I am also grateful for the help I received from the Sitcheran lab members, Dr. Dong Lee, Sowndharya Rajavel, and Jiung Jung, when working on my dissertation project.

I have made wonderful friends through the Genetics program at Texas A&M. I especially want to thank my roommates, Erika Downey-Slinker and Rob Slinker, for their friendship and constant support through the ups and downs of both graduate school and life. I also want to thank Ashley Mattison and Reed Stubbendieck, my first friends in College Station, who went through all aspects of graduate school with me and made everything a lot more interesting and enjoyable.

Finally, I want to thank my family for their endless encouragement and support. They have taught me that you can go a long way by having a good work ethic, a good attitude, and a little bit of fun.

CONTRIBUTORS AND FUNDING SOURCES

CONTRIBUTORS

This work was supervised by a dissertation committee consisting of Professor Bayless [advisor], Professors Sitcheran and Threadgill of the Department of Molecular and Cellular Medicine [Home Department], and Professor Burghardt of the Department of Veterinary and Integrated Biosciences [Outside Department].

The BT114 and BT25 glioma cells were provided by Dr. Ian Parney of the Mayo Clinic. Dr. Albert Baldwin of UNC Chapel Hill provided the *p65*$^{-/-}$ and *p65*$^{-/-}$*;cRel*$^{-/-}$ MEFs. Dr. Denis Guttridge of The Ohio State University provided the *RelB*$^{-/-}$ MEFs. The *NIK*$^{-/-}$ MEFs were provided by Dr. Robert Schreiber of the University of Washington. The glioma biopsy samples were given by Dr. Gerard Toussaint of the Texas A&M University Health Science Center. The UWOS2 and MG63 osteosarcoma cells were provided by Dr. Carl Gregory of the Texas A&M University Health Science Center. Dr. Alan Tackett of the University of Arkansas provided the melanoma cell lines.

The BT114 –Control, NIK(WT), and –NIK(S867A), and the BT25 –Control and sgNIK cell lines were generated by Dr. Dong Lee of the Department of Molecular and Cellular Medicine. The Western blots shown in Figures 2, 4, 5, and 14, and the qPCR analysis shown in Figures 9, 11, and 16 were performed by Dr. Dong Lee. The invasion assays and quantification in Figures 2, 3, 5, and 16 were performed by Sowndharya Rajavel of the Department of Molecular and Cellular Medicine. The flow experiments from Figures 4 and 8, and the staining in Figures 4 and 18 were also performed by Sowndharya Rajavel. Blinded quantifications of cell size and pseudopodial length in

Figures 6 and 7 were analyzed by Connor Pogue of the Department of Molecular and Cellular Medicine. The staining and quantification shown in Figure 17 were performed by Jiung Jung of the Department of Molecular and Cellular Medicine. The invasion assays and qPCR analysis in Figure 28 were provided by Colette Abbey of the Department of Molecular and Cellular Medicine.

All other work conducted for the dissertation was completed by the student independently.

FUNDING SOURCES

This work was supported financially by the Public Health Service and the National Institutes of Health [grant number HL-095786 to K.J.B. and NS-082554 to R.S].

TABLE OF CONTENTS

Page

LIST OF FIGURES

Page

CHAPTER I

INTRODUCTION AND LITERATURE REVIEW

HIGH GRADE GLIOMA

Gliomas are the most common and lethal primary central nervous system (CNS) tumors in adults, and the leading cause of cancer death in children. They are classified by the World Health Organization into grades I-IV, based on mitotic index, cellular density, detection of necrosis, and glial cell types identified. High grade gliomas (grades III-IV) are the most common and malignant, representing about 60-75% of all gliomas (1, 2). Though the cell type of origin remains under debate, high grade gliomas are suggested to be derived through either the transformation of a neural stem cell or glial progenitor cell or through the dedifferentiation of a mature glial cell (3, 4). These tumors exhibit aggressive invasion into the surrounding healthy brain tissue, though they rarely metastasize outside the CNS. Infiltration of the normal brain makes complete surgical removal of the tumor a considerable challenge as this would significantly compromise neurological function and quality of life. The current treatment regime for high grade glioma consists of surgery to remove the bulk of the tumor mass, followed by concurrent radiotherapy and chemotherapy with the cytotoxic DNA alkylating agent, temozolomide (5, 6). Despite this aggressive treatment, high grade gliomas continue to be one of the deadliest cancers with a median survival time between 12 and 15 months (5, 7). Partial removal of the tumor allows the cells that invaded past the margins of resection to regrow the tumor mass, leading to a recurrence rate of 100%.

Several monogenic Mendelian disorders are linked to an increased risk of developing a glioma as an adult, though these patients make up a small portion of the cases (8). Neurofibromatosis 1 and 2, Lynch syndrome and Li-Fraumeni syndrome are a few examples, although these disorders give genetic predisposition to cancers outside the brain as well (8). However, efforts to understand the molecular pathology of high grade glioma have revealed somatic genetic alterations in several signaling pathways (9, 10). Genomic and transcriptomic analysis of glioblastoma by The Cancer Genome Atlas Network found several pathways commonly mutated in glioblastoma, including p53 (*TP53, MDM2, and MDM4*), Rb (*CDKN2A, CDKN2B, CDK4,* and *RB1*), and the PI3K and MAPK pathways (*EGFR, PDGFRA, PTEN, PI(3)K,* and *NF1*) (9, 10).

This gene expression data was used to divide glioblastoma tumors into four subtypes, Proneural, Neural, Classical, and Mesenchymal (11). The Proneural subtype was most frequent in patients under the age of 40, and was characterized by increased expression of *PDGFRA* and mutations of *IDH1*, and *TP53*. The Neural subtype displayed an expression pattern similar to neurons, and these tumors were suggested to be derived from a more differentiated cell. Amplification of *EGFR* was most frequently found in the Classical subtype. Necrosis was most common in the Mesenchymal subtype, as was an increase in expression of mesenchymal markers and genes in the NF-κB pathway, including the noncanonical NF-κB transcription factor, RelB.

NONCANONICAL NF-κB SIGNALING

NF-κB signaling is divided into two main pathways, the canonical pathway with transcription factors p65 (RELA), p50 (NFKB1), and c-Rel (REL), and the noncanonical pathway with transcription factors RelB (RELB) and p52 (NFKB2). The noncanonical pathway regulates several biological processes, including B-cell maturation and survival, lymphoid organ development, and osteoclast differentiation. This pathway relies on the partial processing of the protein, p100 which acts as both an inhibitor to RelB nuclear translocation, and as a precursor of the transcription factor, p52. Noncanonical NF-κB signaling is initiated by activation of specific TNFR superfamily members, including FN14 (12), B-cell activating factor belonging to TNF family receptor (BAFFR) (13), lymphotoxin β-receptor (LTβR) (14), receptor activator for nuclear factor κB (RANK) (15), and TNFR2 (16). Receptor activation leads to stabilization and accumulation of the protein, NF-κB-inducing kinase (NIK or MAP3K14). When cells are unstimulated, NIK interacts with TRAF3 at the N-terminus. After binding NIK, TRAF3 is recruited to the cIAP1/2 E3 ubiquitin ligase complex through binding to TRAF2. cIAP1/2 ubiquitinylates NIK at K48, leading to its proteasomal degradation. NIK can also be phosphorylated by IKKα or TANK-binding kinase 1 (TBK1) leading to NIK proteolysis (17, 18). However, after stimulation of the specific TNF receptors, TRAF3 and TRAF2 are recruited to the activated receptor, leading degradation mediated by ubiquitinylation by cIAP1/2. NIK accumulation causes autophosphorylation, leading to downstream phosphorylation of IKKα. Activated IKKα then mediates the phosphorylation and partial processing of the C-terminus of p100 to p52 through ubiquitinylation by βTrCP. p52-RelB heterodimers

can then translocate to the nucleus where they recognize and bind κB sites on target genes (19, 20).

While the role of canonical NF-κB signaling in immune function and cancer development and progression has been thoroughly investigated (21), much less is known of how the noncanonical NF-κB pathway contributes to the development of disease. Impaired noncanonical NF-κB signaling is associated with compromised lymphoid organogenesis and B-cell maturation (22, 23). Mutations leading to increased activation of noncanonical NF-κB signaling are associated with several cancers, including multiple myeloma, diffuse large B cell lymphoma, Hodgkin's lymphoma, lung cancer, ovarian cancer, and prostate cancer (24-28).

Our previous work has found more invasive glioblastoma cell lines display increased expression of RelB, and knockdown of RelB attenuates glioma cell invasion and tumor progression (29, 30). Further, increased expression of NIK promotes glioma tumor progression in orthotopic tumor xenografts (30). However, the mechanism through which noncanonical NF-κB signaling pathway promotes glioma cell invasion is unknown.

INTEGRINS

Integrins are a large family of cell adhesion molecules which facilitate cell-cell and cell-matrix interactions. The integrin family is composed of 18 alpha subunits which can heterodimerize with 8 beta subunits to form 24 known integrin pairs (31, 32). The alpha and beta subunits are non-covalently linked transmembrane proteins that function to connect the actin cytoskeleton to the ECM. Integrins are critical for mediating cell

adhesion and migration, as well as for integrating signals from both inside and outside the cell. Integrin clustering after matrix adhesion leads to outside-in signaling, while conformational changes to a high-affinity state facilitate inside-out signaling (33). Formation of matrix contacts triggers the assembly of an adhesome complex, and the activation of pro-migratory, proliferative, and anti-apoptotic signaling pathways. These pathways allow sustained cell survival; therefore, integrin adhesion has been implicated in the development of a wide range of pathologies, including tumor cell invasion and metastasis (33).

ITGA11

ITGA11 is one of the four alpha subunits that heterodimerize with ITGB1 to recognize collagen. ITGA11 was originally cloned by the Gullberg lab and found to be highly expressed in the adult uterus, heart and skeletal muscle, and localized to focal adhesions in fibroblasts (34). Like ITGA2, ITGA11 shows preferential binding to fibrillar collagens, recognizing the GFOGER sequence of type I collagen through the alpha-I domain (35). The binding of ITGA11 to collagen is Mg^{2+} dependent, and sensitive to concentrations of Ca^{2+} (35). *ITGA11*$^{-/-}$ mice are viable and fertile, though they display dwarfism and increased mortality, when unchallenged (36). The mice have mutant incisors which could contribute to the dwarfism, though the phenotype is shown before weaning and is not rescued by feeding soft food. This suggests the growth defect cannot be fully contributed to the incisor defect. Mouse embryonic fibroblasts (MEFs) isolated from *ITGA11*$^{-/-}$ mice demonstrate impaired adhesion and spreading on collagen along with a

decreased ability to reorganize and retract collagen gels (36). In wound healing studies, *ITGA11*$^{-/-}$ mice exhibit deficiencies in granulation tissue formation and wound contraction, possibly caused by impaired myofibroblast differentiation and collagen remodeling (37). In the periodontal ligament, sirius red staining indicated an increase in collagen accumulation in *ITGA11*$^{-/-}$ mice, though no change mRNA expression of collagen type I or III was observed (36). Interestingly, MT1-MMP (MMP14) mRNA was decreased in *ITGA11*$^{-/-}$ mice, and it has been previously shown that *MMP14*$^{-/-}$ mice display similar, though more extreme, phenotypes such as dwarfism and collagen remodeling deficiencies (36, 38, 39).

Recently, ITGA11 has been associated with promotion of tumor cell invasion through both increased expression in tumor cells and cancer associated fibroblasts (CAFs) in the tumor microenvironment. Independent studies have found ITGA11 is one of the most highly upregulated genes in non-small cell lung carcinoma (NSCLC) (40, 41). More recently however, gene expression analysis has shown ITGA11 is also upregulated in the CAFs in NSCLC compared to normal lung fibroblasts (42). Furthermore, xenografts of NSCLC in the lungs of *ITGA11*$^{-/-}$ SCID mice demonstrated impaired metastatic potential compared to xenografts in *ITGA11*$^{+/+}$ SCID mice, demonstrating the contribution of stromal ITGA11 during tumor progression (43). These data suggest an involvement of ITGA11 in tumor progression in NSCLC.

ITGA11 has also been implicated in breast cancer, where the mode of cancer dissemination has been studied in detail. Breast cancer cells are known to utilize collective cell invasion to migrate through the normal tissue, where leader cells make contact with

the ECM and degrade it in an MMP-dependent manner. Follower cells trail the leader cells, traveling along the tracks in the ECM created by the leader cells. In breast cancer, *ITGA11* was found to be a marker of leader cells, and knockdown of *ITGA11* attenuated breast cancer cell invasion through a collagen type I and matrigel mixture (44). The expression of ITGA11 within gliomas has not been investigated, nor has a role for ITGA11 been demonstrated in glioma cell invasion.

MT1-MMP

Metalloproteinases have been widely-studied in cell migration and invasion. To migrate through surrounding tissue, tumor cells must adopt an invasive phenotype, undergo cytoskeletal rearrangements, and become polarized as actin-based lamellipodia, filopodia, and nanopodia are projected from the leading edge of cells. These protrusions localize signaling molecules, cell surface receptors and matrix metalloproteinases (MMPs). The MMPs interact with and degrade the basement membrane and the ECM, which can be rich in highly cross-linked type I collagen or fibrin. Translocation of proteases to the actin-rich structures allows for localized breakdown of the surrounding matrix, and subsequent cell migration through tunnels made in the structural barrier (45). These events are precisely coordinated by exogenous factors and intracellular signaling pathways, discussed below.

The matrix metalloproteinase (MMP) family is composed of 26 members that are structurally characterized by a pro-peptide domain, a Zn^{2+} associated catalytic domain, a flexible linker peptide, and a C-terminal hemopexin-like (HPX) domain (46, 47). After

cleavage of the pro-domain to activate the latent zymogens, the MMPs function to degrade components of the ECM. Following stabilization and conformational changes of substrates induced by the C-terminal HPX domain (48), the catalytic domain mediates the degradation of the target protein. Six of the family members, termed membrane-type MMPs (MT-MMPs), contain a transmembrane domain, allowing these proteases to tether to the plasma membrane, creating a short cytoplasmic tail domain. The remaining MMPs are soluble and secreted from the cell to degrade substrates beyond the cell membrane. The MMPs are further classified by the ECM substrates they are able to hydrolyze, including collagen, fibrin, laminin, fibronectin, gelatin, and stromelysin (49, 50).

Early work investigating the role of MMPs in tumor progression focused on the role of soluble MMPs. MMP-2 (also known as gelatinase-A) was previously implicated as an essential protease in cell migration and reported to play a leading role in invasion by complexing with the $\alpha v\beta 3$ integrin at the cell surface, mediating directed migration (51). When MMP-2 and MMP-3 were overexpressed in mammary epithelial cells, the normally non-invasive cells underwent an epithelial to mesenchymal transition (52). While soluble, or secreted MMPs are important for the degradation of denatured type I collagen and other substrates, later studies of MT-MMPs have revealed this membrane-bound class is indispensable for cell invasion events. MMP-14 or membrane-type 1 matrix metalloproteinase (MT1-MMP) has been the most well studied MMP and is essential for invasion through a 3D ECM (53). To compare the necessity of soluble versus membrane-anchored MMPs during invasion, fibroblasts null for MT1-MMP, MMP-2, 3, 8, 9, 13, or TIMP-2 were cultured on type I collagen or chicken chorioallantoic membrane (CAM).

All mutant fibroblasts, except those lacking MT1-MMP, were able to degrade collagen and invade the CAM at similar rates as wild-type fibroblasts. The MT1-MMP null fibroblasts demonstrated no collagen degradation or invasion, demonstrating the particular importance of MT1-MMP during invasion through collagen (54). Similarly, while CHO-K1 and MDCK cells are normally invasion-incompetent, when transfected with MT1-MMP, MMP-1, 2, 7, 9, 11, or 13 and cultured on fibrin matrices with 10% serum, scatter factor, and hepatocyte growth factor, all cells were able to degrade fibrin; however, only MT1-MMP transfected cells exhibited a gain-of-function phenotype and were able to invade the fibrin matrix (55). To further implicate MT1-MMP as the critical MMP, tissue explants and microvascular endothelial cells were isolated from mice null for MT1-MMP, MMP-2 or -9. The MMP-2 and -9 null endothelial cells and explants were indistinguishable from wild-type, forming neovessels and invading collagen matrices in culture (56). However, neovessel formation and collagenolysis were inhibited in MT1-MMP null tissue explants and microvascular cells (56), indicating that MT1-MMP was needed for endothelial cells to remodel and invade the ECM. While MMP-2 null mice exhibited no developmental or physical defects (56), MT1-MMP gene disruption led to abnormalities in osteogenesis, angiogenesis, and collagen turnover leading to reduced neovessel formation, dwarfism, arthritis and premature death (38, 57). Altogether, these experiments point to a critical role for MT1-MMP in cell invasion of the ECM.

Various post-translational modifications direct trafficking of MT1-MMP to the plasma membrane, including furin cleavage, phosphorylation, and O-glycosylation. The pro-domain of the MT1-MMP zymogen contains two recognition sequences for the

proprotein convertase furin, which activates MT1-MMP through cleavage at Tyr112 (58, 59). The MT1-MMP zymogen is a 63 kDa protein and when activated through pro-domain cleavage, it is converted to 60 kDa. During endothelial cell sprouting angiogenesis, a process analogous to tumor and fibroblast cell invasion, the pro-angiogenic phospholipid, sphingosine 1-phosphate, S1P, triggered the migration of MT1-MMP to the plasma membrane by activating the G-protein coupled receptors $S1P_1$ and $S1P_3$ (60). S1P stimulated Src kinase-mediated phosphorylation of tyrosine residue 573 on the cytoplasmic tail of MT1-MMP (61) and induced colocalization between MT1-MMP and the adaptor protein p130Cas at the leading edge of the cell (62). Src-dependent Tyr573 phosphorylation on the cytoplasmic tail of MT1-MMP was shown to be essential for cell migration. Additionally, O-glycosylation of the hinge domain regulates the stability of MT1-MMP through the inhibition of both autolysis and internalization of the active form of the enzyme (63). While only the transmembrane domain was essential for localization to the cell surface, the cytoplasmic domain was critical in the localization of MT1-MMP to the leading edge of the plasma membrane (64, 65). To test for MT1-MMP localization *in vivo*, mice heterozygous for an MT1-MMP allele containing a LacZ reporter gene were generated (66). In tissue explants cultured on type I collagen matrices, β-gal activity was preferentially localized to the invading endothelial tip cells (66). Thus, proper post-translational modifications direct MT1-MMP to the cell surface to facilitate successful invasion events.

The proteolytic activity of MT1-MMP is coordinated with integrins and receptor tyrosine kinases. Cell migration and invasion requires cleavage of the ECM, which

presents a structural barrier consisting of cross-linked type I collagen networks and other substrates (67). MT1-MMP hydrolyzes collagen type I, II, III, proteoglycan, fibronectin, vitronectin, type 1 gelatin, the alpha chain of laminin-1, the gamma-2 chain of laminin-5, integrins, and cell surface receptors (61, 68-70). Following the degradation of type I collagen by MT1-MMP, cryptic binding sites for the αvβ3 integrin are exposed (71, 72). The αvβ3 integrin binds to the ECM and associates with the tyrosine kinase receptor VEGFR-2, leading to increased migration in endothelial and other invasive cells (73, 74). Thus, matrix proteolysis through MT1-MMP may allow complex formation between integrins and receptor tyrosine kinases, which work together to facilitate invasion. In endothelial cells, MT1-MMP complexes with the α2β1 integrin to promote endothelial cell assembly into interconnected networks in 3D collagen matrices (75).

CELL INVASION

Cell invasion into surrounding tissue requires coordinated matrix adhesion, remodeling, and degradation (76). A critical component of cell invasion is the integration of signals between the extracellular environment and the cell cytoskeleton. These bidirectional signals are controlled by ligation of integrins to proteins in the basement membrane and extracellular matrix (ECM). Integrin activation and clustering lead to the recruitment of actin binding proteins, such as talin and paxillin, to the sites of matrix adhesion, forming focal adhesions and connecting the actin cytoskeleton to ECM. Many signaling molecules and pathways are activated downstream of integrin activation and focal adhesion formation, including Src, FAK, the family of small Rho GTPases, and the

PI3K and MAPK signaling pathways. Activation of small Rho GTPases, Rac and Cdc42, causes dynamic actin remodeling to form protrusive actin-based pseudopodia into the surrounding matrix (77, 78). After formation of these adhesive protrusions, matrix proteases, such as MT1-MMP, are activated and recruited which allows directed proteolysis (79, 80). MT1-MMP has been shown to complex with integrins within these adhesive sites where it proteolyzes matrix proteins in a controlled manner (81-83). This matrix degradation allows for coordinated proteolysis, cell motility into the space created through ECM degradation, and also reveals cryptic sites in the ECM proteins and a reservoir of signaling molecules trapped within the matrix which promote invasion (84-87). As the leading edge of the cell migrates through the surrounding tissue, integrins bind to the newly exposed matrix, creating focal adhesions and sending additional actin-based protrusions to examine the nearby environment. Concomitantly, the rear of the cell releases its adhesions to the ECM by cleaving the cytoplasmic integrin tails attached to the ECM through calpain activity or by decreasing the integrin affinity for the ECM substrate (88, 89).

Pseudopodia and other actin-based degradative structures are common characteristics of more motile and invasive cells (90, 91). Formation and maturation of pseudopodia is dependent on attachment of integrins to the ECM (92), and inhibition of pseudopodia formation attenuates tumor cell migration and invasion in several tumor cell lines, including the U87 glioblastoma cell line (93). Further, many of the proteins known to localize to focal adhesions and pseudopodia, such as Arp2/3, fascin, cortactin, and alpha-actinin, are upregulated in cancer (94, 95). Although pseudopodia are linked with

tumor progression, a role for noncanonical NF-κB signaling in the development of pseudopodia has not been established.

While the mechanism of cell invasion described above is considered to be utilized during single cell tumor cell invasion, tumor cells can employ various mechanisms to invade collectively through their respective surroundings (96). Tumors are made up of a heterogeneous population of cells, and not all within the tumor are capable of degrading and invading their surrounding matrix. One mode tumors can use to overcome this barrier is through collective invasion. In some ways analogous to endothelial cell tip and stalk cell relationships during angiogenesis, in collective cell invasion, a cell with an invasive phenotype degrades the matrix and invades while the cells which are not capable of degrading the matrix follow behind (97). Although not proliferative, leader cells are invasion-competent and proteolyze the ECM in an MMP-dependent manner (98, 99). The follower cells, while proliferative, cannot degrade the matrix and thus cannot invade through the surrounding barrier. These populations can form a commensal relationship where the leader cells degrade the matrix and invade, leaving a tunnel in the matrix which the follower cells can migrate through in an MMP-independent manner. It has been suggested that the follower cells could actually be the population which colonizes the sites of metastasis (44). This mode of collective invasion has been found to be utilized in breast cancer (44, 100), melanoma (101), colon cancer (102), glioblastoma (103), and during neural crest development (104, 105).

To study cell invasion, we utilize a 3D *in vitro* assay where tumor cells isolated from glioblastoma patient tumors are seeded onto a polymerized 3D type I collagen matrix

(29, 127). Though not normally expressed in the brain, type I collagen has been found to be a prominent component of the glioma ECM (107). To mimic the properties of the *in vivo* ECM, the collagen is reconstituted using acid which preserves the collagen telopeptides, allowing fibril formation and crosslinking, creating a matrix requiring MMP-dependent degradation for cell invasion (108, 109). We have shown previously that glioma cells invade this matrix in a MMP-dependent manner (30). In these studies, we use this model system to investigate mechanisms through which noncanonical NF-κB signaling regulates glioma cell invasion.

CHAPTER II

NIK REGULATES MT1-MMP ACTIVITY AND PROMOTES GLIOMA CELL INVASION INDEPENDENTLY OF THE CANONICAL NF-κB PATHWAY*

SUMMARY

A growing body of evidence implicates the noncanonical NF-κB pathway as a key driver of glioma invasiveness and a major factor underlying poor patient prognoses. Here, we show that NF-κB-inducing kinase (NIK/MAP3K14), a critical upstream regulator of the noncanonical NF-κB pathway, is both necessary and sufficient for cell-intrinsic invasion, as well as invasion induced by the cytokine TWEAK, which is strongly associated with tumor pathogenicity. NIK promotes dramatic alterations in glioma cell morphology that are characterized by extensive membrane branching and elongated pseudopodial protrusions. Correspondingly, NIK increases the phosphorylation, enzymatic activity and pseudopodial localization of membrane type-1 matrix metalloproteinase (MT1-MMP/MMP14), which is associated with enhanced tumor cell invasion of three-dimensional collagen matrices. Moreover, NIK regulates MT1-MMP activity in cells lacking the canonical NF-κB p65 and cRel proteins. Finally, increased expression of NIK is associated with elevated MT1-MMP phosphorylation in orthotopic xenografts and co-expression of NIK and MT1-MMP in human tumors is associated with

*Part of this research was originally published in the journal *Oncogenesis.* Duran CL, Lee DW, Jung JU, Ravi S, Pogue CB, Toussaint LG, Bayless KJ, Sitcheran R (2016). NIK regulates MT1-MMP activity and promotes glioma cell invasion independently of the canonical NF-κB pathway. *Oncogenesis.* 2016. 5(6):e231. © Nature Publishing Group.

poor glioma patient survival. These data reveal a novel role of NIK to enhance pseudopodia formation, MT1-MMP enzymatic activity, and tumor cell invasion independently of p65. Collectively, our findings underscore the therapeutic potential of approaches targeting NIK in highly invasive tumors.

INTRODUCTION

The persistent invasiveness of high-grade glioma cells into healthy brain tissue is a major factor underlying the therapy resistance and poor prognosis of this malignancy. NF-κB transcription factors have been shown to play key roles in regulating tumor-promoting functions including cell migration and invasion (110, 111). There are two main pathways controlling NF-κB activation. In the context of glioma, most studies have focused on the canonical NF-κB pathway, which is dependent on IκB Kinase-β (IKKβ) and mediated by p65 (RELA)- or cRel (REL)-containing transcription factor complexes. However, we and others have demonstrated that constitutive, noncanonical NF-κB signaling, mediated by RelB-p52 complexes, predominates in aggressive, mesenchymal glioma where it promotes cell migration, invasion and tumor recurrence (11, 29, 30, 112). Activation of the noncanonical NF-κB pathway is dependent on NF-κB-inducing kinase (NIK, also known as MAP3K14), a constitutively active kinase that is continuously targeted for proteasomal degradation in unstimulated cells (17-19). In response to specific cytokines, NIK degradation is attenuated, resulting in activation of IKKα, phosphorylation-dependent proteolytic processing of the RelB-inhibitory protein p100 to p52, and nuclear translocation of RelB-p52 heterodimers (20). We have recently shown

TNF-like weak inducer of apoptosis (TWEAK, also known as TNFSF12) preferentially activates noncanonical NF-κB RelB and p52 proteins and promotes the invasive properties of glioma cells (30).

Tumors must degrade the surrounding extracellular matrix (ECM) to invade into nearby healthy tissue (113). Invasive cancer cell phenotypes show elevated formation of invadopodia, which are specialized actin- and cortactin-rich membrane protrusions that mediate attachment to and degradation of the ECM (79). Invadopodia formation in 2D is associated with greater invasive behavior in 3D, where cells must extend larger protrusions, termed pseudopodia, to migrate successfully (98, 114). Membrane type-1 matrix metalloproteinase (MT1-MMP, also known as MMP-14), is the predominant ECM-degrading enzyme localized to invadopodia (98, 113, 114). MT1-MMP is highly expressed in invasive human cancers and is associated with poor patient survival (115-118). MT1-MMP is activated by furin cleavage (119, 120), and once phosphorylated on Y573 (121), MT1-MMP is directed to the plasma membrane (122), where it can degrade multiple ECM proteins (123). Notably, the signals that regulate MT1-MMP localization to the cell surface during invasion are not fully understood.

Several studies have established a role for canonical NF-κB-dependent (p65-mediated) regulation of MT1-MMP expression (124, 125). In addition, Fritz and colleagues demonstrated that noncanonical NF-κB signaling (RelB-p52-mediated) regulates MT1-MMP expression and tumor cell invasion induced by the scaffold protein CNK1 (126). Thus, while both canonical and noncanonical NF-κB signaling have been linked to regulating MT1-MMP expression, whether these pathways control activation and

localization of MT1-MMP during invasion have not been established. Importantly, the role of NIK in both constitutive and TWEAK-induced invasion of glioma cells is not well understood. In this study, we establish novel functions for NIK in regulating MT1-MMP.

MATERIALS AND METHODS

Reagents

TNFα was obtained from Promega (Madison, WI), rhTWEAK was purchased from PeproTech (Rocky Hill, NJ), TAPI-2 was obtained from Calbiochem (San Diego, CA). MG132 was purchased from Cell Signaling Technology (Danvers, MA). Collagen type I was isolated and prepared as previously described (127) or purchased from Corning (Corning, NY).

Cells and culture conditions

BT25 and BT114 cell lines were obtained from human glioma patients and described previously (128). Glioma lines were maintained as tumorspheres in Neural Stem Cell (NSC) medium (DMEM/F12, 1x B-27 Supplement minus Vitamin A, 1x Glutamax, 50 ng/ml EGF, 50 ng/ml bFGF, 1x Pen/Strep). Spontaneously immortalized mouse embryonic fibroblasts (MEFs) from $p65^{-/-}$, $cRel^{-/-}p65^{-/-}$ animals and their corresponding WT MEFs were a kind gift from Dr. Albert S. Baldwin Jr. (UNC, Chapel Hill), $RelB^{+/+}$ and $RelB^{-/-}$ MEFs were generously provided by Dr. Denis Guttridge (The Ohio State University), and $NIK^{+/+}$ *and* $NIK^{-/-}$ MEFs were obtained from Dr. Robert Schrieber (University of Washington). HEK293FT cells were purchased from Invitrogen (Grand

Island, NY). MEF and HEK293FT cells were cultured in DMEM+10% FBS (Invitrogen). All cells were incubated at 37°C with 5% CO_2.

Constructs

pLenti6 overexpression constructs for NIK were generated by subcloning cDNA into pLenti6-V5-DEST (Addgene, Cambridge, MA) using the GATEWAY™ Cloning System. Luciferase (Promega, Madison, WI) coding sequences were subcloned into pLenti6-V5-DEST and used as controls for NIK overexpression. NIK(S867A) mutation was obtained by PCR cloning using oligo primers containing the mutation.

CRISPR-Cas9 NIK gene knockout cell clones

Lenti-CrispR-v2 (Addgene, Cambridge, MA) was used to express both *Cas9* and human *NIK* sgRNA (sgNIK-1: GCUCCUUCGGAGAGGUGCAC, sgNIK-2: GAAAGCGUCGCAGCAAAGCC, or sgNIK-3: AGUACCGAGAAGAAGUCCAC). BT25 cells were transduced with mixture of lentiviruses carrying these sgRNAs then selected against 0.6 μg/ml puromycin. 1507 bp and 33 bp deletions around sgRNA target sequences were identified by sequencing and loss of NIK expression was confirmed by immunoblot, qPCR and/or immunofluorescence microscopy analysis of puromycin-resistant cells. Single colony cells were isolated by serial dilution and experiments were repeated with at least two clones.

Lentiviral production

HEK293FT cells were transfected with 24 μg of lentiviral plasmids using 72 μg of polyethyleneimine (Polysciences Inc., Warrington, PA). Lentiviruses were harvested after three days and used to infect $2x10^5$ BT114 or MEF cells. Transduced cells were grown for 72 hours in NSC medium or DMEM with 10% FBS containing 6 μg/ml or 0.1 μg/ml blasticidin (Invivogen, San Diego, CA), respectively, to select cells with stable transduction.

Invasion assays

Invasion assays were established as previously described (127). Briefly, 3D collagen type-I matrices were prepared at a final concentration of 2 mg/ml, containing indicated concentrations of TWEAK (0 or 10 ng/ml). Following collagen polymerization, dissociated cells (40,000 cells/100 μl DMEM) were seeded and incubated at 37°C with 5% CO_2. To inhibit MMPs, DMSO, 2.5 or 5 μM TAPI-2 was preincubated with the cells for 20 minutes at 37°C. Cells, combined with the inhibitors, were seeded onto collagen matrices. Invasion assays were fixed after 24-48 hours incubation, as indicated, with 3% glutaraldehyde in PBS and stained with 0.1% toluidine blue in 30% methanol.

Quantification of invasion responses

Invasion density was quantified manually in toluidine blue-stained invasion assays as the average number of structures invading past the monolayer, per field, using an eyepiece fit with a 10x10 ocular grid. At least four wells per treatment group were counted,

per experiment, for three independent experiments. To visualize invasion responses, after fixation and staining, collagen gels were removed from the well, cut and imaged from the side using an Olympus CKX41 microscope with a Q-Color 3 camera or a Nikon Ti Eclipse inverted microscope and DS-Fi1 5-Meg Color C-Mount Camera at 20x magnification.

RNA isolation, cDNA synthesis, and quantitative-RT-PCR

Total RNA was isolated from cells using PurelinkTM RNA Mini Kit (Life Technologies). cDNA was synthesized from 1 μg of total RNA using Super-Script® III Reverse Transcriptase (Life Technologies) following manufacturer's instructions. Quantitative RT-PCR was performed using SYBR® Green PCR Master Mix (Applied Biosystems, Foster City CA). Expression of mRNA was normalized to either GAPDH or RPLP0 expression levels. The following primers were used: GAPDH 5′-AATGAAGGGGTCATTGATGG-3′, 5′-AAGGTGAAGGTCGGAGTCAA-3′; RPLP0 5′- TCGTCTTTAAACCCCTGCGTG-3′, 5′-TGTCTGCTCCCACAATGAAAC-3′; MMP-14 (human) 5′-TGCCTACCGACAAGATTGATG-3′ 5′-ATCCCTTCCCAGACTTTGATG-3′; MMP14 (mouse) 5'-GGATGGACACAGAGAACTTCG-3' 5'-TTTTGGGCTTATCTGGGACAG-3; NIK 5′-TTCAGCCCCACCTTTTCAG- 3′ 5′-ACGCTTTCCCTTCCAACAC-3′. Three independent experiments were performed in triplicate wells. qRT-PCR data was analyzed using StepOne Software (version 2.1). ΔΔCT values were normalized to GAPDH expression values for each sample, set relative to indicated treatment, and converted to $2^{-\Delta\Delta CT}$ to compare the relative mRNA fold change expression between treatment groups.

Immunostaining

$2.5x10^5$ cells were seeded on collagen (50 μg/ml) coated 12 mm coverslips in a 24 well plate. After 16 hours incubation, cells were treated as indicated, fixed in 4% paraformaldehyde, permeabilized with 0.5% Triton X-100 in PBS, and blocked overnight in 0.1% Triton X-100, 1% BSA/1% goat serum in TBS at 4°C. To examine the effects of TWEAK treatment on pMT1-MMP localization in MEFs, cells were serum-starved for 2 hours, treated with TWEAK (10 ng/ml) for 4 hours and subsequently fixed and processed as described above. 1.09 μM DAPI (Invitrogen) was used for staining nuclei and the following primary antibodies were used: cortactin (Upstate, Lake Placid, NY, 05-180), p65 (SC-8008), custom generated Y573 pMT1-MMP (21st Century Biochemicals, as previously described (121), NIK (Abcam, Cambridge, MA, ab7204), and either Alexa Fluor 488 Phalloidin (Invitrogen, A12379) or Alexa Fluor 647 Phalloidin (Invitrogen, A22287). Cells were imaged using a Nikon TI A1R inverted confocal microscope to capture Z-stacked images with a 0.225 μm step size. Fluorescence was quantified using Nikon Elements Software (see Figure 6B).

MT1-MMP activity assays

MT1-MMP activity assays were performed on cell lysates (not conditioned media) using a Sensolyte, AS-72025 kit, with several modifications; to inhibit soluble MMPs and specifically evaluate MT1-MMP activity after 8-24 hours invasion, lysates from cells invading collagen were incubated with conditioned media collected from TIMP-1-transfected HEK293FT cells (129). The MT1-MMP sensitive substrate was added to equal

amounts of cell lysate and incubated for 30 minutes. Fluorescence intensity was measured at Ex/Em 490/520 nm using Victor X3 Multilabel Reader 2030. Relative fluorescence units (RFUs) were calculated by subtracting the control reading from each sample and averaging the remaining RFU value of the replicates. Gelatin zymography was performed as previously described (130).

Western blotting

Whole cell extracts were prepared using RIPA. To detect NIK protein expression, cells were pre-treated with 5 μM MG132 for 1 hour and with or without 10 ng/ml TWEAK for 5 hours, as indicated. Proteins were subjected to western blotting as previously described (30, 129), using the following specific antibodies: α-Actin (Calbiochem, CP01), MT1-MMP (Millipore, MAB3328), pMT1-MMP (Y573) NIK (CST-4994), p65 (SC-8008), p-p65 (Ser536, CST-3033), RelB (SC-226), p100/p52 (CST-4882), and GAPDH (Abcam, ab8245).

Immunohistochemical analysis of mouse xenograft tissue

Intracranial xenografts were previously performed (30). Animals from that experiment were perfused, brains were removed and fixed with 4% paraformaldehyde and embedded in OCT. 10 μm-thick sections were immunostained with incubated with NIK-specific antibody (Abcam, ab7204) and Alexa Fluor® 488-secondary antibody (Invitrogen, A-11008) and DAPI mounting media (Invitrogen). Images were acquired using a Nikon TI A1R inverted confocal microscope. Adjacent tumor sections were used

for immunohistochemical detection of pMT1-MMP (Y573) using the Vectastain ABC elite kit (Vector Laboratories). The signal was developed using DAB peroxidase substrate (Vector Laboratories), counterstained with haematoxylin and images were acquired on the Nikon Eclipse Ti microscope.

Ex vivo glioma tumor tissue staining

The use of de-identified human glioblastoma tissue was approved by the Institutional Review Boards (IRBs) of Saint Joseph Regional Health Center, Bryan, TX (IRB2012-001), and Texas A&M University (IRB2014-0318D). Sections of human glioma biopsy samples were stained with DAPI and antibodies specific for pMT1-MMP (Y573) and NIK (Abcam, ab7204). NIK-ab7204 was pre-conjugated to AF488 using an antibody labeling kit (Molecular Probes®/Invitrogen, A20181) and immunostaining was performed sequentially using the pre-labeled NIK antibody last. Imaging was performed as described above.

Glioma database analysis

Gene expression data for glioblastoma (GBM) patients from The Cancer Genome Atlas (TCGA), Cell 2013 dataset (10) and lower grade glioma (LGG) patients from the TCGA (Provisional raw data set, NCI) were downloaded from cBioPortal for Cancer Genomics (131, 132) and analyzed using Prism 6 (Graphpad Software, Inc.). Kaplan-Meier plots were generated from GBM and LGG patients with increased NIK (MAP3K14) and MT1-MMP (MMP14) mRNA expression with a z-score of 1.5. GBM dataset can be

accessed at http://bit.ly/1IFXIKA and LGG dataset can be accessed at http://bit.ly/1IFY43S.

Statistical analyses

All statistical analyses were performed using Prism 6 (Graphpad Software, Inc.). Student's *t*-test was performed on data comparing two samples, unless otherwise indicated. One-way or two-way ANOVA with Holm-Šídák or Tukey's Honest Significant Difference (HSD) post-hoc test for comparing multiple samples. Kruskal-Wallis with Dunn's post-test was used to assess statistical significance between log2-base NIK and MT1-MMP gene expression data. For ANOVA analyses, multiplicity adjusted P-values are reported (133) with significance value of alpha =0.05. Survival and disease free patient data was analyzed using a Log-rank Mantel-Cox test. Unpaired Welch t-test was used to analyze mean survival GBM patients. No statistical method was used to predetermine sample size. Experiments were not randomized. The investigators were not blinded to sample allocation during experiments.

RESULTS

NIK is required for constitutive and TWEAK-induced glioma cell invasion

We previously demonstrated that patient-derived glioma cell lines exhibit distinct invasive potentials that correlate more strongly with noncanonical NF-κB/RelB signaling than with canonical NF-κB/p65 activity (29, 30). To address the role of NIK, a key upstream regulator of noncanonical NF-κB signaling, in glioma invasion and

pathogenesis, we first sought to determine whether NIK was sufficient to promote cell invasion in BT114 glioma cells, which exhibit low invasive activity (30). In addition to expressing wild-type NIK (NIK(WT)), which is continuously degraded under unstimulated conditions, we also used a more stable form of NIK that allowed greater protein accumulation and facile immunological detection. Specifically, a S867A substitution at the conserved TBK1 phosphorylation site renders human NIK resistant to degradation (17), and immunoblot analysis of BT114 glioma cells confirmed that NIK(S867A) is expressed at higher levels than NIK(WT) (Figure 1A). Using 3-dimensional (3D) collagen type I invasion assays, we observed that NIK transfected cells were more invasive than controls cells, and NIK(S867A) exerted a significantly stronger effect than NIK(WT) (Figure 1B and C). Furthermore, ectopic expression of NIK in several additional glioma lines, including BT116, U87, and BT25 cells, promoted cell invasion in this assay (Figure 2).

Next, we investigated the effects of NIK knockdown using CRISPR/Cas9/small-guide (sg)RNA-mediated deletion of *NIK*. For these experiments we took advantage of the highly invasive BT25 glioma line (30). NIK protein is no longer detectable in both untreated and TWEAK-treated BT25-sgNIK cells, indicating efficient sgRNA-mediated deletion of *NIK* (Figure 3A). We also confirmed loss of NIK expression in BT25-sgNIK cells by immunofluorescence staining, flow cytometry and impaired p100 processing and p52 nuclear localization (Figure 4A-C). Importantly, loss of NIK significantly diminished the invasive potential of both untreated, as well as TWEAK-treated, BT25-sgNIK cells (Figure 3B and C). Similarly, loss of NIK in BT114-sgNIK cells significantly attenuated

invasion in unstimulated and TWEAK-treated cells (Figure 5A-C). Together, these data identify a critical role for NIK in regulating both constitutive and TWEAK-induced glioma cell invasion.

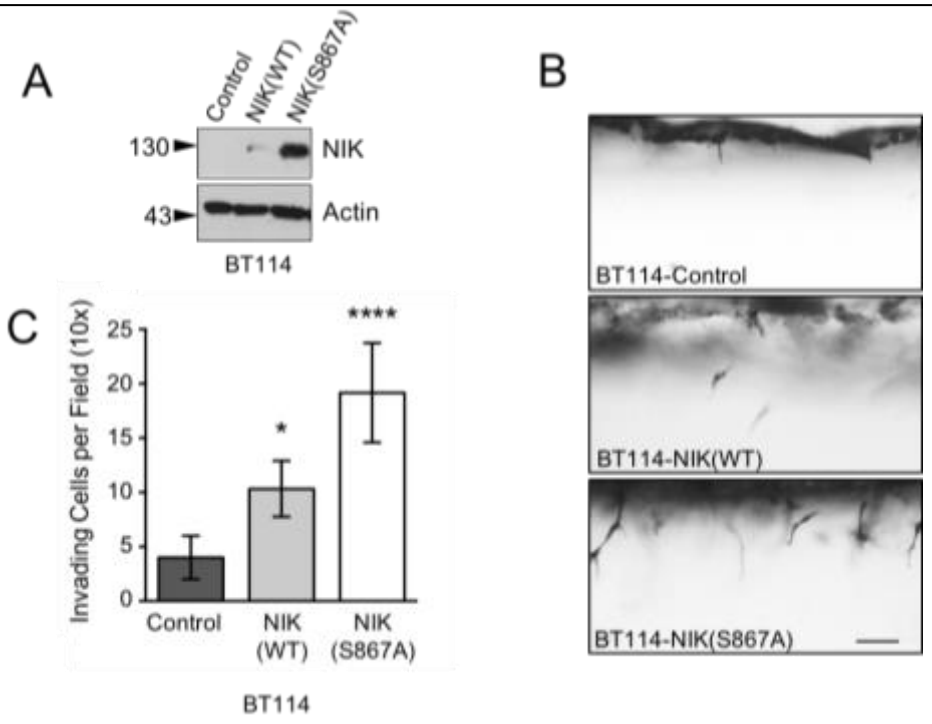

Figure 1. NIK promotes glioma cell invasion.
(A) Western blot analysis of BT114 glioma cells transduced with lentiviral vectors expressing luciferase (Control), NIK(WT) or NIK(S867A). Whole cell detergent lysates were probed with indicated antibodies. **(B)** Side-view images of BT114-Control, -NIK(WT) and -NIK(S867A) cells after 24 hours invasion in 3D collagen matrices. Cells in collagen matrices were fixed, stained with toluidine blue, cut into thin slices and imaged with light microscopy. Scale bar = 50 µm. **(C)** Quantification of invasion density of BT114-Control, -NIK(WT) and -NIK(S867A) cells in (B) represented as the average numbers of invading cells per 1-mm^2 field (top-view) ± SD after 24 hours of invasion. At least 6 wells were quantified per experiment for four independent experiments. Graph shows a representative experiment. Statistical significance was calculated with 2-way ANOVA and Tukey's HSD post test. Multiplicity adjusted P-values: * 0.0109 for Control vs. NIK(WT) and **** <0.0001 for Control vs. NIK(S867A).

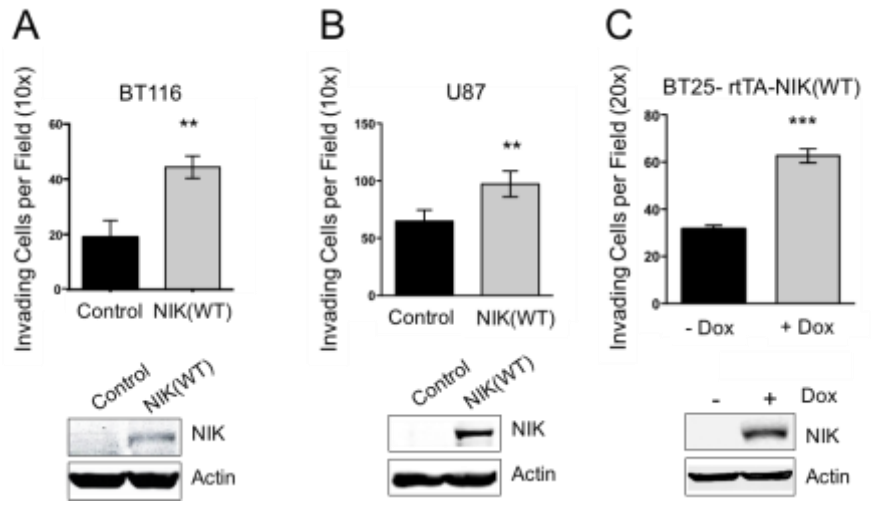

Figure 2. NIK promotes invasion in different glioma lines.
(A) BT116 cells expressing vector (Control) or NIK(WT) were seeded onto 3D collagen matrices and allowed to invade 24 hours. Graph shows average number of invading cells +/- SD in a 0.25 mm^2 field. At least 4 wells were quantified per cell type for three independent experiments. Unpaired t-test P-value: ** 0.0037 Control vs. NIK(WT). Western blot analysis of BT116 cells expressing vector (Control) or NIK(WT) confirming exogenous NIK expression. **(B)** U87 cells expressing vector (Control) or NIK(WT) were seeded onto 3D collagen matrices and allowed to invade 24 hours. Graph shows average invasion density. At least 4 wells were quantified per cell type for three independent experiments. Unpaired t-test P-value: ** 0.0012 Control vs. NIK(WT). Western blot analysis of U87 cells expressing vector (Control) or NIK(WT) confirming exogenous NIK expression. **(C)** BT25 cells expressing NIK under control of reverse tetracycline- controlled transactivator (rtTA), inducible through doxycycline, were not treated (-Dox) or treated with 5ng/ml (+Dox) for 48 hours before seeding onto collagen matrices and allowing to invade 48 hours. Graph shows average invasion density. At least 4 wells were quantified per cell type for three independent experiments. Unpaired t-test: ***P <0.0001 -Dox vs. +Dox. Western blot analysis of BT25 cells treated with (+Dox) or without doxycycline (-Dox) confirming induced NIK expression.

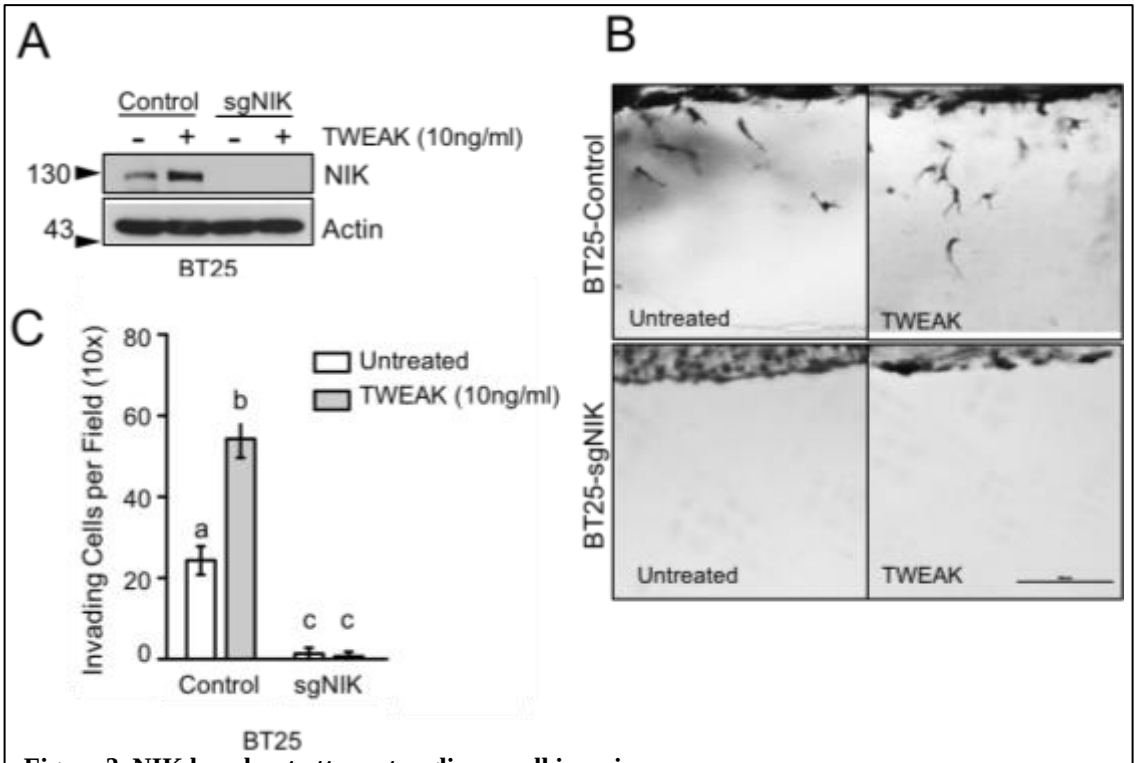

Figure 3. NIK knockout attenuates glioma cell invasion.
(A) Western blot analysis of whole cell lysates from BT25-Control and clonally selected BT25-sgNIK cells. Cells were first treated with MG132 for 1 hour to prevent NIK degradation and then untreated, or treated with TWEAK (10 ng/ml), as indicated for 5 hours. Extracts were probed with indicated antibodies. **(B)** Side view images of invasion assays with untreated or TWEAK-treated (10 ng/ml) BT25-Control and BT25-sgNIK cells allowed to invade 3D collagen matrices for 24 hours. Scale bar = 100 μm. **(C)** Invasion densities for (B) were quantified as described above in (1C), quantifying at least 3 wells of invading cells were quantified per experiment for three independent experiments. Graph shows a representative experiment. Different letters represent statistically significant differences calculated with two-way ANOVA and Tukey's HSD post test. Multiplicity adjusted P-values for all differences is <0.0001.

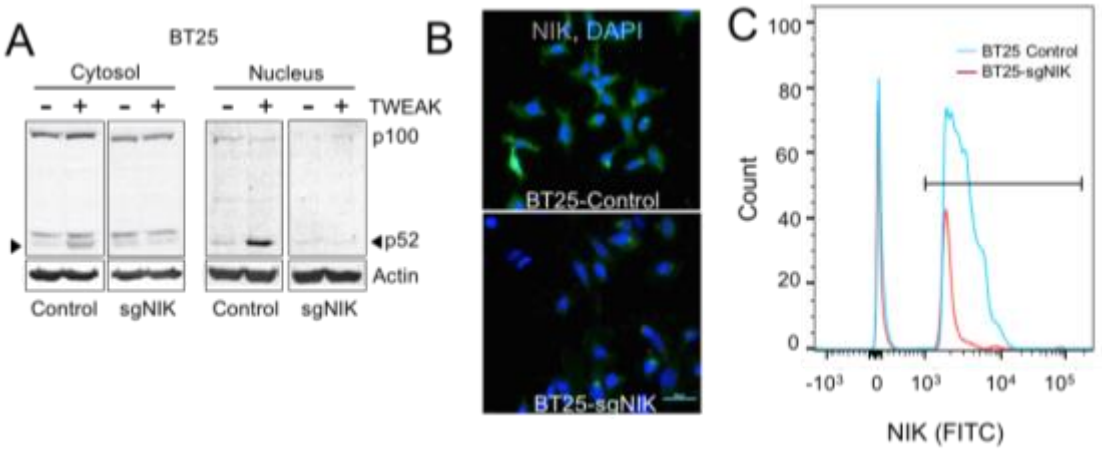

Figure 4. Glioma cells expressing sgNIK have decreased NIK expression.
(A) Nuclear and cytoplasmic fractions were isolated from BT25 cells expressing vector (Control) or sgNIK treated with (+) or without (-) 10 ng/ml TWEAK for 24 hours. Extracts were probed with antibodies directed to Actin and p100/p52 to assess p100 processing and p52 nuclear translocation downstream of NIK. **(B)** BT25-Control and BT25-sgNIK cells were seeded onto collagen coated coverslips and immunostained with antibodies directed to NIK (green) and DAPI (blue) to demonstrate loss of NIK expression in sgNIK cells, and specificity of antibody. Scale bar = 10 μm. **(C)** Flow cytometry was performed to quantify NIK staining in BT25-Control and BT25-sgNIK cells. $3x10^5$ cells were fixed, permeabilized in 0.3% Triton in PBS, and incubated with antibodies directed to NIK or isotype controls followed by incubation with FITC-conjugated secondary antibody. At least 10000 events were analyzed with a BD LSRFortessaTM X-20 cell analyzer and data was analyzed, normalizing to mode, with FLowJo software (v-X).

NIK promotes pseudopodia formation

Because changes in morphology can be predictive of cell motility and metastatic potential (134), we sought to determine whether the ability of NIK to promote invasion of glioma cells was associated with changes in cell shape. Examination of BT114 cells in 2D culture revealed that both NIK(WT) and NIK(S867A) significantly altered cell morphology, specifically by inducing the formation of F-actin- and cortactin-dense, branched cellular processes resembling the pseudopodia of invasive cells (Figure 6A). Quantification of these features (Figure 6B) revealed that total cell area as well as the

length of extended pseudopodial cell processes were increased in both NIK(WT) and NIK(S867A) cells, compared with vector control cells (Figure 6C and D).

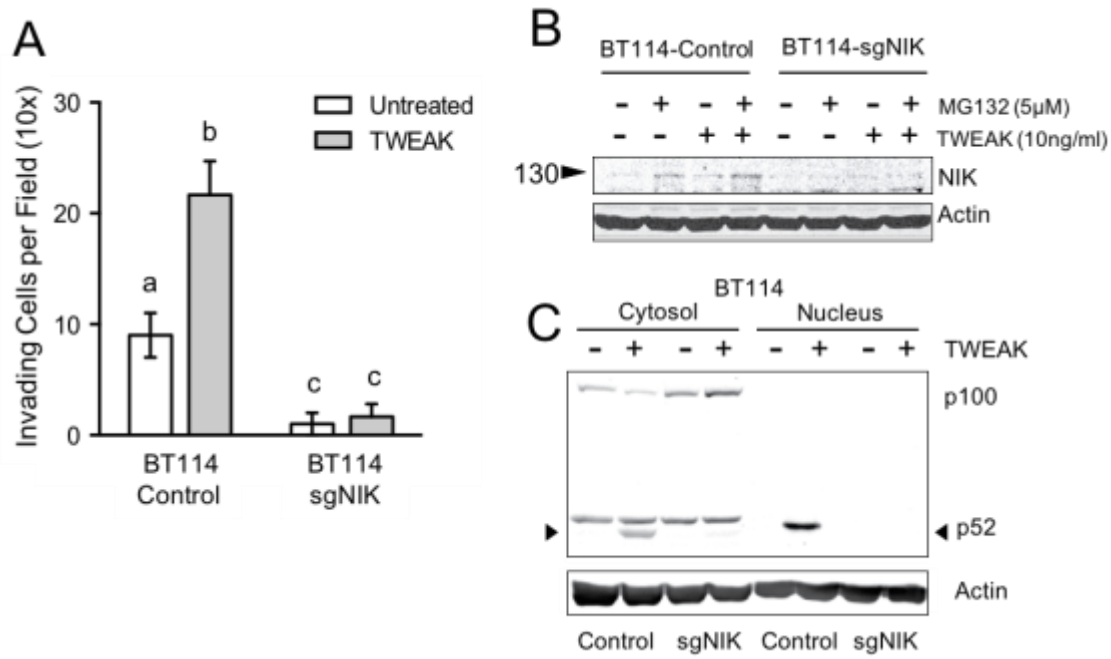

Figure 5. Cells expressing sgNIK do not invade in response to TWEAK.
(A) BT114-Control and BT114-sgNIK cells were seeded onto collagen matrices with or without 10 ng/ml TWEAK and allowed to invade 24 hours. Representative graph from three independent experiments shows average invasion density counted from three wells per treatment. Statistical analysis was calculated using 2-way ANOVA and Tukey's HSD post test. Different letters indicate statistically significant differences with the following multiplicity adjusted P-values: $p=0.0002$ for "a vs. b"; $p<0.01$ for "b vs. c" and "a vs. c". **(B)** Western blot analysis of BT114 cells expressing vector (Control) or sgNIK treated with or without MG132 (5 μM) for 1 hour to prevent NIK degradation and then untreated, or treated with TWEAK (10 ng/ml), as indicated for 5 hours. Whole cell lysates were probed with indicated antibodies. **(C)** Western blot analysis of BT114 cells expressing vector (Control) or sgNIK treated as in Figure 4A. Extracts were probed with antibodies directed to Actin and p100/p52 to demonstrate inhibition of p100 processing and p52 nuclear translocation in BT114-sgNIK cells.

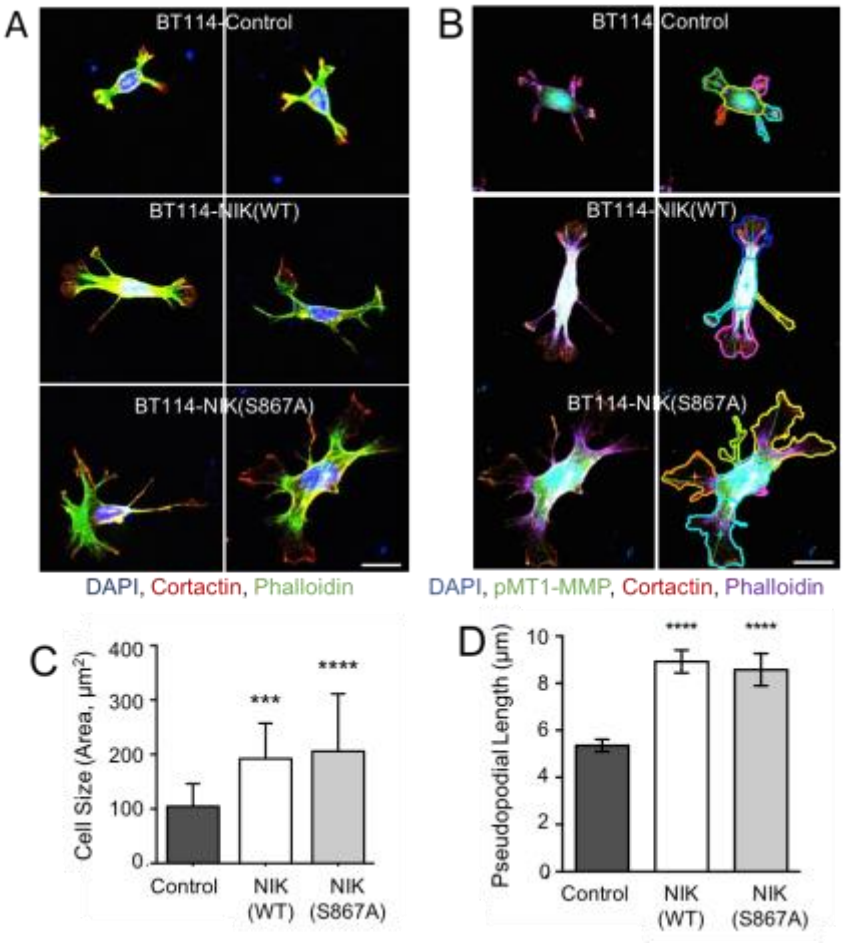

Figure 6. NIK enhances pseudopodia formation.
(A) BT114 -Control), -NIK(WT), or -NIK(S867A) cells were seeded onto collagen coated coverslips and fixed after 16 hours. Cells were stained with DAPI (blue), Alexa Fluor 488-phalloidin (green), and cortactin (red) and imaged using confocal microscopy. Images of representative cells are shown. Scale bar = 10 µm. **(B-D)** Quantification of cell size and pseudopodial length of BT114 cells in (A). At least 65 cells (Control, NIK(WT) or NIK(S867A)) from three independent staining experiments were used for the following blinded quantifications: **(B)** Cells were seeded onto collagen-coated coverslips and stained with DAPI (blue) and antibodies directed to pMT1-MMP (green), cortactin (red), and Alexa Fluor 647-phalloidin (Cy-5). Only single cells containing one nucleus and not in contact with another cell were used for quantifications. The average pseudopodial length was then quantified by drawing a line starting from the line tangent to the cell body, and extending to the furthest cortactin- pMT1-MMP-positive point of the protrusion. The average cell area was quantified by creating an ROI outlining the cell. At least 65 protrusions per treatment group were used for blinded quantifications. Scale bar=10 µm. **(C)** Average cell size (area, μm^2) ± SEM. Statistical significance was calculated with one-way ANOVA and Tukey's HSD post test. Multiplicity adjusted P-values: *** 0.0002 for Control vs. NIK(WT); **** <0.0001 for Control vs. NIK(S867A), **(D)** Average length (µm) of pseudopodial structures extended from the cell body ± SEM. Statistical significance was calculated with one-way ANOVA and Tukey's HSD post test. Multiplicity adjusted p-values: **** <0.0001 for Control vs. NIK(WT) and vs. NIK(S867A).

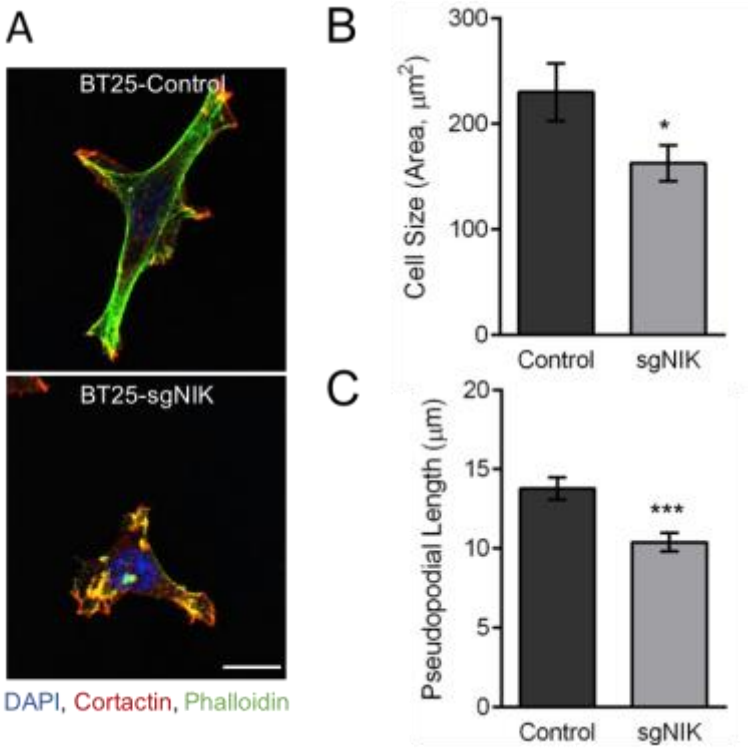

Figure 7. NIK silencing attenuates pseudopodia formation.
(A) BT25-Control or BT25-sgNIK cells were treated and imaged as described in (Figure 6A). Representative cells shown. Scale bar = 10 μm. 7B and C were quantified as described in Figure 6B. **(B)** Average cell size (area, μm^2) ± SEM for BT25-Control or BT25-sgNIK cells. Unpaired t-test P-value: *0.0330 for Control vs. sgNIK. **(C)** Average length (μm) of pseudopodial structures extended from the cell body ± SEM. Unpaired t-test P-value: *** <0.0002 for Control vs. sgNIK. At least 50 cells from three independent experiments were used for quantification (Figures 7B, 7C).

Conversely, we observed that BT25-sgNIK cells were smaller and less elongated compared with BT25 control cells (Figure 7A-C). These data establish a role for NIK in increasing the formation of pseudopodial membrane protrusions, cell size and cell elongation.

NIK increases MT1-MMP pseudopodial localization and enzymatic activity

The matrix-degrading enzyme, MT1-MMP (also known as MMP-14), is the predominant proteolytic component of invasive pseudopodia (98, 113, 114). Unlike soluble, secreted MMPs, cell surface localization of active, phosphorylated MT1-MMP (pMT1-MMP, Y573) is required for degradation of ECM proteins and tumor cell invasion (121, 122, 135-137). We therefore investigated whether NIK promoted pseudopodia formation through regulation of MT1-MMP. First, we noted a positive correlation between glioma invasion, NIK expression, MT1-MMP expression and MT1-MMP enzymatic activity in BT25 and BT114 cells (Figure 8). We previously demonstrated that MT1-MMP mRNA levels were not altered by TWEAK treatment (30). Consistent with this observation, we found that NIK(WT) does not significantly affect the expression of MT1-MMP at protein or mRNA level in BT114 cells (Figure 9A, B). MT1-MMP mRNA levels are unaltered in BT114-sgNIK cells irrespective of treatment with TWEAK (Figure 9C). The increase of MT1-MMP in BT114-NIK(S867A) cells compared with BT114-NIK(WT) cells is likely due to higher expression levels of transfected NIK in the former compared to the latter cells (Figure 9A, B). BT114-NIK(S867A) cells also show slightly increased levels of RelB, but total and phosphorylated (P536) p65 levels remain unchanged. However, BT114 cells overexpressing NIK(WT) and NIK(S867A) exhibit increased levels of pMT1-MMP (Figure 9A), suggesting a role for NIK in regulating MT1-MMP localization to invasive pseudopodia.

We next evaluated the effect of ectopic NIK expression on pMT1-MMP subcellular distribution. BT114-Control cells exhibit a punctate pMT1-MMP staining

pattern throughout pseudopodial structures at the cell periphery (Figure 10A). When to compared to these controls, BT114 cells expressing NIK(WT) or NIK(S867A) showed an increase in pMT1-MMP pseudopodial staining, with NIK(S867A) having a stronger effect than NIK(WT) (Figure 10A). Quantification of pMT1-MMP staining demonstrated that the percent of pMT1-MMP at the pseudopodia is significantly increased in NIK(WT)- and NIK(S867A)-expressing cells, and correlates with levels of NIK expression (Figure 10B). Volumetric views of these immunostaining experiments demonstrated that pMT1-MMP co-localizes with the pseudopodia marker cortactin (Figure 10C), which is required for pseudopodia assembly and maintenance (79). Consistent with these observations, we observed that MT1-MMP enzymatic activity is increased in cells expressing NIK(WT) or NIK(S867A) (Figure 10D). Loss of NIK in BT25-sgNIK cells did not affect expression of MT1-MMP mRNA or total protein, but did diminish levels of pMT1-MMP (Figure 11A and 4B). Furthermore, we also observed that pseudopodial localization of pMT1-MMP was significantly diminished in the absence of NIK (Figure 11C, D). Taken together, both gain-of-function and loss-of-function studies support a working model whereby NIK predominantly regulates MT1-MMP at the post-transcriptional level.

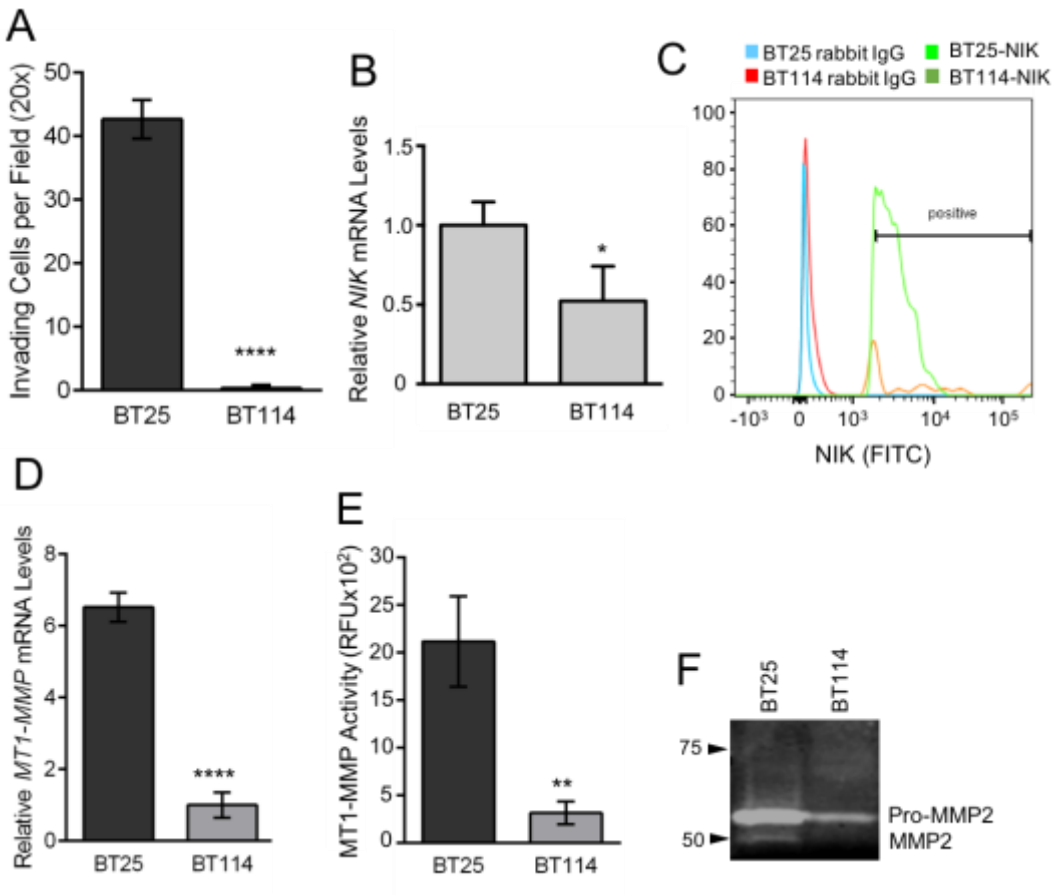

Figure 8. Glioma cell invasiveness correlates with MT1-MMP expression and activity.
BT25 and BT114 glioma cell lines were seeded onto collagen matrices and allowed to invade 24 hours. Cultures were fixed in 3% glutaraldehyde, stained with toluidine blue. **(A)** Invasion density was quantified as the average number of invading cells +SD in a 0.25 mm2 field. At least 4 wells were quantified per cell type for three independent experiments. Unpaired Student's test P-value ****p<0.0001. **(B)** Quantitative RT-PCR was performed to analyze *NIK* mRNA expression in BT25 and BT114 glioma cells. Graph shows fold change *NIK* expression relative to BT25 cells, averaged from triplicate wells from one representative experiment. Unpaired test P-values:*p=0.0351. **(C)** NIK protein expression in BT25 and BT114 cells was compared using flow cytometry with antibodies directed to NIK (Abcam, 7204) or isotype controls. **(D)** Quantitative RT-PCR was performed to analyze expression of *MT1-MMP* in BT25 and BT114 cells. Graph shows fold- change *MT1-MMP* expression relative to BT114 cells, averaged from triplicate wells from one representative experiment. Student's t-test P-value ****p<0.0001. **(E)** MT1-MMP activity was assayed using the Sensolyte 520-MMP-14 Assay kit (AnaSpec) with extracts made from the indicated cells after 8 hours of invasion and incubation with TIMP-1 conditioned media. Graph from one representative experiment (n=3) is depicted, showing average RFU (relative fluorescence units) from three replicates per cell type. Unpaired Student's t-test P-value **p=0.0031. **(F)** Gelatin zymogram was performed to evaluate matrix degradation by BT25 and BT114 cells.

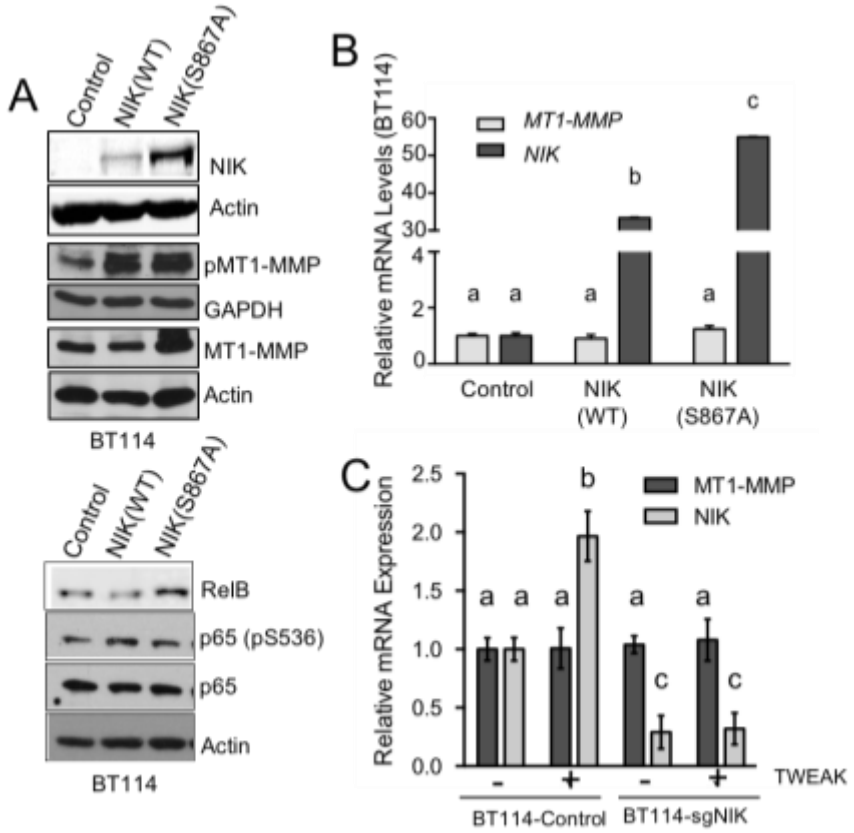

Figure 9. NIK increases MT1-MMP phosphorylation, but not mRNA expression.
(A) Representative western blot analysis (n=4) of BT114-Control, -NIK(WT) or -NIK(S867A) cells. Whole cell lysates were probed with indicated antibodies. **(B)** qPCR analysis was performed to analyze expression of *MT1-MMP* and *NIK* in BT114 cells expressing Control, NIK(WT) or NIK(S867A). Graph shows fold-change *MT1-MMP* and *NIK* expression relative to BT114-Control cells. Average gene expression was calculated from triplicate wells from a representative experiment that was repeated three times. *GAPDH* expression was used as endogenous control. Statistical analysis of gene expression data was calculated using 2-way ANOVA with Tukey's HSD post test. Different letters indicate statistically significant differences with multiplicity adjusted P-values < 0.0001 for all comparisons. **(C)** Quantitative RT-PCR analysis was performed to analyze expression of *MT1-MMP* and *NIK* in BT114-Control and BT114-sgNIK cell untreated or treated with TWEAK (10ng/ml) for 24 hours. Graph shows fold-change *MT1-MMP* and *NIK* expression relative to untreated BT114-Control cells from triplicate wells from one representative experiment that was repeated three times. *RPLP0* expression was used as endogenous control. Statistical analysis of gene expression data was calculated using 2-way ANOVA with Tukey's HSD post test. Different letters indicate statistically significant differences with multiplicity adjusted P-values: a vs. b and b vs. c < 0.0001; a vs. c = 0.0004.

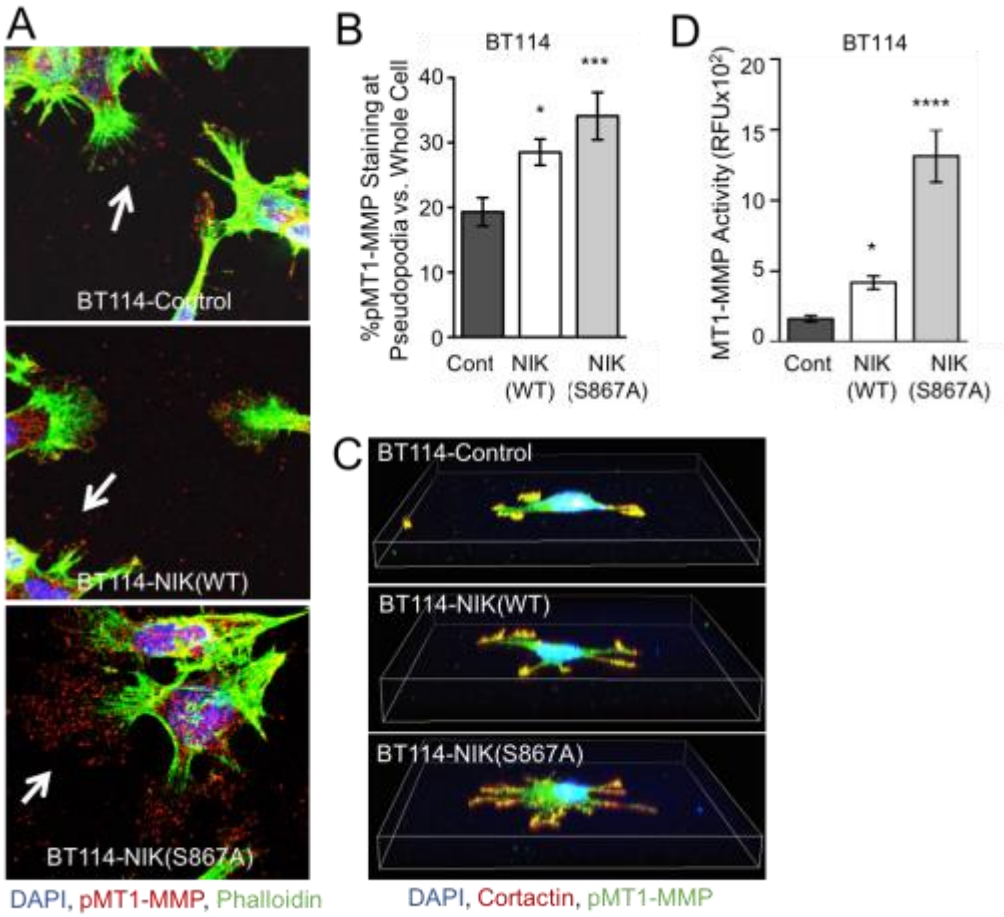

Figure 10. NIK increases MT1-MMP pseudopodial localization.
(A) BT114 cells expressing Control, NIK(WT) or NIK(S867A) grown on collagen-coated coverslips were stained with DAPI (blue), Alexa Fluor 488-phalloidin (green), and anti-pMT1-MMP (Y573) (red). Confocal microscopy was used to evaluate subcellular localization of pMT1-MMP. Images of representative cells from one of six experiments are shown. Arrows indicate pMT1-MMP localized to pseudopodia. **(B)** Quantification of pMT1-MMP staining that localized to pseudopodia was performed using images from obtained in (A) and normalized to total cellular pMT1-MMP staining: at least 30 cells from six different experiments were used for quantification. One-way ANOVA with Tukey's HSD post test multiplicity adjusted P-values: * 0.0394 Control vs. NIK(WT); *** 0.0009 Control vs. NIK(S867A). **(C)** Immunofluorescence staining of BT114 cells expressing Control, NIK(WT) or NIK(S867A) grown on collagen-coated coverslips was performed to demonstrate colocalization between pMT1-MMP and cortactin at pseudopodial structures. Cells were stained with DAPI (blue), pMT1-MMP (green), and cortactin (red), and imaged using confocal microscopy. Volumetric views of confocal Z-stacks were made using Nikon NIS Elements software and rotated to show 3D view of pseudopodia. **(D)** MT1-MMP activity was assayed in the indicated cells after 16 hours of invasion using the Sensolyte 520-MMP-14 Assay kit (AnaSpec) with modifications to specifically quantify MT1-MMP activity. Representative graph from three experiments depicts average RFU (relative fluorescence units) ± SD. One-way ANOVA with Holm-Sidak post test multiplicity adjusted P-values: * 0.0301 for NIK(WT) vs. Control; **** <0.0001 for NIK(S867A) vs. Control.

To test the hypothesis that NIK enhances MT1-MMP activity post-transcriptionally, we used a heterologous assay involving ectopic co-expression of NIK(S867A) and MT1-MMP in HEK293FT cells. Control HEK293FT cells (vector only) lack MT1-MMP, exhibit low MT1-MMP activity and do not invade collagen (Figure 12A, B, D, E). Ectopic expression of NIK(S867A) alone in HEK293FT cells does not increase endogenous MT1-MMP protein, mRNA or enzymatic activity (Figure 12A, B, C), and does not enhance the invasive potential of these cells (Figure 12D, E). While ectopic expression of a CMV-driven MT1-MMP promotes HEK293FT cell invasion as previously reported (138), co-expression of NIK and CMV-MT1-MMP significantly increased HEK293FT cell invasion (see side-view images of collagen matrices and quantification of invasion cell densities; Figure 12D, E). Consistent with increased cell invasion, we observed that HEK293FT cells co-expressing NIK and MT1-MMP have increased MT1-MMP enzymatic activity compared with expression of MT1-MMP alone (Figure 12B). These data demonstrate that NIK can enhance MT1-MMP enzymatic activity and localization within pseudopodia without increasing MT1-MMP expression.

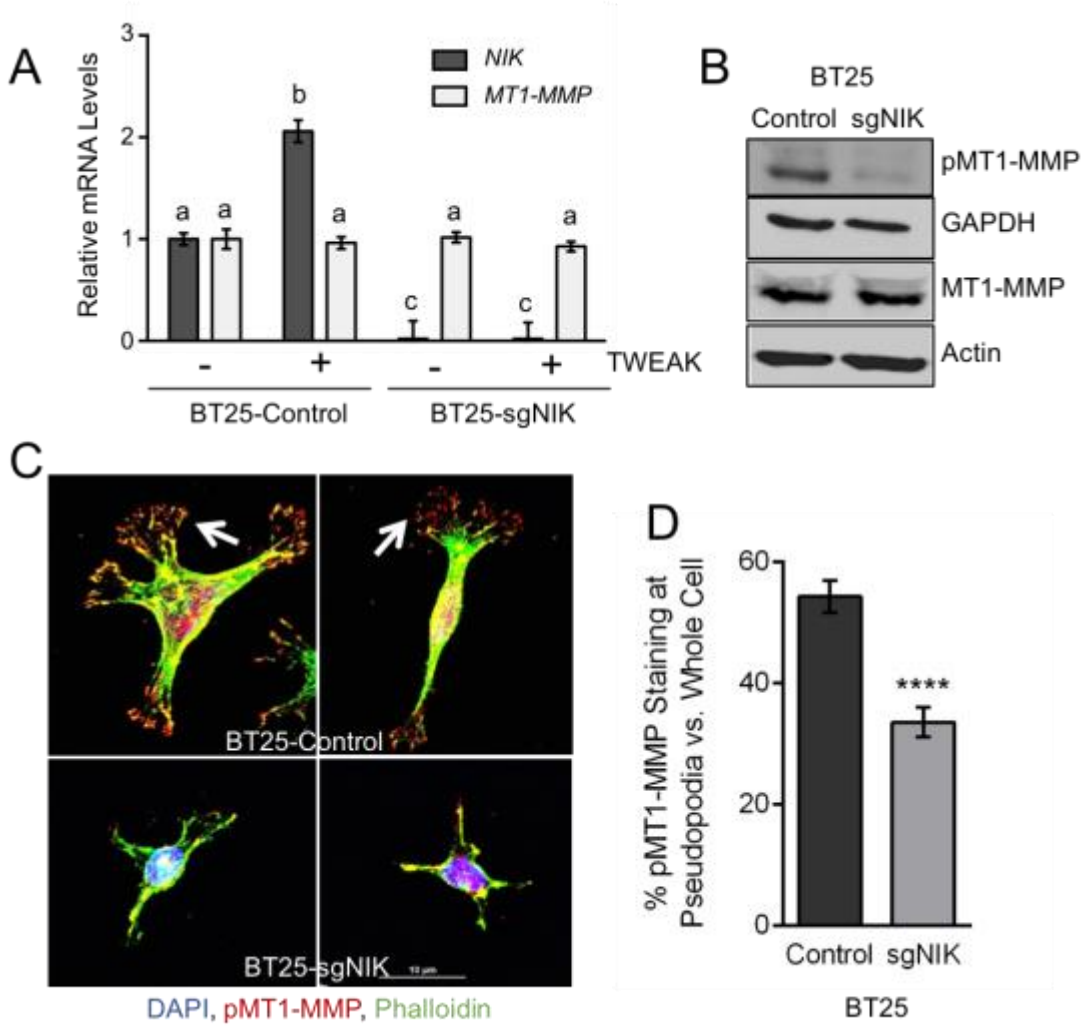

Figure 11. Loss of NIK decreases invasion and results in loss of pseudopodial pMT1-MMP localization.

(A) qPCR analysis of *NIK* and *MT1-MMP* mRNA expression in BT25-Control and BT25-sgNIK cells that were untreated or treated with TWEAK for 24 hours. Graph shows data from triplicate wells from one representative experiment that was repeated three times. *GAPDH* expression was used as endogenous control. Statistical analysis of gene expression data was calculated using 2-way ANOVA with Tukey's HSD post test. Different letters indicate statistically significant differences with the following multiplicity adjusted P-values: $p<0.0001$ for "a vs. b"; $p=.001$ for "a vs. c". **(B)** Representative western blot analysis of pMT1-MMP (Y573) and MT1-MMP expression in BT25-Control and BT25-sgNIK cells. Whole cell lysates were probed with the indicated antibodies. **(C)** BT25-Control and BT25-sgNIK cells grown on collagen-coated coverslips were stained with DAPI (blue), Alexa Fluor 488-phalloidin (green), and anti-pMT1-MMP (Y573) (red). Confocal microscopy was used to evaluate subcellular localization of pMT1-MMP. Images of representative cells from one of three experiments are shown. Arrows indicate pMT1-MMP localized to pseudopodia. Scale bar = 10 μm. **(D)** Quantification of pMT1-MMP staining that localized to pseudopodia was performed using images obtained in (C) and normalized to total cellular pMT1-MMP staining: BT25-Control (n= 30 cells) and BT25-sgNIK (n=30 cells). Cells from three different experiments were used for quantification. Unpaired Student's test P-value ****$p<0.0001$.

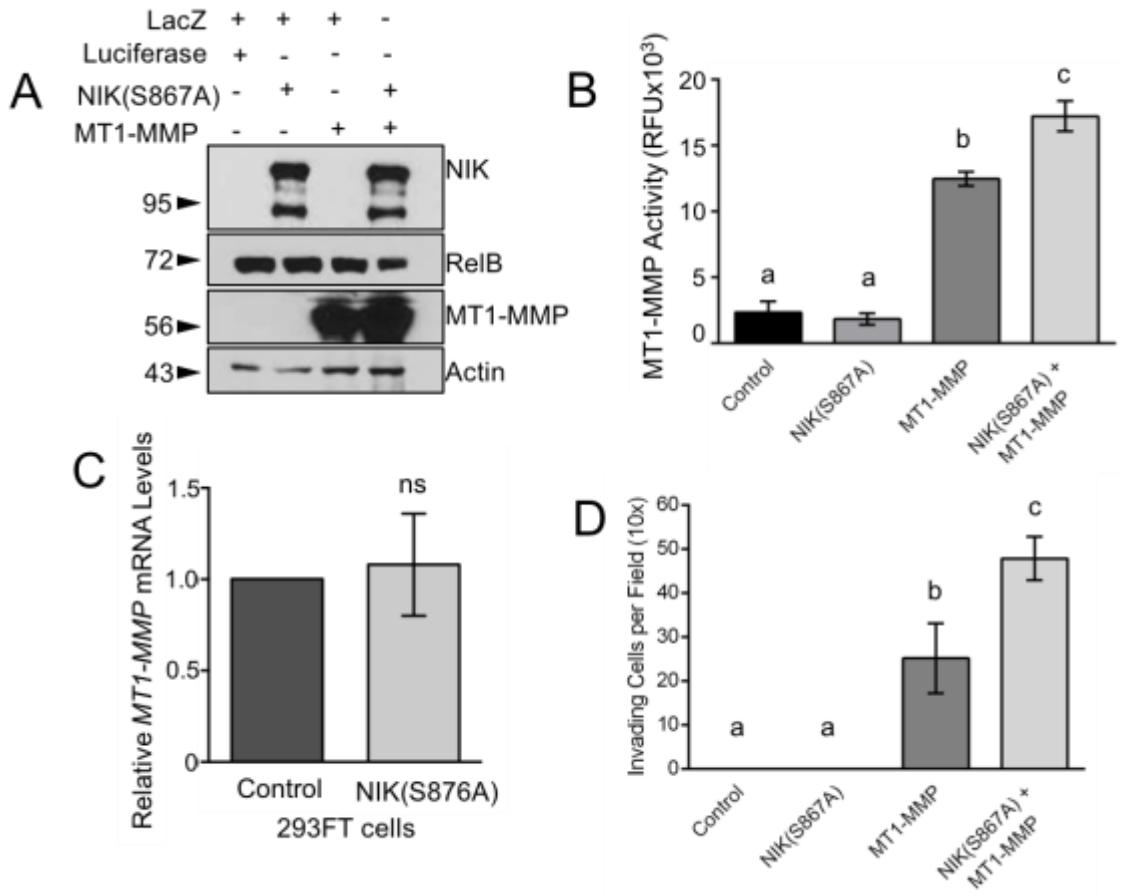

Figure 12. NIK increases MT1-MMP activity and invasion in a heterologous HEK293FT system. HEK293FT cells were transfected to express LacZ and Luciferase, LacZ and NIK(S867A), LacZ and MT1-MMP, or NIK(S867A) and MT1-MMP. **(A)** Whole cell lysates were probed with antibodies directed against NIK, RelB, MT1-MMP and Actin using western blotting. **(B)** MT1-MMP activity assays were performed as described in Figure 3E, using lysates made from HEK293FT cells after 24 hours of invasion. RFU= relative fluorescence units. One-way ANOVA with Tukey's HSD post test was used for statistical analysis. Different letters indicate statistical significance. Multiplicity adjusted P-value <0.0001 for all comparisons. **(C)** Quantitative RT-PCR was performed to analyze *MT1-MMP* mRNA expression in 293FT cells transfected to express luciferase (Control) or NIK(S867A). Graph shows fold change *MT1-MMP* expression relative to 293FT cells expressing Luciferase (Control), averaged from triplicate wells from one representative experiment. Unpaired Student's t-test P-values = 0.6453 (ns). **(D)** Quantification of average number of invading cells per field ± SD. At least 4 wells were quantified per cell type for three independent experiments. A representative graph is shown. Significance was calculated using one-way ANOVA with Tukey's HSD test and letters indicate statistically significant differences. Multiplicity adjusted P-values: p <0.0001 for all comparisons. **(E)** Invasion assays were fixed with 4% paraformaldehyde, stained with Alexa Fluor 488-phalloidin (green) and DAPI (blue) and imaged using confocal microscopy. Z-stacks were compressed and rotated to demonstrate side-view of invasion.

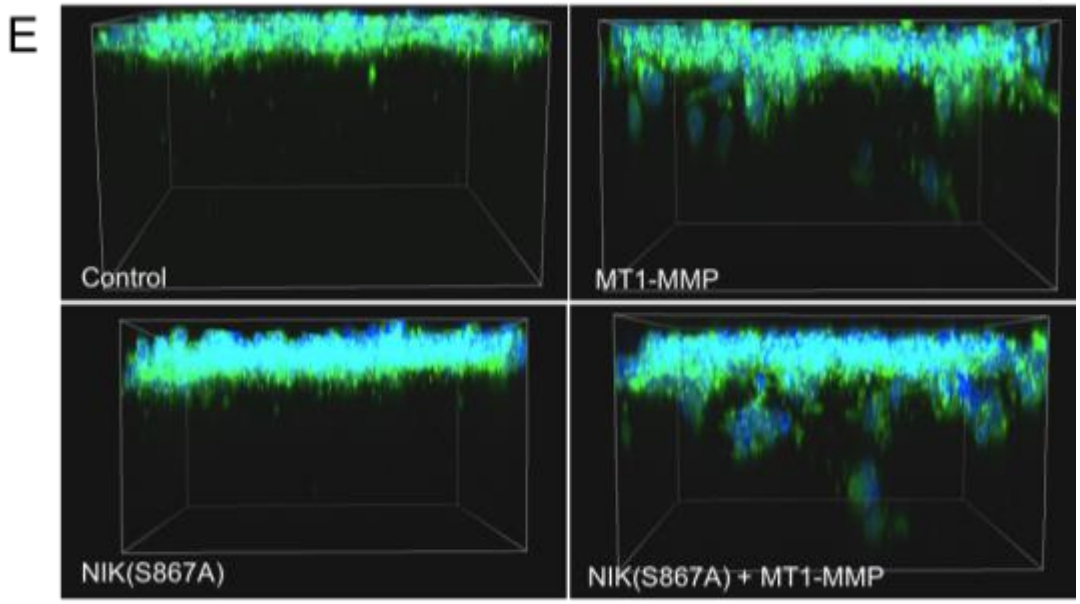

Figure 12. Continued.

TWEAK and NIK promote invasion and increase pseudopodial pMT1-MMP localization independently of the canonical NF-κB pathway

NIK is required for activation of noncanonical NF-κB transcription factors, but can also regulate canonical NF-κB proteins (p65- and cRel) (26, 139, 140). Since RelA/p65 was previously reported to regulate expression of MT1-MMP (124, 125), we sought to determine whether TWEAK- or NIK- induced invasion and regulation of pMT1-MMP required canonical NF-κB signaling. We first noted that neither NIK(WT) or NIK(S867A) affected p65 phosphorylation (pS536), a marker of p65 transcriptional activation (141) (see Figure 9A). Moreover, neither TWEAK treatment nor NIK expression significantly affected p65 nuclear translocation(30) (Figure 13), suggesting that NIK does not significantly enhance p65 activity in these cells.

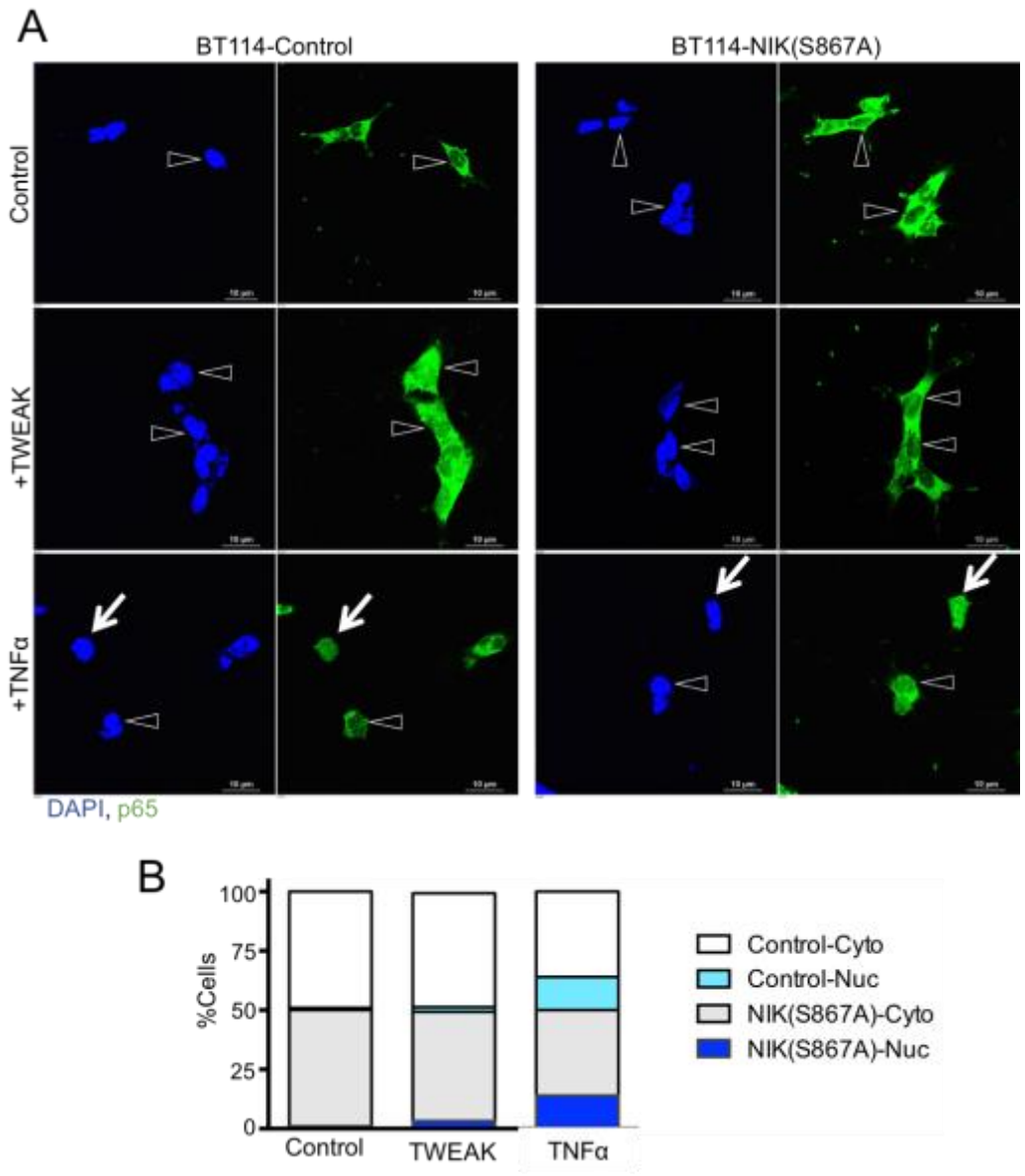

Figure 13. NIK expression or TWEAK treatment does not induce canonical NF-κB.
BT114 cells expressing Vector (Control) or NIK(S867A) seeded onto collagen- coated coverslips were treated with nothing (Control), 10 ng/ml TWEAK for 4 hours or 20 ng/ml TNFα for 30 minutes, as a control to demonstrate p65 movement to nucleus, before fixing with 4% paraformaldehyde. **(A)** Coverslips were immunostained with antisera directed to p65 (green), stained with DAPI (blue) to visualize nuclei, and imaged using confocal microscopy. Arrowheads indicate p65-negative nuclei. Arrows indicate p65-positive nuclei. Scale bars = 10 μm. **(B)** 50 cells per treatment per experiment (n=3) were examined for the percentage of p65 localization to the nucleus (Nuc) or cytoplasm (Cyto). A representative experiment is shown.

To test the effects of TWEAK and NIK on invasion in the absence of specific NF-κB proteins (Figure 14A-C), we exploited the ability of mouse embryonic fibroblasts (MEFs) to invade collagen in an MMP-dependent manner (Figure 14D). MEFs derived from homozygous *p65*$^{-/-}$ or *p65*$^{-/-}$*;cRel*$^{-/-}$ mice showed significantly reduced invasion compared to their corresponding pooled wild-type MEFs, while *RelB*$^{-/-}$MEFs invasion was almost completely abrogated (Figure 14E). TWEAK treatment significantly enhanced invasion in all MEFs, with the exception of *RelB*$^{-/-}$ MEFs (Figure 14E, F). Notably, TWEAK-enhanced invasion of *p65*$^{-/-}$ MEFs was accompanied by a significant increase of pMT1-MMP located within pseudopodia (Figure 15A, B).

We explored the invasion potential of *NIK*$^{-/-}$ MEFs and their corresponding *NIK*$^{+/+}$ wild-type controls (142). In contrast to the wild-type control MEFs of NF-κB mutant strains (see above), *NIK*$^{+/+}$ MEFs were only minimally invasive in 3-D collagen matrices, as were *NIK*$^{-/-}$ MEFs (Figure 15C). We speculate that the variability in WT MEF invasion may be due to different genetic backgrounds of mice from which the MEFs were isolated. Regardless, the *NIK*$^{+/+}$ MEFs exhibited robust TWEAK-induced invasion, which was significantly impaired in *NIK*$^{-/-}$ MEFs (Figure 15C). Moreover, we also observed decreased pseudopodial localization of pMT1-MMP in *NIK*$^{-/-}$ MEFs compared with *NIK*$^{+/+}$ MEFs (Figure 15D, E).

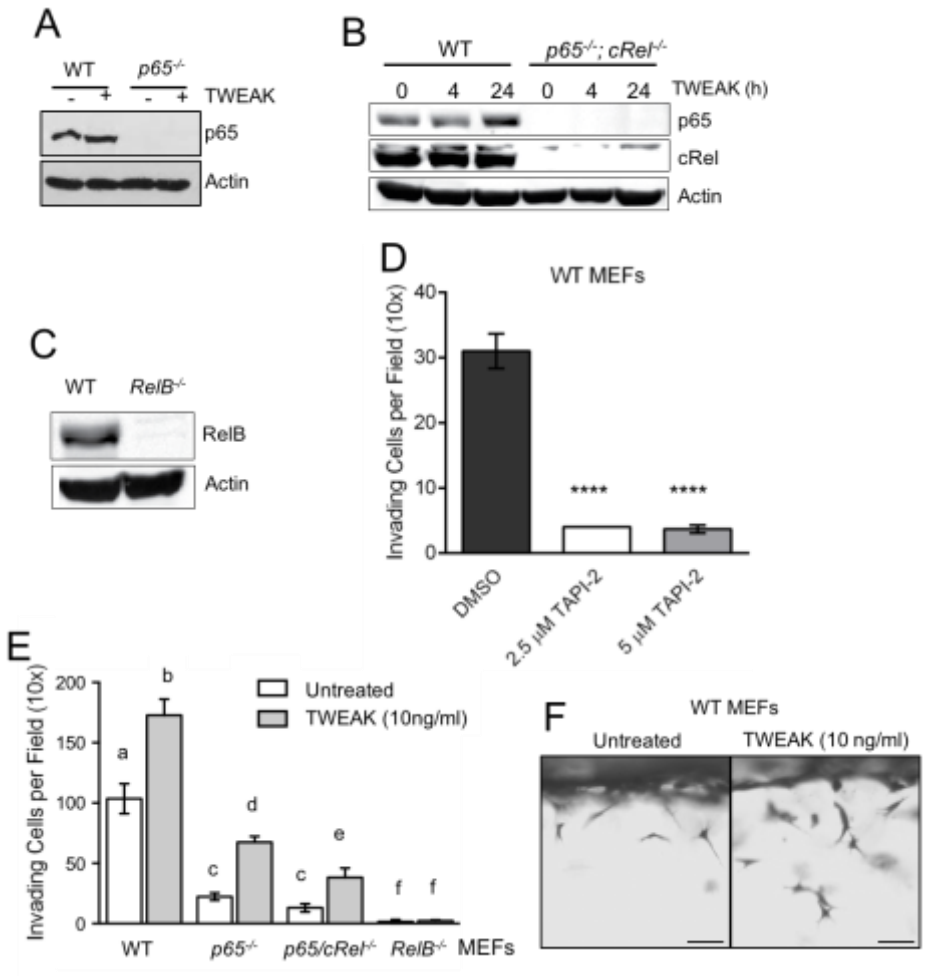

Figure 14. MEF invasion is MMP dependent and MT1-MMP expression and localization to pseudopodia increases with TWEAK treatment.

(A) Western blot analysis confirms loss of p65 in null MEFs ± TWEAK treatment (10ng/ml for 24 hours) using indicated antibodies. **(B)** WT and *p65*$^{-/-}$*; cRel*$^{-/-}$ MEFs were treated with 10 ng/ml TWEAK for indicated times. Western blot analysis confirms loss of NF-□B proteins, p65 and cRel in null MEFs, using indicated antibodies (cRel: Cell Signaling Technology, CST4727). **(C)** Western blot analysis confirms loss of RelB in null MEFs, using indicated antibodies. **(D)** Average invasion density quantification ± SD using WT MEFs treated with vehicle control (DMSO) or the MMP inhibitor TAPI-2 (2.5 or 5 μM) before seeding onto 3D collagen matrices. Four wells were quantified per experiment for three independent experiments. Statistical significance was calculated with one way ANOVA with Dunnett's multiple comparisons test where ****p<0.0001 for 2.5 and 5 μM TAPI-2 vs. DMSO. **(E)** WT mouse embryonic fibroblasts (MEFs) and NF-κB null MEFs were allowed to invade collagen matrices ± 10 ng/ml TWEAK. WT represents pooled invasion data from *p65*$^{+/+}$, *p65/cRel*$^{+/+}$ and *RelB*$^{+/+}$ MEFs (± TWEAK). Three independent experiments were performed counting three invading wells per treatment. Differences between untreated and TWEAK treated samples of a given genotype, as well as differences among untreated or TWEAK treated cells of different genotypes were analyzed using 2-way ANOVA with Tukey's HSD post test. Statistically significant differences are indicated by different letters. Multiplicity adjusted P-values: ****<0.0001 between all letters, except ***<.001 for "c vs. e" and *<0.01 for "c vs. f." **(F)** Untreated or TWEAK-treated WT MEFs were seeded onto collagen matrices and allowed to invade 24 hours. Side view images of invasion are shown. Scale bar

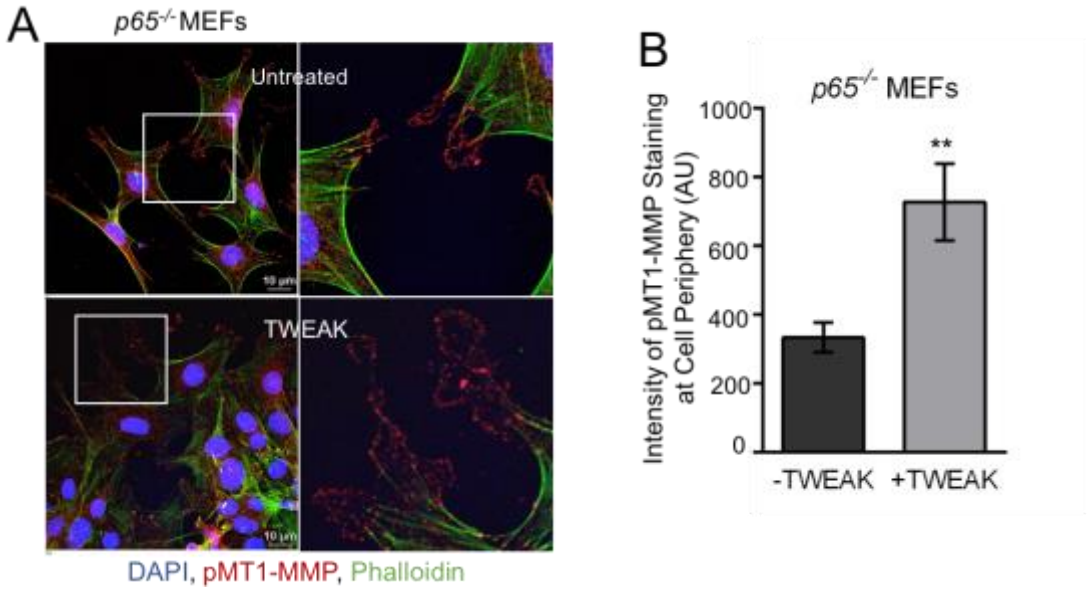

Figure 15. Loss of NIK in MEFs abrogates surface localization of pMT1-MMP in response to TWEAK.

(A) *p65*$^{-/-}$ MEFs were seeded onto collagen coated coverslips and treated with or without (Untreated) 10 ng/ml TWEAK for 4 hours. Cells were fixed and stained with anti-pMT1-MMP (red), Alexa Fluor 488-phalloidin (green), and DAPI (blue), and imaged using confocal microscopy. Scale bar = 10 μm. Right panels show the zoomed portion of the boxed image on the left. Images of representative cells from one of three experiments are shown. **(B)** Blinded quantification of pMT1-MMP intensity beyond actin-rich protrusions expressed in arbitrary units (AU) ± SEM of images of *p65-/-* MEFs ± TWEAK (10ng/ml). At least 30 cells per treatment from three independent experiments were used for quantifications. **p<0.01 using unpaired Student's *t*-test. **(C)** Invasion density of WT *NIK-/-* MEFs, untreated or treated with TWEAK (10 ng/ml) and allowed to invade 3D collagen matrices for 48 hours. Three wells were quantified per treatment in three independent experiments. Graph depicts one representative experiment. Statistical analysis of invasion data was calculated using 2-way ANOVA. Different letters indicate statistically significant differences with multiplicity adjusted P- value of p<0.0001 for all comparisons. **(D)** WT and *NIK-/-*MEFs were seeded onto collagen coated coverslips, and treated and stained with anti-pMT1-MMP antibody (red), Alexa Fluor 488-phalloidin (green), and DAPI (blue), and imaged using confocal microscopy. Scale bar = 10 μm. **(E)** Intensity of pMT1-MMP staining beyond actin-rich protrusions expressed in arbitrary units (AU) ± SEM of images from Figure 15D of WT and *NIK-/-* MEFs untreated or treated with 10ng/ml TWEAK. Statistical significance was calculated using 2-way ANOVA with Tukey's HSD post test. Statistically significant differences are indicated by different letters. Multiplicity adjusted P-values: <0.0001 for "a vs. b." **(F)** WT and *NIK-/-* MEFs were treated with or without MG132 (5 μM) for 1 hour to prevent NIK degradation and then untreated, or treated with TWEAK (10 ng/ml), as indicated for 5 hours. Western blot analysis using indicated antibodies confirms loss of NIK protein in *NIK-/-* MEFs.

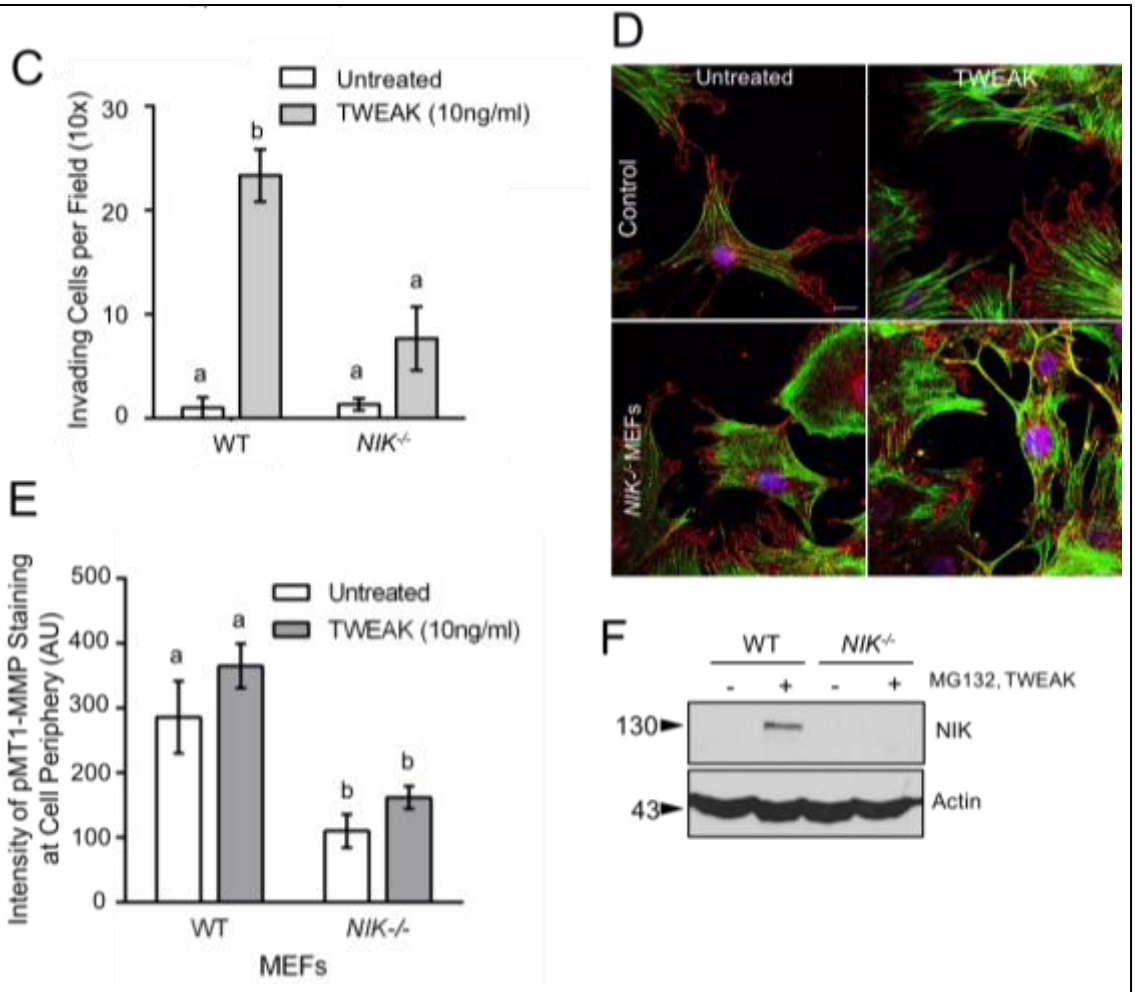

Figure 15. Continued.

Next, we tested whether NIK is sufficient to promote MEF invasion in the absence of canonical NF-κB proteins. Expression of NIK(WT) in *p65*$^{-/-}$*;cRel*$^{-/-}$ MEFs increased invasion (Figure 16A) and pseudopodial localization of pMT1-MMP (Figure 16B). Moreover, expression of NIK(WT) did not significantly alter expression of MT1-MMP (Figure 16C), consistent with our results in BT114 cells (Figure 9B). Together, these

results demonstrate that TWEAK and NIK promote invasion and pMT1-MMP localization within pseudopodia, independently of the canonical NF-κB pathway.

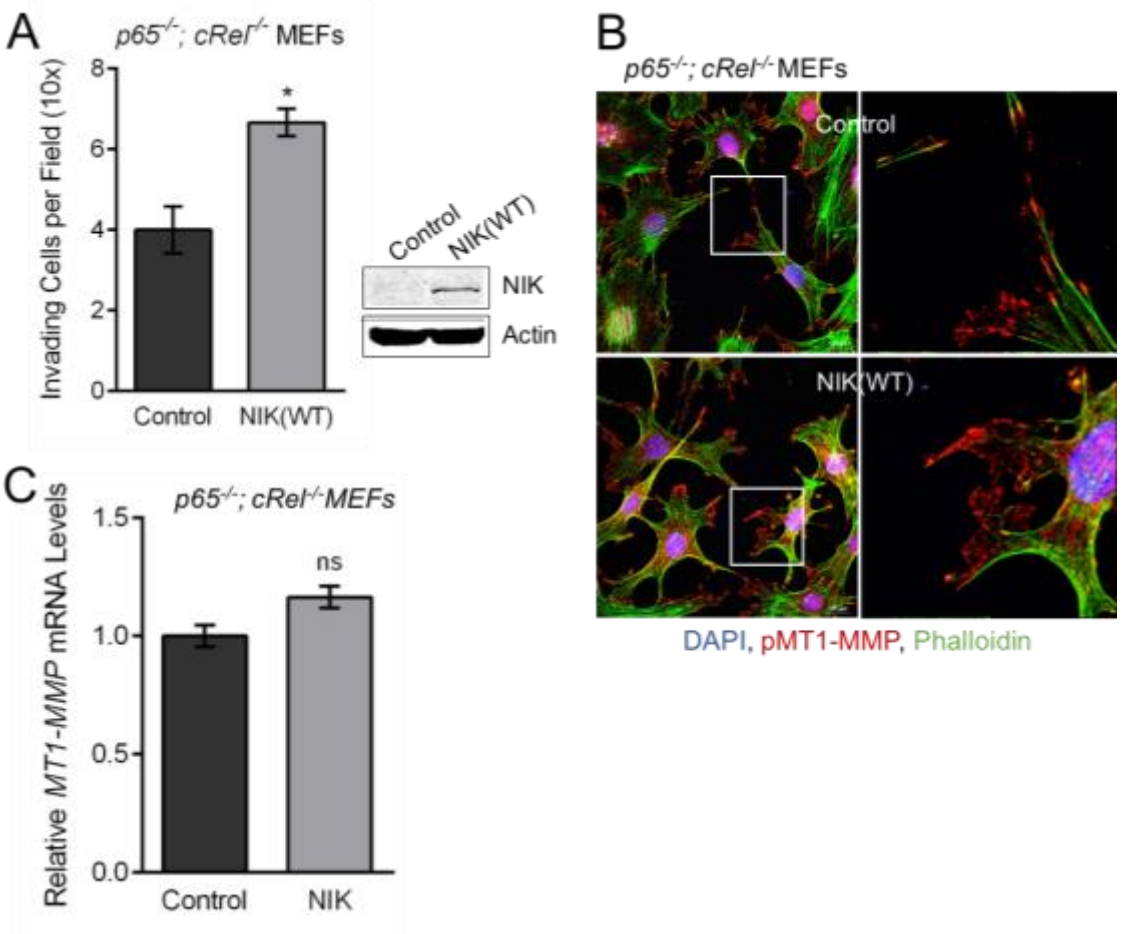

Figure 16. TWEAK increases invasion and pMT1-MMP pseudopodia localization in the absence of canonical NF-κB p65/cRel proteins.
(A) Invasion density of *p65*$^{-/-}$*;cRel*$^{-/-}$ knockout MEFs transduced to express vector (Control) or NIK(WT). At least four wells were quantified per treatment for three independent experiments. Graph depicts one representative experiment. Unpaired t-test P-value: *0.01. Panel shows western blot analysis of *p65*$^{-/-}$*;cRel*$^{-/-}$ knockout MEFs expressing vector (Control) or NIK(WT) confirming exogenous NIK expression. **(B)** *p65*$^{-/-}$*;cRel*$^{-/-}$MEFs were seeded onto collagen coated coverslips, and treated and immunostained as described in Figure 15A. Scale bar = 10 μm. **(C)** Quantitative RT-PCR was performed to analyze MT1-MMP expression in *p65-/-;cRel-/-* MEFs expressing vector alone (Control) or NIK. *GAPDH* expression was used as endogenous control. Gene expression data was averaged from triplicate wells from one representative experiment of three total experiments. Unpaired Student's t-test P-values = 0.0654 (ns).

NIK expression is associated with increased pMT1-MMP in orthotopic xenograft tumors

We previously demonstrated that BT114-NIK cells formed larger tumors *in vivo*, compared with BT114-Control cells (30). We used tumor tissue from these animals for immunohistochemical analyses. Immunofluorescence staining verified increased NIK expression in BT114-NIK tumors compared with BT114-Control tumors (Figure 17A, B).

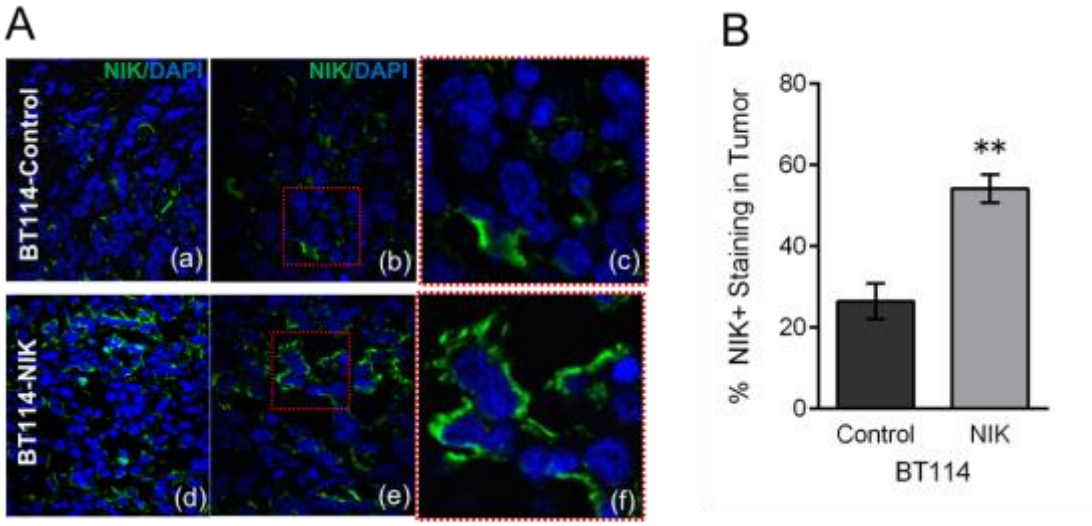

Figure 17. NIK increases tumor growth and pMT1-MMP *in vivo*.
(A) Tumor sections derived from BT114-Control (n=3) or BT114-NIK (n=3) xenograft tumors were stained with DAPI (blue) and anti-NIK (green), and imaged using confocal microscopy. Scale bars=20μm (panels a, d) and 50μm (panels b, e). Red outlined boxes are in panels b and e are magnified in panels c and f, respectively. **(B)** Graph shows percent NIK expression in tumors quantified from five sections of each tumor using Image J software analysis. **p=0.0011 vs. BT114-Control using unpaired Student's *t*-test. **(C, D)** Immunohistochemical diaminobenzidine (DAB) staining (brown) of sections from BT114-Control **(C)** or BT114-NIK **(D)** tumors with anti-pMT1-MMP (Y573) antibody. The portion of the image marked with a red dotted square is shown as a zoomed image on the right. Sections from non-injected brain region are shown as a negative control. Scale bar = 50 μm. **(E)** Graph shows quantification of pMT1-MMP staining (Figure 17C-D) from 5 sections of tumors derived from BT114-Control or BT114-NIK cells using IHC profiler (143) to measure positive pixel counts for DAB staining; ± SEM **p=0.0014 vs. BT114-Control using unpaired Student's *t*-test.

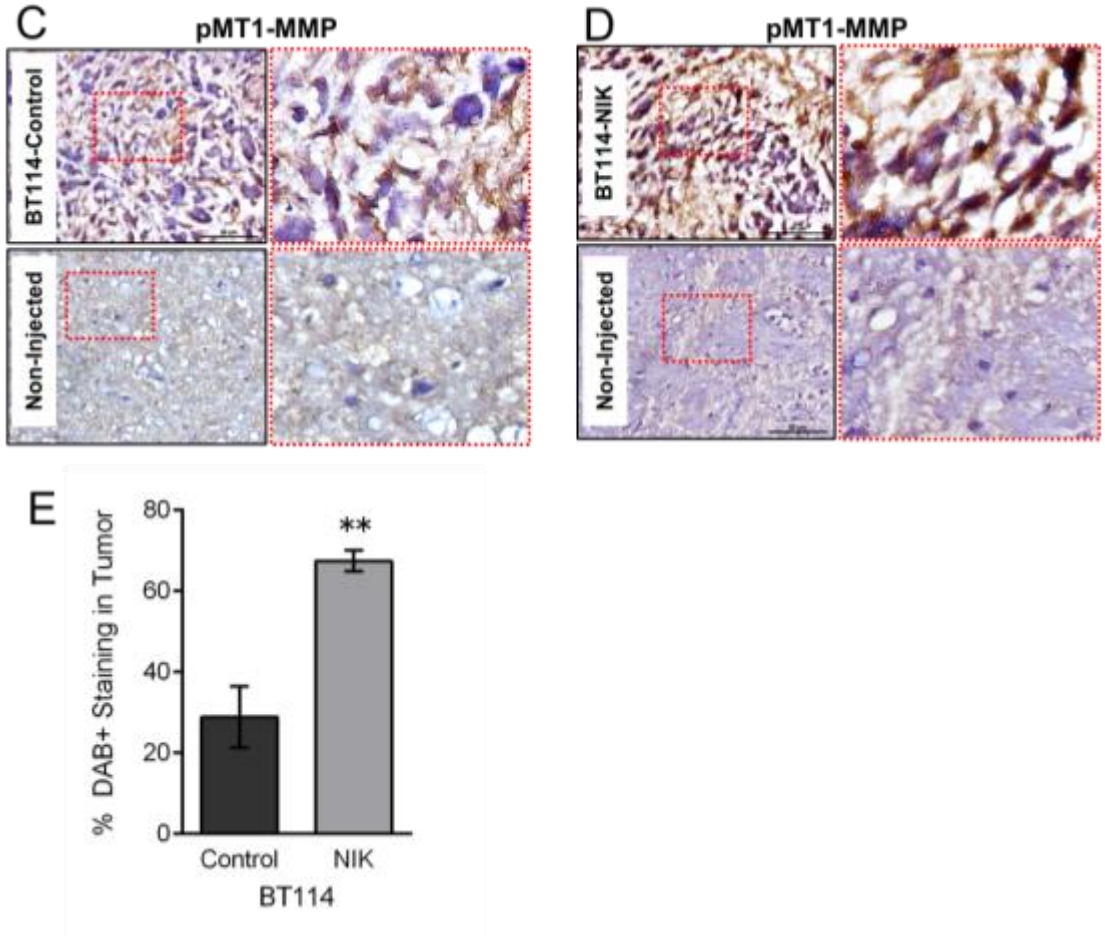

Figure 17. Continued.

Adjacent tumor sections were used for immunohistochemical staining, which revealed increased expression of pMT1-MMP in BT114-NIK tumors, compared to BT114-Control tumors (Figure 17C-E). As a control, we examined pMT1-MMP staining in sections from the non-injected brain hemisphere without tumor growth (Figure 17C, D; bottom panels) (143). These data demonstrate that increased NIK expression in tumors increases levels of pMT1-MMP, which is associated with increased tumor spreading.

NIK and MT1-MMP expression in human glioma correlates with poor survival

To investigate the significance of NIK and MT1-MMP in human tumors, we examined their expression ex-vivo in human glioma tissue. Results from these experiments revealed co-expression of NIK and pMT1-MMP in three patient-derived tumor samples (Figure 18A). To determine whether the observed co-expression of NIK and MT1-MMP is relevant for disease pathogenesis, we analyzed NIK and MT1-MMP expression in TCGA datasets through the cBioPortal Cancer Genome for Cancer Genomics (131, 132). Kaplan-Meier plots reveal that increased NIK and MT1-MMP mRNA expression correlates with poor survival of glioblastoma (GBM) patients (Figure 18B, C). The mean survival of GBM patients with increased NIK and MT1-MMP expression (5% of cases) is 10.6 months compared with 14.1 months for patients with unaltered expression (Figure 18C). In lower grade glioma (LGG), the correlation between high NIK and MT1-MMP expression (12% of cases) and poor patient survival was even higher (Figure 18D), suggesting that high NIK and MT1-MMP expression is a prognostic indicator for LGGs that are likely to progress to more aggressive tumors. Furthermore, the time to disease progression for LGG patients with high NIK and MT1-MMP expression is significantly shorter and is reflected by a higher rate of relapse (Figure 18E). Collectively, these results demonstrate a strong correlation between NIK and MT1-MMP expression levels and glioma pathogenesis.

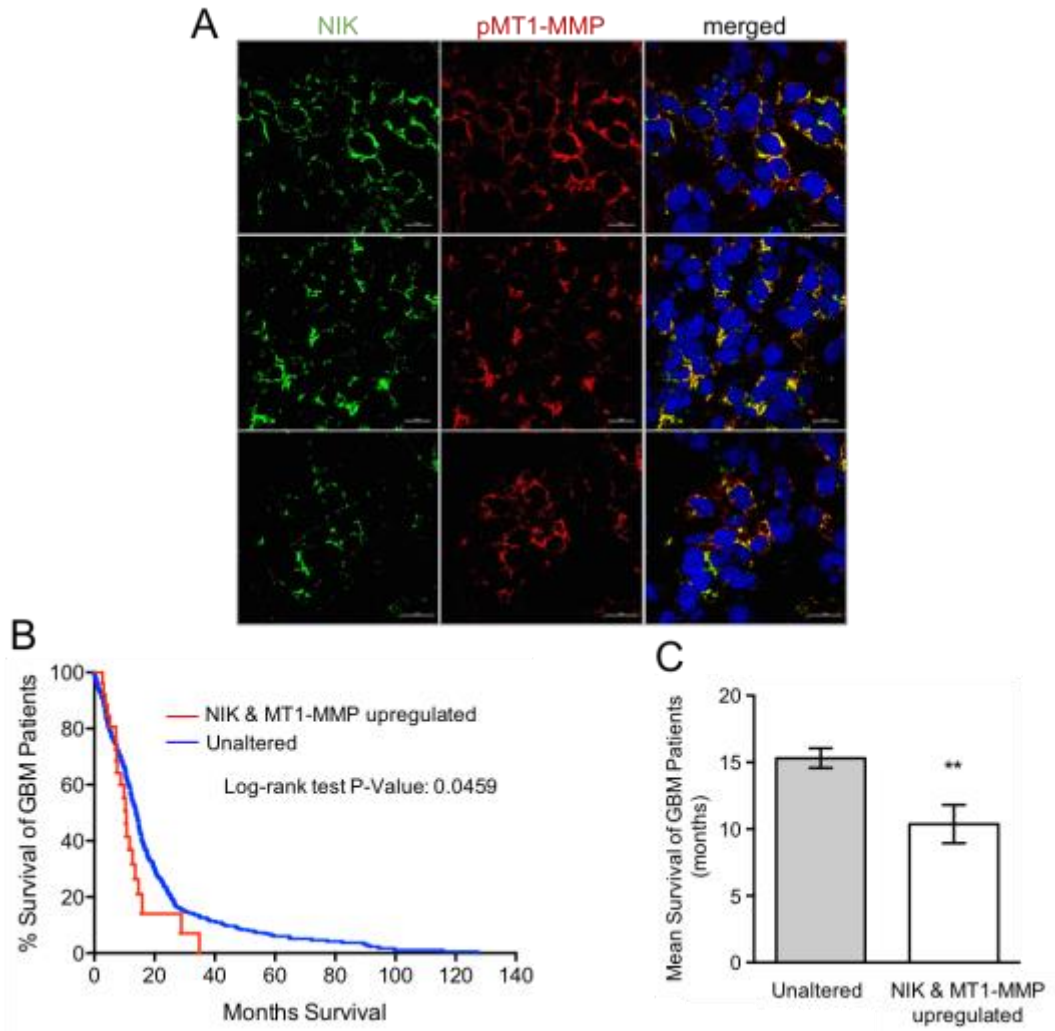

Figure 18. NIK and MT1-MMP are co-expressed in human glioma and correlate with poor patient survival.

(A) Sections of human glioma ex-vivo biopsy tissue were stained with antibodies specific for pMT1-MMP (Y573) (red) and NIK (pre-conjugated with AF488; green). Representative images are shown from three tumors. **(B)** Kaplan-Meier curve representing TCGA patient survival data from glioblastoma (GBM) patients with upregulated NIK (MAP3K14) and MT1-MMP (MMP14) mRNA expression. Data was downloaded from cBioPortal for Cancer Genomics TGCA, Cell 2013 dataset (10). Log-rank Mantel-Cox test indicates statistical significance with p=0.0459. **(C)** Mean survival (months) of GBM patients with unaltered (n=509) or upregulated NIK and MT1-MMP expression (n=27). Unpaired Welch t-test indicates statistical significance with ** p=0.0038. **(D)** Kaplan-Meier curve representing TCGA patient survival data from lower grade glioma (LGG) patients with upregulated NIK and MT1-MMP mRNA expression (LGG Provisional raw data at the NCI). Log-rank Mantel-Cox test indicates statistical significance with $p=5.42e^{-5}$. **(E)** Kaplan Meier curve representing disease-free time for LGG patients with upregulated NIK and MT1-MMP. Log-rank Mantel-Cox test indicates statistical significance with p=0.0202.

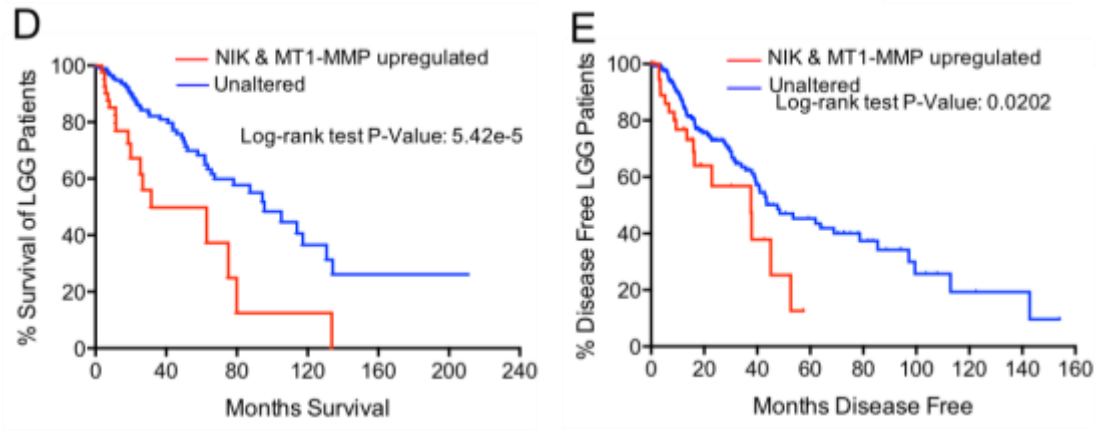

Figure 18. Continued.

DISCUSSION

Aberrant activation of NIK has been shown to have oncogenic roles in several cancers, including melanoma, ovarian cancer, and multiple myeloma (27, 144, 145), primarily through regulation of proliferation and cell survival (139, 145, 146). However, the role of NIK in CNS tumor pathogenesis, and particularly in tumor cell invasion, has not been clearly established. Here, we demonstrate that NIK plays a critical role in regulating MT1-MMP phosphorylation, pseudopodial localization and enzymatic activity to drive cell invasion. Our data suggest that NIK regulates MT1-MMP activity through a mechanism that is both post-transcriptional and indirect. A post-transcriptional process is indicated since we observed that NIK increases MT1-MMP phosphorylation and activity, but does not affect MT1-MMP mRNA expression (Figures 9B, 11A). Since phosphorylation of Y573 is the critical step in enhancing movement of MT1-MMP to the cell surface (122), and NIK is a serine-threonine kinase, we speculate that NIK-induced

MT1-MMP phosphorylation is indirect. However, we cannot rule out the possibility that NIK phosphorylates MT1-MMP at either the T567(147) or S577 residues within the cytoplasmic tail, which may, in turn, regulate Y573 phosphorylation. Alternatively, NIK may regulate MT1-MMP at the step of furin cleavage[19, 20]. Collectively, this study is the first to demonstrate that NIK expression promotes tumor cell invasion by regulating MT1-MMP at the post-transcriptional level.

We demonstrate a strong correlation between cell invasion and expression of NIK at the protein and mRNA levels (Figures 1, 2). This correlation is consistent with analyses of both low and high grade glioma databases, indicating that increased expression of NIK and MT1-MMP is associated with poor patient survival (Figure 18). Therefore, high NIK and MT1-MMP co-expression may be key prognostic indicators, not only for high-grade gliomas, but also for lower grade gliomas that are likely to progress to more aggressive, therapy-resistant tumors. In support of this hypothesis, NIK was recently identified in an analysis of protein interaction networks associated with glioma chemoresistance (148).

Our study is the first to link expression of NIK to pro-invasive cell shape phenotypes (Figure 6, 7), which play a central role in driving cancer cell dissemination through healthy tissue (91). NIK expression significantly enhances pMT1-MMP localization within pseudopodia, to promote increased invasion of 3D matrices (Figures 10, 11, 15, 16). The expansion of pseudopodia length in 2D coupled with increased invasion responses in 3D matrices suggest that NIK may enhance or stimulate the transition from invadopodia to pseudopodia (149, 150), which is critical for cell invasion (91). Interestingly, differences in cell shape were recently shown to influence the extent

of canonical NF-κB activation (151). Although NIK does not require RelA/p65 to promote cell invasion and localization of pMT1-MMP to pseudopodia (Figure 15, 16), NIK may be part of a feedback mechanism that tunes the levels of canonical NF-κB activation through regulation of cell shape.

Current therapeutic strategies for targeting NF-κB signaling in high-grade glioma, as well as other tumors, focus on inhibition of the canonical/p65-mediated pathway (152), which has well-established tumor-promoting functions (153, 154). Here, we have established new roles for NIK in regulating MT1-MMP activity and tumor cell invasion that are independent of RelA/p65, underscoring the importance of developing treatment strategies that target both the canonical and noncanonical NF-κB pathways. Indeed, since invadopodia and pseudopodia formation drive dissemination and metastasis of several cancers (91), inhibition of NIK may be an efficacious therapeutic approach in many invasive tumor types.

CHAPTER III

NIK CONTROLS GLIOMA CELL ADHESION AND INVASION THROUGH REGULATION OF LEADER CELL MARKER, ITGA11

SUMMARY

A hallmark of high grade glioma is highly aggressive, diffuse invasion into normal brain tissue, contributing to a 100% recurrence rate and resistance to current therapies. Recent efforts to determine molecular differences in high grade glioma and define tumor subtypes have revealed that the noncanonical NF-κB transcription factor RelB is upregulated in the highly aggressive mesenchymal subtype, as well as in recurrent tumors. We have found noncanonical NF-κB signaling drives directed glioma cell invasion into 3D collagen matrices. Stabilization of NF-κB-inducing kinase (NIK), a critical driver of noncanonical NF-κB signaling, promoted glioma cell adhesion, spreading, and pseudopodia formation on collagen substrates. While normal brain tissue expresses low levels of collagen, collagen type I is upregulated within the stroma and surrounding tissue of glioma. As NIK expression appeared to regulate glioma cell behavior on collagen, we investigated whether NIK controls the expression of collagen-binding and other integrins. We found NIK expression upregulated the integrin alpha 11 subunit (ITGA11), while it did not significantly affect the expression of ITGA1, ITGA2, or ITGA10. Analysis of human tumor samples revealed that ITGA11 expression was increased in glioma tissue compared to normal brain tissue. Furthermore, when testing multiple glioma lines, ITGA11 expression positively correlated with invasiveness into 3D collagen matrices. In

a heterologous system, ITGA11 and MT1-MMP, a key matrix metalloproteinase, formed a complex, suggesting these transmembrane proteins could interact in glioma cells to facilitate coordinated recognition and degradation of collagen during invasion. Silencing of ITGA11 in an invasive glioma line attenuated invasion into 3D collagen matrices. NIK expressing cells were capable of enhancing the invasiveness of normally non-invasive glioma cells. Collectively, these data reveal an ability of NIK to promote collective glioma cell invasion, pseudopodia formation, and ITGA11 expression. These data suggest ITGA11 could serve as a novel marker for more invasive glioma and a potential therapeutic target in glioma.

INTRODUCTION

High grade gliomas are uniformly fatal. These devastating tumors are the most common primary brain tumor and have a median survival time of approximately one year (2). A hallmark of these tumors is aggressive, diffuse invasion into normal brain tissue. Though surgical resection can remove the majority of the tumor, a balance between removal of the tumor while maintaining neurological function leads to incomplete excision of the tumor. While adjuvant chemotherapy and radiation have improved survival time (155), the tumors retain a 100% recurrence rate due to survival and regrowth of the cells that invaded past the margins of resection. Therefore, understanding the mechanisms controlling the invasiveness of these tumors is of fundamental importance to the development of therapeutics to combat this disease.

Genetic profiling of high grade glioma has defined distinct subtypes based on molecular and clinical signatures (11, 156). In particular, tumors of the mesenchymal subtype are characterized as more aggressive and endothelial-like, expressing markers of angiogenesis. Patients with the mesenchymal subtype have shorter survival time, relative to other subtypes. Further, regardless of the original subtype, most glioma tumors recur as the mesenchymal subtype (156). Separate studies found the noncanonical NF-κB transcription factor RelB was upregulated in mesenchymal tumors (11), and the recurrent tumors often had increased RelB copy number (112). Noncanonical NF-κB signaling is driven by the stabilization of NF-κB inducing kinase (NIK or MAP3K14) in response to specific cytokines, such as TWEAK, leading to downstream translocation of RelB to the nucleus where it can act on target genes (17-19, 30). Our previous work demonstrated that RelB expression positively correlated with mesenchymal glioma tumor invasiveness into 3D type I collagen matrices and RelB silencing attenuated glioma invasiveness and tumor growth (29, 30).

Consistent with RelB, stabilization of NIK also stimulates glioma cell invasion (30, 157). Furthermore, Chapter II found that NIK regulates the phosphorylation and activity of the type I collagen matrix metalloproteinase, MT1-MMP (or MMP14) and the localization of MT1-MMP to pseudopodial structures. NIK also controlled glioma cell spreading and pseudopodia formation on collagen in 2D. In human patients, upregulation of NIK and MT1-MMP is negatively correlated with survival time (157). However, the manner through which noncanonical NF-κB signaling drives glioma cell growth and invasion is largely unknown.

The extracellular matrix (ECM) composition of normal brain differs substantially from glioma. While type I collagen is the most highly expressed protein in the body, the normal brain expresses very little collagen, making it a very soft tissue. However, the ECM of glioma is composed of collagen, hyaluronan, tenascin-C, and vitronectin (107, 158, 159). Expression of type I collagen within the tumor stroma has been shown to positively correlate with increasing grade of glioma; grade IV glioblastoma multiforme tumors express the highest levels of type I collagen (107). The presence of collagen within the tumor microenvironment can provide adhesive scaffolding for migrating cells, release growth factors to promote invasion and proliferation, and induce the activation of pro-invasive signaling after recognition by collagen binding receptors (160, 161). Thus, the increased expression of collagen in glioma likely contributes to aggressive behavior in glioma, although a specific mechanism has not been identified.

Integrins are transmembrane receptors for ECM and basement membrane proteins that consist of heterodimers of alpha and beta subunits. Currently there are 18 alpha and 8 beta subunits, which can form 24 integrin pairs, providing substrate specificity (162). Once integrins adhere to an ECM protein, the intracellular tails will unfold to reveal a binding site for the actin binding protein, talin. Therefore, integrins couple the extracellular environment and the actin cytoskeleton (163). Integrin attachment to the ECM forms a nascent adhesion which will develop into a focal adhesion, containing hundreds of proteins, including F-actin, and the actin binding proteins, talin, paxillin, vinculin, and alpha-actinin. Several signaling molecules are activated during focal adhesion assembly, including FAK, Src, and members of the small Rho GTPase family,

Rac1 and Cdc42. Downstream actin remodeling events stimulate the production of actin-rich invasive structures. Pseudopodia develop from sites of integrin-matrix adhesion and localize proteases that degrade the ECM (164-167). In particular, MT1-MMP has been found to be recruited to integrin adhesive sites and initiate collagen degradation, and promote invasion (79, 81, 82, 113, 114, 168, 169).

Integrins have been shown to be upregulated in many solid tumors and are thought to stimulate tumor cell migration (170). In glioma, the αvβ3 and αvβ5 integrins display increased expression at the border between the tumor and normal brain tissue and may contribute to glioma cell invasion (171). Expression of the integrin subunits that form collagen-binding integrins has not been studied in glioma, however. There are four alpha integrin subunits, ITGA1, ITGA2, ITGA10, and ITGA11, which heterodimerize with ITGB1 to bind type I collagen, recognizing the GFOGER motif within fibrillar collagen (35, 172). Notably, an association between ITGA11 expression and tumor cell invasion and progression has been recently investigated. Increased ITGA11 expression was found in the subset cells that initiate collective cell invasion in breast cancer lines and its expression correlates with progression of non-small cell lung cancer (41, 44). A role for ITGA11 in mediating glioma cell invasion has not been determined. In this study, we demonstrate noncanonical NF-κB signaling regulates the expression of ITGA11 to control invasion of high grade glioma.

MATERIALS AND METHODS

Reagents

Collagen was isolated and prepared as previously described (127). Osteopontin was isolated as previously described (173). Human fibronectin was purchased from Sigma Aldrich (F-1141).

Cells

BT25 and BT114 cell lines were obtained from human glioma patients and described previously (128). U87 glioma cells were purchased from ATCC. Glioma lines were maintained in Neural Stem Cell (NSC) medium (DMEM/F12, 1x B-27 Supplement minus Vitamin A, 1x Glutamax, 50 ng/ml EGF, 50 ng/ml bFGF, 1x Pen/Strep). HEK293FT cells were purchased from Invitrogen (Grand Island, NY) and were cultured in DMEM (Invitrogen) supplemented with 10% FBS (Invitrogen). All cells were incubated at 37°C with 5% CO_2. Osteosarcoma and melanoma cells were a kind gift of Carl Gregory (174) and Alan Tackett, respectively, and both cell lines were grown in DMEM supplemented with 10% FBS.

Constructs

pLenti6 overexpression constructs for NIK were previously described (157). Briefly, NIK cDNA was subcloning cDNA into pLenti6-V5-DEST (Addgene, Cambridge, MA) using the GATEWAY™ Cloning System. Luciferase (Promega, Madison, WI) coding sequences were subcloned into pLenti6-V5-DEST and used as controls for NIK

overexpression. NIK(S867A) mutation was obtained by PCR cloning using oligo primers containing the mutation. *NIK* gene–knockout cells (BT25-sgNIK) were described previously (157). MT1-MMP-His cloning has been previously described (175). The enhanced GFP construct has been detailed previously (176). ITGA11 expression constructs were amplified from human umbilical vein endothelial cell cDNA using primers (5'-ACTGGTCGACGCCACCATGGACCTGCCCAGGGG-3') and (5'-ACTGGGTACCCTCCAGCACTTTGGGGGTGG-3') and inserted into the pFlag-CMV2 vector (Sigma) to generate a C-terminal Flag tag on ITGA11. Positive clones were tested for expression by transfection into HEK293FT cells and fidelity by sequencing.

Lentiviral production

HEK293FT cells were transfected with 24 μg of lentiviral plasmids using 72 μg of polyethyleneimine (Polysciences Inc., Warrington, PA). Lentiviruses were harvested after three days and used to infect $2x10^5$ BT114 or U87 cells. Transduced BT114 and U87 cells were selected for 14 days in NSC medium 6 μg/ml blasticidin or 200 ng/ml puromycin, respectively, (Invitrogen, San Diego, CA) to verify stable transduction.

Invasion assays

Invasion assays were established as previously described (127). Briefly, 3D collagen type I matrices were prepared at a final concentration of 2 mg/ml. Before polymerization, 28 μl of collagen matrix was added to each well of a half-area 96-well plate and allowed to polymerize for 45 minutes at 37°C with 5% CO_2. Following collagen

polymerization, dissociated cells (40,000 cells/100 µl DMEM) were seeded and allowed to incubate at 37°C with 5% CO_2. Invasion assays were fixed after 48 hours incubation, with 3% glutaraldehyde in PBS and stained with 0.1% toluidine blue in 30% methanol. Co-culture invasion assays were established as described above. BT25-Control and BT25-sgNIK cells were labeled with 1 µg/ml DiO or DiI (Thermo Fisher, V22886, V22885) by incubating for 20 minutes and washing per manufacturer's instructions. Labeled cells were seeded individually in separate wells at 40,000 cells/100 µl DMEM or combined at 20,000 cells of each type/ 50 µl DMEM per cell type. Unlabeled cells were also seeded in separate wells at 40,000 cells/100 µl DMEM, as a control. Cells were fixed after 48 hours in 4% paraformaldehyde for 30 minutes, and rinsed with Tris-Glycine buffer, containing 0.3% Tris and 1.5% glycine, and stained with 1 µM DAPI (Molecular Probes) for 30 minutes. Collagen gels were cut, mounted, and imaged from the side using a Nikon TI A1R inverted confocal microscope to capture Z-stacked images with a 0.5 µm step size.

Quantification of invasion responses

Invasion density was quantified manually in toluidine blue stained invasion assays as the average number of structures invading past the monolayer, per field, using an eyepiece fit with a 10x10 ocular grid. At least four wells per treatment group were counted, per experiment, for three independent experiments. To visualize invasion responses, after fixation and staining, collagen gels were removed from the well, cut and imaged from the side using an Olympus CKX41 microscope with a Q-Color 3 camera at 10x magnification.

Adhesion assays

High binding EIA/RIA 96-well plates were coated with 1.25µg/ml of collagen type I, fibronectin, or osteopontin and allowed to coat overnight at 4°C with gentle mixing. The matrix proteins were removed and the wells were blocked with 10 mg/ml BSA for 1 hour. Negative controls consisted of blank wells blocked with BSA alone. BT114, BT25, or U87 cells were seeded in triplicate at 40,000 cells per well and allowed to attach for 30 minutes at 37°C. Unattached cells were washed before fixing in 3% formalin and staining with 0.1% amido black in 10% acetic acid and 30% methanol. Stained wells were rinsed with water and dried before adding 50 µl 2N NaOH. Absorbances at 595 nm were read using a Victor X3 Multilabel Reader (PerkinElmer).

RNA isolation, cDNA synthesis and quantitative RT-PCR

Cells were lysed in 700 µl RLT buffer (Qiagen, Valencia, CA) with 7µl 2-mercaptoethanol (Sigma). Total RNA was isolated using the Qiagen RNeasy mini kit, according to manufacturer's instructions. RNA was treated with RNase-Free DNase (Qiagen) to degrade DNA for 15 minutes at 22°C. RNA samples were run on a 1% acrylamide gel to test for RNA quality and stored at -80°C. 1 µg RNA was reverse transcribed into cDNA using Superscript III First-Strand Synthesis System (Invitrogen), following manufacturer's instructions and cDNA samples were diluted 1:6 in DEPC treated water. Quantitative RT-PCR (qPCR) assays were performed using SYBR Green PCR Master Mix (Applied Biosystems, Foster City, CA) and 10 µM primers to amplify GAPDH (5'-AATGAAGGGGTCATTGATGG-3', 5'-

AAGGTGAAGGTCGGAGTCAA-3'), β-Actin (5'-CATCACCATTGGCAATGAGC-3', 5'-CGATCCACACGGAGTACTTG3'), ITGA1 (5'-TGGGTGCTTATTGGTTCTCC-3', 5'-TTCACCTCTCCCAACTGGAC-3'), ITGA2 (5'-TCACTTTGTTGCTGGTGCTC-3', 5'-CCTCGGTGAGCCTGAATAAC-3'), ITGA3 (5'-TTCAAACGGAACCAGAGGATG-3', 5'-ACCTGAAGGTCCCTTGTGTG-3'), ITGA6 (5'-GCGGTGTTATGTCCTGAGTC-3', 5'-CCATCACAAAAGCTCCAATC-3'), ITGA10 (5'-GGTGAGAGCAGCAAAGAACC-3', 5'-TGGGACTGACTGAACCCTTC-3'), ITGA11 (5'-CCAGAAGGAGGACTCAGACG-3', 5'-GAAGGGATAGCTGACGTTGC-3'), ITGAV (5'-CCCCGAGGGAAGTTACTTCG-3', 5'-ATGGATCATCCTTGGCATAATCTC-3'), ITGB1 (5'-ACTGATTGGCTGGAGGAATG-3', 5'-AACAATGCCACCAAGTTTCC-3'), ITGB4 (5'-CATAGAGTCCCAGGATGGAG-3', 5'-CTGCTGTACTCGCTTTGCAG-3'). Three independent experiments were performed in triplicate wells. qPCR data was analyzed using StepOne Software (version 2.1). ΔΔCT values were normalized to GAPDH expression values for each sample, set relative to vector (Control), and converted to $2^{-\Delta\Delta CT}$ to compare the relative mRNA fold change expression between treatment groups.

Western blotting

Whole cell protein extracts were prepared by pelleting equal numbers of cells and lysing the cells in 1.5x boiling Laemmli sample buffer containing 2% β-mercaptoethanol. Proteins were separated on 7% SDS-PAGE gels and transferred to Immobilon PVDF

membranes (EMD Millipore, Billerica, MA). Membranes were blocked with 5% evaporated non-fat milk in 0.1% Tween-20 in TBS and incubated with primary antibodies diluted in milk blocking buffer at 4°C, overnight. The following primary antibodies were used in this study: α-Actin (Calbiochem, CP01), MT1-MMP (Millipore, MAB3328), ITGA11 (Millipore, ab6031), and GAPDH (Abcam, ab8245). After washing in 0.1% Tween-20/TBS, membranes were incubated for 1 hour at room temperature with HRP-conjugated antibodies (DAKO, Carpinteria, CA) directed against the appropriate species and diluted in 5% evaporated non-fat milk. Immobilon Western Chemiluminescent HRP Substrate (EMD Millipore) was used for detection of HRP with HyBlot CL autoradiography film (Denville Scientific, Metuchen, NJ).

Transient transfection and immunoprecipitation

HEK293FT cells were transiently transfected in solution with 1 μg DNA and 8 μl Lipofectamine (Invitrogen) and seeded at $1x10^6$ cells per well in a 6-well plate coated with 20 μg/ml collagen type I. Cells were allowed to incubate overnight at 37°C with 5% CO_2. The next day, the plate was placed on ice and washed two times with 2 ml PBS with cations (0.9 mM Mg^{2+} and Ca^{2+}). Cells were lysed in 1 ml cold lysis buffer containing 0.5% NP-40 in PBS with cations, 1x protease inhibitor (Roche Diagnostics) and 25x HALT phosphatase inhibitor. Cells were incubated for 20 minutes on ice and scraped every 5 minutes to aid the lysis. Lysates were collected and centrifuged at 16,000xg for 15 minutes at 4°C. The supernatants were precleared by gentle rotation with 5 μl protein G magnetic beads for 1 hour at 4°C. The supernatants were incubated with 2 μg antibodies

directed to MT1-MMP (Abcam, ab38971) or species specific IgG (Invitrogen) for 14 hours at 4°C. 10 µl protein G magnetic beads were added to the lysates and gently rotated for 2 at 4°C. Beads were washed 6 times with 1 ml lysis buffer, without protease and phosphatase inhibitors. Proteins were eluted from the beads using 1.5x Laemmli sample buffer. Lysates were reduced with 2 % β-mercaptoethanol and analyzed by western blotting, as described above.

Human protein atlas

Human cerebral cortex and glioma stained tissue sections are from The Human Protein Atlas available from www.proteinatlas.org (177). The tissue sections are stained for the alpha 1 chain of collagen type I (COL1A1), ITGA11, and MT1-MMP (MMP14).

Statistical analyses

All statistical analyses were performed using Prism 5 or Prism 6 (Graphpad Software, Inc.). Student's *t*-test was performed on data comparing two samples. One-way ANOVA with Tukey's Honest Significant Difference (HSD) post-hoc test was performed when comparing more than two samples. For ANOVA and Student's *t*-test analyses, significance was considered with a p value of alpha =0.05.

RESULTS

NIK increases expression of collagen binding integrin subunit alpha 11

Studies in Chapter II show glioma cell invasion into 3D collagen matrices is variable and can be controlled by noncanonical NF-κB signaling activation or inhibition (29, 30, 157). NF-κB-inducing kinase (NIK or MAP3K14) is constitutively degraded under basal conditions, but when stimulated, NIK expression is stabilized leading to activation of noncanonical NF-κB signaling through RelB nuclear translocation to act on target genes (17-19). In addition to regulation of invasion, Chapter II shows that expression of NIK controlled formation of pseudopodia and cell spreading on collagen in glioma cells (157). To investigate a mechanism by which NIK regulates these responses on collagen, we performed an initial screen of integrin subunits which form receptors for multiple ECM proteins to determine whether NIK could control pseudopodia formation and cell spreading through specific integrins. Initial experiments compared non-invasive BT114 glioma cells expressing a Vector Control to BT114 cells expressing a stabilized, constitutively active from of NIK (NIK(S867A)). We found that mRNA expression of the integrin α11 (ITGA11) subunit, which binds type I collagen, was upregulated in BT114-NIK(S867A) cells compared to BT114 cells expressing a vector control (BT114-Control) (Figure 19). No significant changes were seen in expression of the ITGA1, ITGA2, ITGA3, ITGA6, ITGAV, ITGB1, or ITGB4 subunits, indicating a selective upregulation of the ITGA11 subunit.

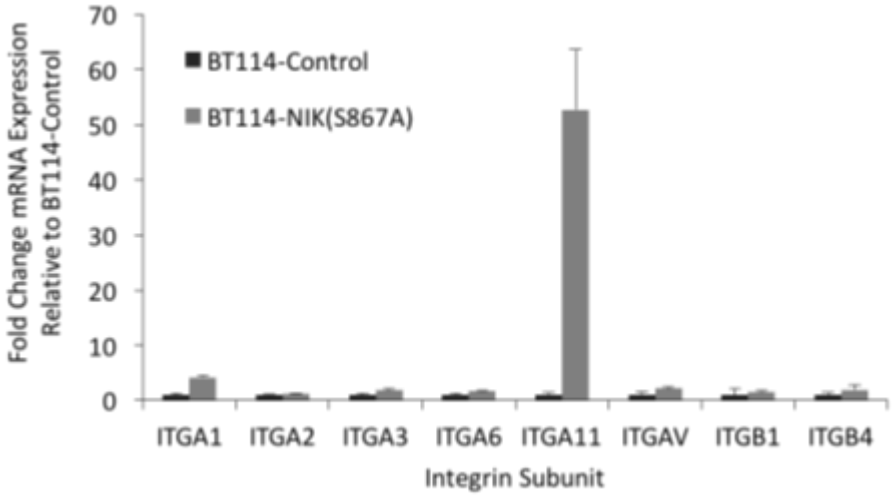

Figure 19. Expression of NIKS867A in non-invasive BT114 cells increases ITGA11 mRNA expression.
mRNA was isolated from BT114 cells expressing a Vector Control (Control) or NIK(S867A). qPCR analysis was performed using primers directed to ITGA1, ITGA2, ITGA3, ITGA6, ITGA11, ITGAV, ITGB1, ITGB4, and GAPDH. All ΔΔCT values were normalized to the GAPDH value for each respective sample and set relative to the Vector Control. ΔΔCT values were converted to $2^{-\Delta\Delta CT}$ to compare the relative mRNA fold change expression between BT114 -Control and -NIK(S867A) cells.

Previously we have found, and show here, that glioma lines isolated from primary tumors display different invasive capabilities into collagen, which positively correlates with expression of the noncanonical NF-κB transcription factor, RelB (29, 30, 157). Based on this observation, we next determined whether glioma cell invasion into collagen correlated with ITGA11 subunit expression. Wild-type glioma cells (BT114, BT25, and U87) were seeded onto 3D collagen matrices and allowed to invade overnight. Side view images of invasion and quantification of invasion density demonstrate that BT25 and U87 cells were more invasive than BT114 cells (Figure 20A, B). To examine cell attachment to collagen, a phenotype controlled by integrin ligation to matrix proteins, we performed an adhesion assay where equal numbers of BT114, BT25, and U87 cells were seeded onto

collagen, and allowed to attach for 30 minutes before washing away unattached cells and fixing, as described previously (178). While all cell lines were able to attach to immobilized collagen, the more invasive BT25 and U87 cells were significantly more adherent than BT114 cells (Figure 20C). Using quantitative real time PCR (qPCR), we examined mRNA expression of the four integrin subunits (ITGA1, ITGA2, ITGA10, and ITGA11) known to dimerize with the ITGB1 subunit to form collagen receptors. Compared to the other alpha chains, ITGA11 was the most highly upregulated in the more invasive glioma lines, BT25 and U87, compared to the non-invasive BT114 cells (Figure 20D). These data demonstrate more invasive glioma cells display both increased adherence to collagen and expression of the collagen binding integrin subunit, ITGA11.

Type I collagen, ITGA11, and MT1-MMP expression are upregulated in human glioma

The ECM of the normal brain consists mostly of hyaluronan, tenascin-C, proteoglycans, and basement membrane proteins surrounding the vasculature (158). Normal brain expresses very little fibrillar matrix proteins, such as type I collagen, making it a soft tissue. Recently, Huijbers et al., showed positive Masson's Trichrome staining for collagen fibers in glioblastoma multiforme (GBM) and further, the two alpha subunits which make up type I collagen are in the top one hundred genes upregulated in GBM compared to grade III gliomas (107). Staining performed by The Human Protein Atlas (177) demonstrates that type I collagen, ITGA11 and the membrane-bound protease which degrades collagen, MT1-MMP, are upregulated in high grade glioma, compared to normal brain tissue (Figure 21). These data demonstrate upregulation of collagen and the ITGA11

collagen receptor in glioma, reinforcing the relevance of studying ITGA11 in glioma invasion.

NIK expression controls ITGA11 expression in high grade glioma

To test whether NIK controlled the expression of ITGA11 beyond the initial screen of integrin subunits (Figure 19), we examined glioma cell adherence to collagen and the expression of all collagen binding integrin subunits after modulation of NIK expression.

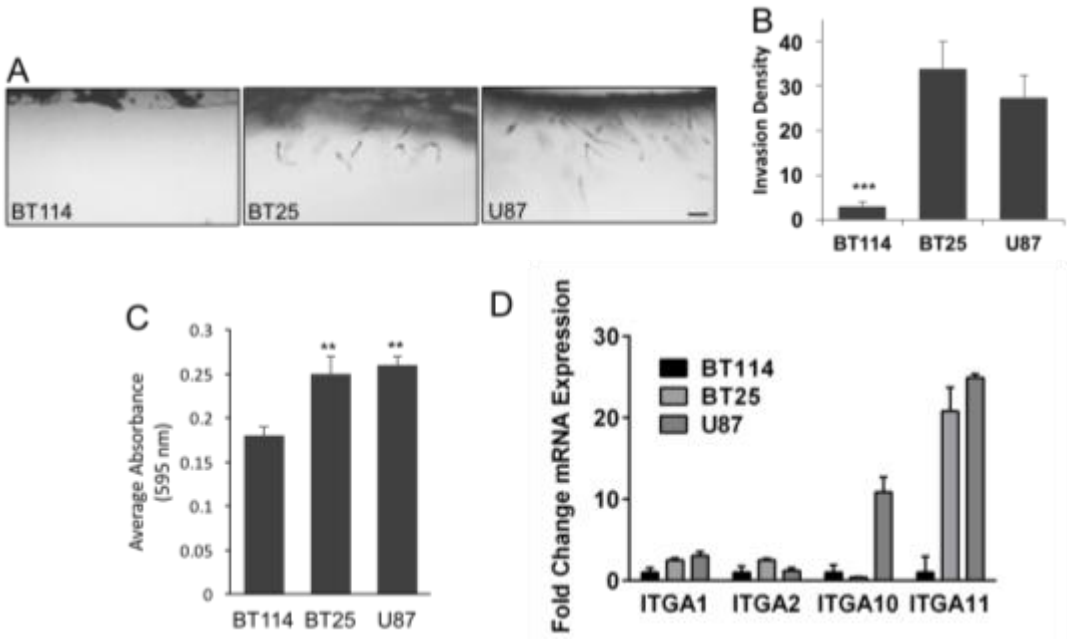

Figure 20. Glioma cell invasiveness and adhesion to type I collagen is correlated with ITGA11 expression.
(A) BT114, BT25 and U87 glioma cells were seeded onto 2 mg/ml collagen matrix and allowed to invade 24 hours, fixed and stained with toluidine blue. Side view images of invasion shown, scale bar = 50μm. **(B)** Average invasion densities +/-SD from panel A. ***$p<0.01$ using Student's t-test. **(C)** Average absorbance values +/-SD from BT114, BT25, and U87 cells stained with 0.1% amido black after adhesion assays on 1.25 ug/ml col I. **$p<0.01$ using Student's t-test. (D) qPCR analysis using indicated primer pairs, showing fold change gene expression relative to BT114 cells. All values were normalized to RPLPO control. Representative experiment shown (n=2).

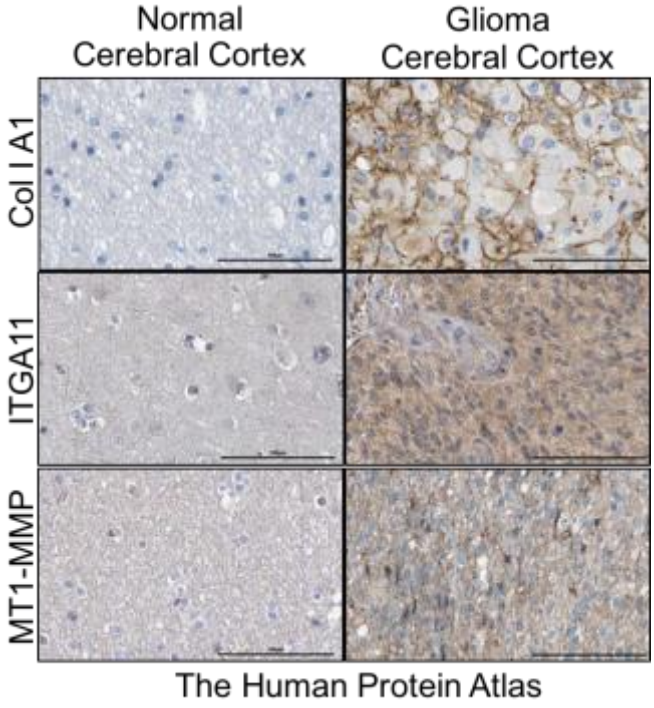

Figure 21. Col I A1, ITGA11, and MT1-MMP are upregulated in glioma.
Collagen I, subunit A1 (Col I A1), ITGA11 and MT1-MMP staining of normal or glioma tissue in the cerebral cortex. Scale bars=100 µm. Staining performed by The Human Protein Atlas.

Our previous findings indicated that increased NIK expression enhanced BT114 cell invasion compared to BT114 cells expressing luciferase control (Chapter II, (157)). In adhesions assays, BT114-NIK(S867A) cells displayed increased adhesion to collagen compared to BT114-Control cells. However, cell adhesion to osteopontin (OPN), a ligand for integrins that recognize RGD and LDV sequences, was not affected by increased NIK expression (Figure 22A). We next examined mRNA expression of the integrin alpha subunits that form collagen receptors in BT114-Control cells, BT114 cells expressing a wild-type NIK construct (NIK(WT)), and BT114-NIK(S867A) cells. Compared to the other alpha subunits, ITGA11 was the most highly upregulated in the cells expressing

NIK(WT), or NIK(S867A), (4- and 42- fold greater, respectively) compared to Control cells (Figure 22B). Further, examination of ITGA11 protein expression by western blotting revealed a corresponding upregulation of ITGA11 in BT114 cells expressing NIK(WT) and NIK(S867A) compared to Control cells (Figure 22C).

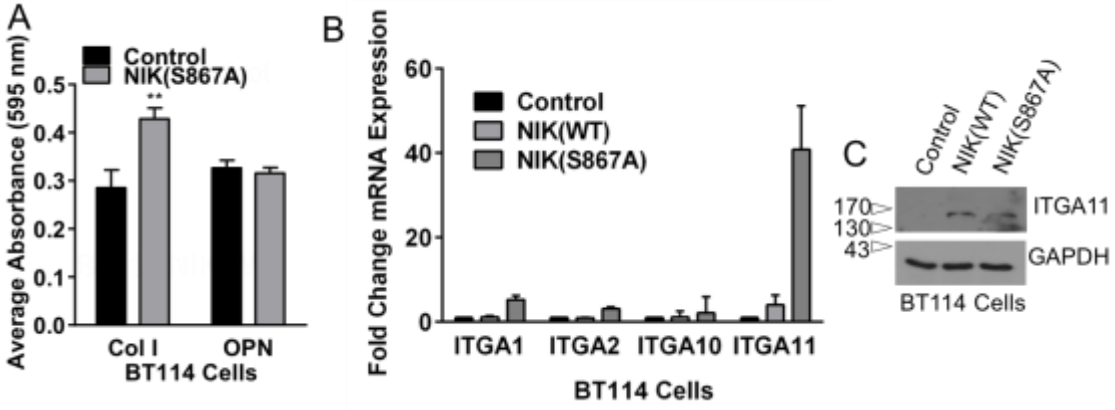

Figure 22. NIK promotes glioma cell spreading, attachment, and pseudopodia formation. **(A)** BT114 cells expressing the vector (Control) or NIK(S867A) were seeded onto 1.25 µg/ml collagen type I (Col I) or osteopontin (OPN) and allowed to attach 30 minutes. Cells were rinsed and remaining cells were stained with 0.1% amido black. Graph shows average absorbance at 595 nm after adhesion assay. **p<0.01 using Student's t-test. **(B)** mRNA was isolated from BT114 -Control, -NIK(WT), and -NIKS867A cells and used for qPCR analysis with primers directed to ITGA1, ITGA2, ITGA10 and ITGA11, showing fold change gene expression relative to BT114-Control. All values were normalized to RPLPO control. **(C)** Western blotting analysis of lysates made from BT114 -Control, -NIK(WT), and -NIKS867A cells using antibodies against ITGA11 and GAPDH.

We next examined adherence to collagen and integrin expression in the invasive BT25 glioma cell line after NIK had been knocked out using CRISPR/Cas9/small guide RNA-mediated deletion of *NIK* (sgNIK). We have previously found that deletion of NIK in BT25 cells significantly attenuates BT25 cell invasion into 3D collagen (Chapter II, (157)). In adhesion assays, BT25-sgNIK cells were less adherent to collagen compared to BT25 cells expressing a vector control (Control), while adherence to OPN was not affected

(Figure 23A). Examination of ITGA1, ITGA2, ITGA10 and ITGA11 mRNA expression revealed that deletion of NIK in BT25 cells decreased expression of ITGA11 compared to BT25-Control cells (Figure 23B). Correspondingly, BT25-sgNIK cells also exhibited decreased ITGA11 expression at the protein level (Figure 23C). These data indicate that NIK controls the adhesion of glioma cells to collagen, possibly by regulating the expression of the collagen binding integrin, ITGA11.

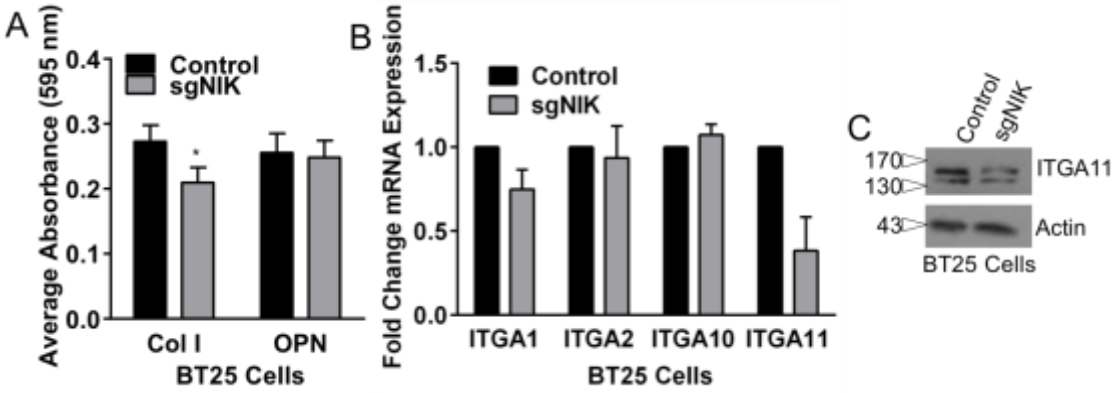

Figure 23. NIK silencing inhibits glioma cell spreading, attachment, and pseudopodia formation. **(A)** BT25 cells expressing the vector (Control) or sgNIK were seeded onto 1.25 µg/ml collagen type I (Col I) or osteopontin (OPN) and allowed to attach 30 minutes. Cells were rinsed and remaining cells were stained with 0.1% amido black. Graph shows average absorbance at 595 nm after adhesion assay. *$p<0.05$ using Student's t-test. **(B)** mRNA was isolated from BT25 -Control and –sgNIK cells and used for qPCR analysis with primers directed to ITGA1, ITGA2, ITGA10 and ITGA11, showing fold change gene expression relative to BT25-Control cells. All values were normalized to RPLPO control. **(C)** Western blotting analysis of lysates made from BT25 -Control and -sgNIK cells using antibodies against ITGA11 and Actin.

ITGA11 silencing attenuates glioma cell invasion

To evaluate a role for ITGA11 in glioma cell invasion, we used lentiviral-mediated delivery of short hairpin RNAs to knockdown ITGA11 (shITGA11) or GAPDH (shGAPDH) expression, as a control. We used the U87 glioma cell line to knockdown expression of ITGA11 as we have found these cells to be highly invasive (29, 30, 157) and express high levels of ITGA11 (Figure 20). We first confirmed knockdown of *GAPDH* and *ITGA11* in the U87-shGAPDH and U87-shITGA11 cells, respectively. Additionally, ITGA11 shares strong sequence similarity with ITGA1 and ITGA2; therefore, we confirmed that the ITGA11 short hairpin did not have significant unintended off target effects on mRNA expression of ITGA1 and ITGA2 (Figure 24A). In invasion assays, we observed that knockdown of ITGA11 significantly diminished U87 invasion into 3D collagen matrices, compared to shGAPDH control cells (Figure 24B). Side view images of invasion demonstrate dramatic attenuation of both invasion density and distance into the collagen matrix in U87-shITGA11 cells (Figure 24C). Together, these results support that NIK controls the expression of ITGA11, which plays a significant role in the invasion of glioma cells into 3D collagen matrices.

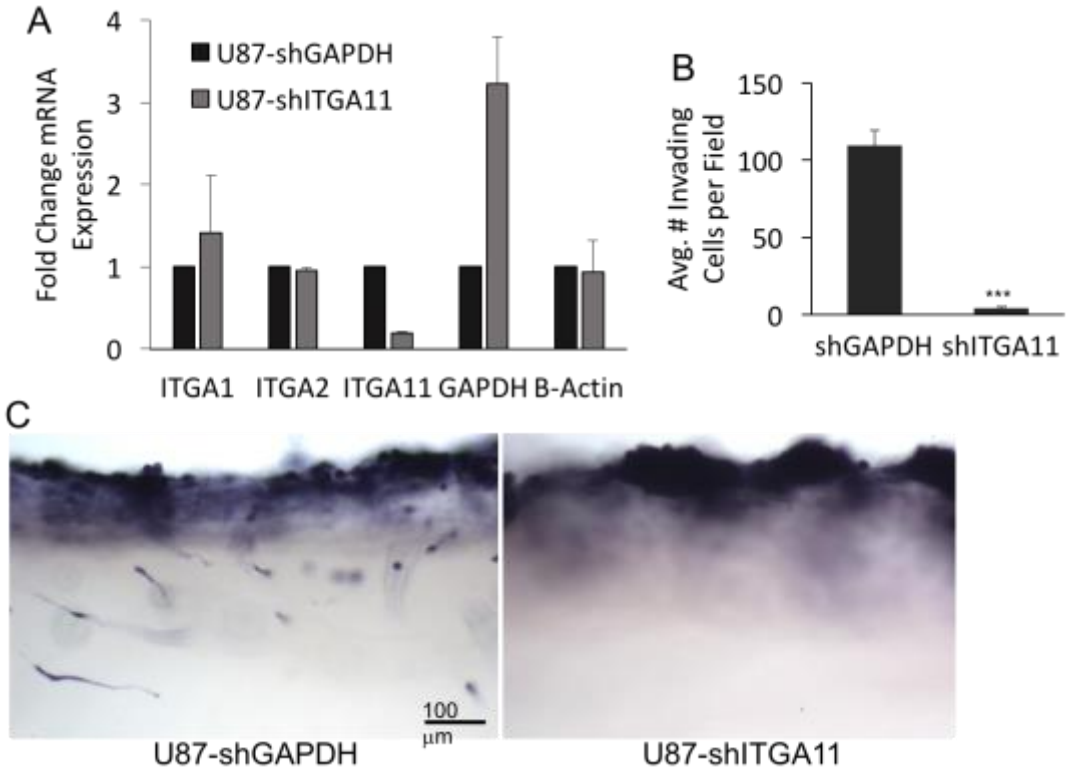

Figure 24. Silencing of ITGA11 decreases U87 invasion.
U87 cells were transduced with shRNA directed to GAPDH or ITGA11, seeded onto 2 mg/ml collagen type I matrices, and allowed to invade 48 hours. **(A)** mRNA was isolated from U87 –shGAPDH and -shITGA11 cells and used for qPCR analysis comparing integrin, GAPDH, and B-actin mRNA expression. **(B)** Quantification of average invasion density +/- SD ***$p<0.001$ using Student's *t*-test. Data shown are average values +/- s.d. **(C)** Side view images of invasion shown, scale bar = 100µm.

ITGA11 complexes with MT1-MMP

We have previously found that NIK regulates MT1-MMP phosphorylation (Y573) and localization to cortactin-rich pseudopodial structures (Chapter II, (157)). MT1-MMP degrades collagen, along with other basement membrane and ECM proteins to facilitate cell invasion. Phosphorylation of MT1-MMP at Y573 directs the protease to the plasma membrane, where it is tethered and can interact with other transmembrane proteins, the basement membrane, and ECM components (121-123). Notably, MT1-MMP is recruited

and enriched at sites of integrin-matrix adhesion to initiate directed collagen degradation and invasion (79, 81, 82, 113, 114, 168, 179). We therefore investigated whether MT1-MMP could form a complex with ITGA11. Using a heterologous system, MT1-MMP was co-expressed in HEK293FT cells with either GFP or ITGA11-Flag. Immunoprecipitation experiments determined ITGA11 complexed with MT1-MMP when co-expressed in HEK293FT cells (Figure 25). These data suggest that ITGA11 complex formation with MT1-MMP in glioma cells could enable coordinated, localized matrix degradation at sites of integrin adhesion to stimulate directed cell migration.

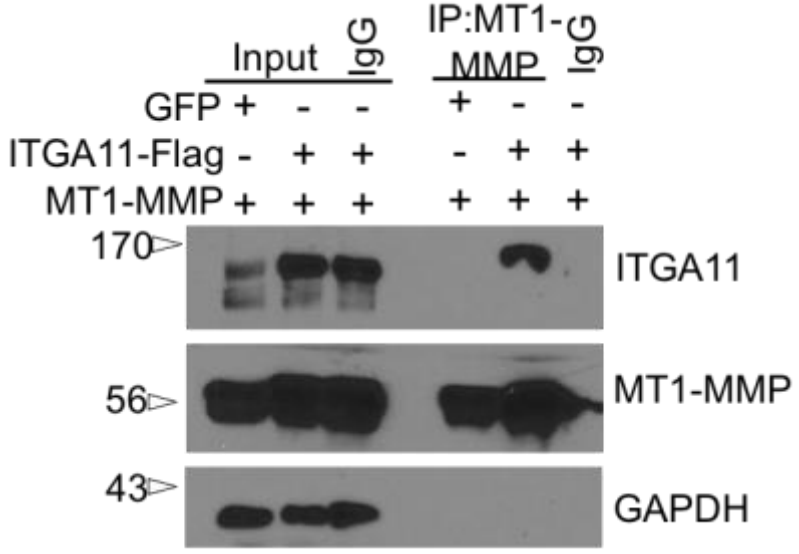

Figure 25. ITGA11 complexes with MT1-MMP in HEK293FT cells.
HEK293FT cells were transiently transfected to express MT1-MMP and either Flag-tagged ITGA11 or GFP control. MT1-MMP or isotype control were immunoprecipitated from cleared lysates and eluates were probed for MT1-MMP, ITGA11, and GAPDH during western blotting.

NIK promotes a leader cell phenotype in glioma

In breast cancer, ITGA11 has recently been identified as a marker of leader cells which facilitate collective cell migration (44). As we found NIK could regulate the expression of ITGA11 in glioma cells, we wondered whether NIK might drive a leader cell phenotype in 3D collagen matrices. We tested this through invasion assays using the invasive BT25-Control cells, which have relatively high NIK expression (157) and the BT25-sgNIK cells where NIK has been deleted (Figure 26A). As before, BT25-Control cells showed significant invasion into collagen matrices, while the BT25-sgNIK cells were less invasive (Figure 26B). However, when both cell types were combined, the number of invading BT25-sgNIK cells increased significantly (Figure 26A, B). Quantification of invasion distance past the original monolayer demonstrated BT25-Control cells invaded significantly further than the BT25-sgNIK cells, when seeded separately. When the two cell types were seeded in equal ratios, the BT25-sgNIK gained the ability to invade comparably to the BT25-Control cells (Figure 26C). This suggests a leader and follower cell relationship between cells with high NIK expression and cells lacking NIK, respectively, where NIK promotes a leader cell phenotype, stimulating the invasion of cells less capable of invading on their own.

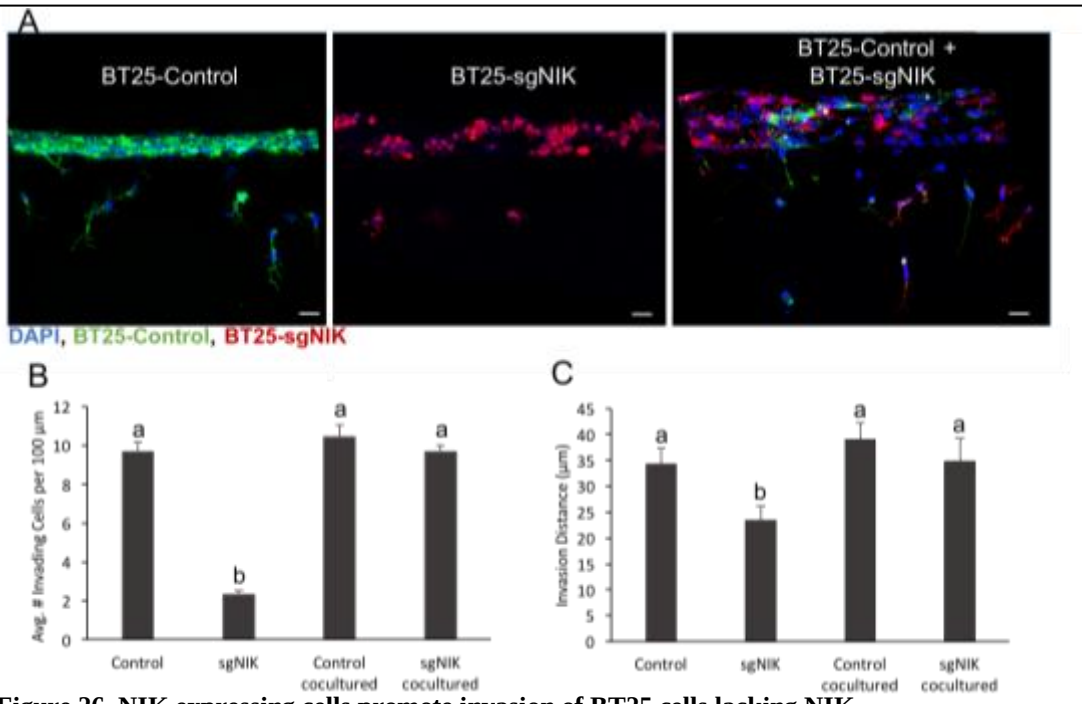

Figure 26. NIK expressing cells promote invasion of BT25 cells lacking NIK.
(A) BT25 cells expressing a vector control (BT25-Control) were labeled with DiO (green) and BT25-sgNIK were labeled with DiI (red). Cells were seeded separately or together into 2 mg/ml collagen type I matrices and allowed to invade 48 hours. Nuclei were labeled with DAPI (blue). Side view of invasion shown. Scale bar = 10µm. **(B)** Graph shows quantification of invasion density. After removing fixed collagen gels from the wells, gels were cut, mounted, and imaged from the side using confocal microscopy. The average number of invading cells per 100 µm +/- SD is shown. Different letters represent statistically significant differences calculated with an ANOVA and Tukey's HSD. **(C)** Quantification of invasion distance. Data shown are average values +/- SEM. Different letters represent statistically significant differences calculated with an ANOVA and Tukey's HSD.

ITGA11 expression correlates with invasiveness in other collagen-rich tumors

Since the expression of ITGA11 positively correlates with glioma cell invasiveness and promotes glioma cell invasion through 3D collagen matrices, we were interested in investigating if ITGA11 expression correlated with invasiveness of other tumor types. We chose to examine osteosarcoma and melanoma tumors, which typically must invade through dense type I collagen matrices. During invasion assays, MG63 human osteosarcoma cells were more invasive than UWOS2 cells (Figure 27A and B) and

correspondingly, also had increased expression of ITGA11 mRNA (Figure 27C). M4, M7 and M9 human melanoma cells were less invasive than the M6, M8, M10, WM115, and WM266 cells (Figure 28A and B) and also expressed relatively less ITGA11 mRNA during qPCR analyses (Figure 28C). Taken together, these data suggest that ITGA11 could be used as a general marker for more invasive human tumors. Together, our data in glioma support a correlation between NIK or noncanonical NF-κB signaling and ITGA11 expression. Whether this holds true in other tumors remains to be determined.

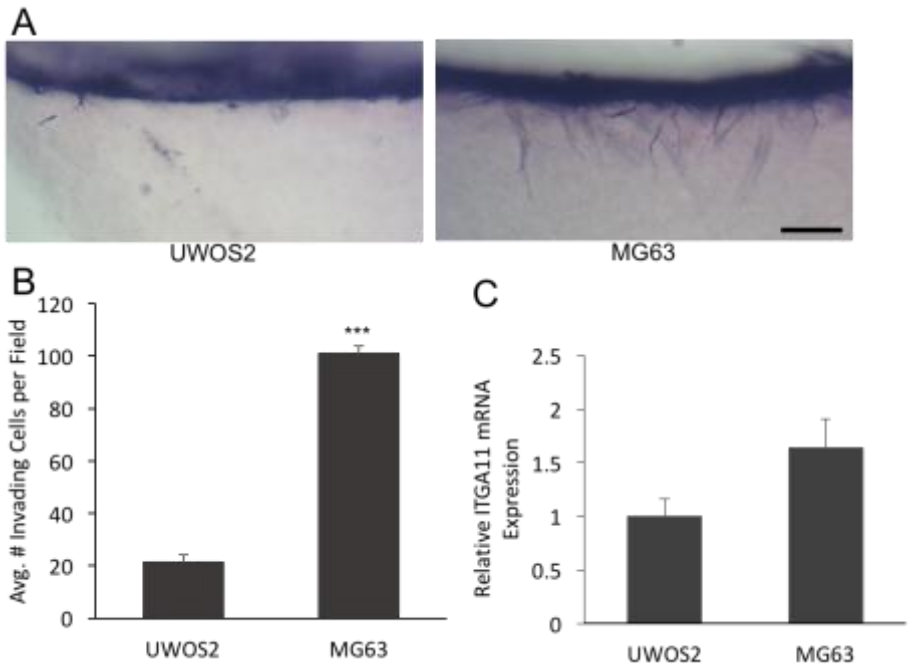

Figure 27. ITGA11 expression correlates with invasiveness of human osteosarcoma cells. UWOS2 and MG63 osteosarcoma cells were seeded onto 2 mg/ml collagen type I matrices, and allowed to invade 48 hours. (A) Side view images of invasion shown, scale bar = 50μm. (B) Quantification of average invasion density +/- SD ***$p<0.001$ using Student's *t*-test. (C) mRNA was isolated from UWOS2 and MG63 cells and used for qPCR analysis comparing ITGA11, showing fold change gene expression relative to UWOS2 cells. All values were normalized to GAPDH control.

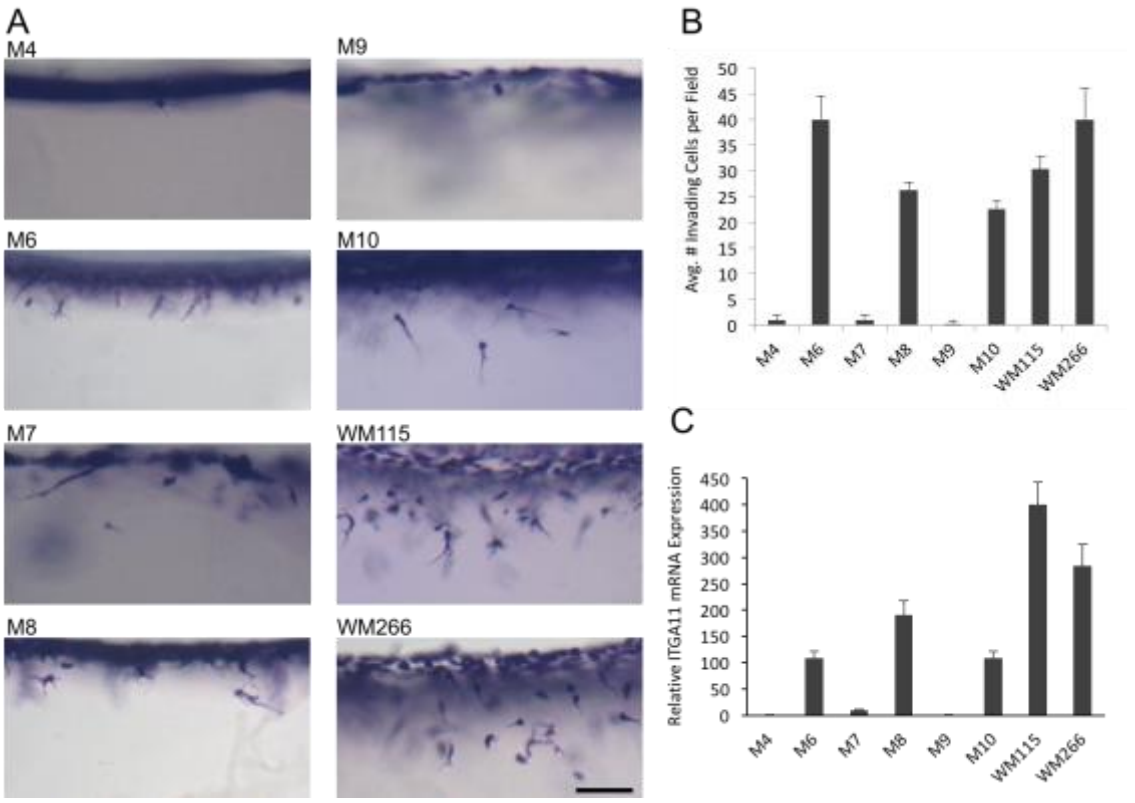

Figure 28. ITGA11 expression correlates with invasiveness of human melanoma cells.
M4, M6, M7, M8, M9, M10, WM115, and WM266 melanoma cells were seeded onto 2 mg/ml collagen type I matrices, and allowed to invade 48 hours. **(A)** Side view images of invasion shown, scale bar = 50μm. **(B)** Quantification of average invasion density +/- SD. **(C)** mRNA was isolated from indicated melanoma cells and used for qPCR analysis comparing ITGA11, showing fold change gene expression relative to M4 melanoma cells. All values were normalized to GAPDH control.

DISCUSSION

Although it has become increasingly apparent that noncanonical NF-κB signaling, through increased NIK activity, mediates the development and progression of a number of cancers (24-28), the mechanism by which NIK regulates tumor cell invasion is not well known. In the context of glioma, our previous studies have found NIK promotes glioma tumor growth (30), activation of MT1-MMP, and formation of invasive pseudopodial

structures (157). Here we provide evidence that in glioma cells, NIK increases the expression of ITGA11, and promotes a leader cell phenotype in collagen. Consistent with studies of breast cancer (44), ITGA11 was required for glioma cell invasion, and ITGA11 expression correlated with increased invasiveness in glioma, melanoma, and osteosarcoma cells.

In agreement with findings of collagen deposition within the glioma tumor stroma (107), staining from The Human Protein Atlas demonstrates increased expression of type I collagen in glioma tumor sections. While the normal brain is a soft tissue, the deposition of collagen within the tumor increases the stiffness of the tumor stroma. Using ultrasound, several studies have found glioma tissue is stiffer than the surrounding environment (180, 181). Increased collagen stiffness has been found to activate canonical NF-κB signaling (182), though whether noncanonical NF-κB signaling is activated by the same mechanism is unknown.

Recent studies have found the aggressiveness of glioma and poor patient prognosis are correlated with increased stiffness of the glioma ECM (183). Correspondingly, collagen deposition correlates with increasing glioma tumor grade (107). Furthermore, glioma cell invasion often follows stiffer areas of the brain, such as white matter and along the basement membrane of blood vessels (184, 185). Increased collagen stiffness has been found to enhance glioma cell motility, invasiveness, and proliferation (186-188). These studies of collagen in glioma relate to investigations in breast cancer, where tissue stiffness is known to promote the conversion of normal breast epithelial cells to tumor cells (189, 190). Increased breast density, caused by collagen deposition, is one of the greatest

independent risk factors for development of breast cancer, conferring a 4-6 increased risk in patients (191-194). Stromal collagen deposition increases matrix stiffness causing activation of signaling pathways which promote tumor cell invasion, survival, and growth (195). Our finding that ITGA11 expression correlates with more invasive glioma cells provides an explanation for how glioma cells could recognize and respond to the increased collagen deposition to promote a more invasive phenotype.

Our study is the first to show NIK can promote collective invasion, enhancing the invasiveness of glioma cells not capable of invading into collagen. NIK controls the expression of ITGA11, a marker of leader cells which initiate collective invasion in breast cancer (44). Knockdown of ITGA11 in glioma cells abrogated invasion, suggesting NIK-dependent ITGA11 expression may be a critical component of collective invasion, in glioma as well. ITGA11 expression correlated with melanoma and osteosarcoma cell invasiveness, although whether NIK regulates ITGA11 expression to promote invasiveness in these tumors remains to be determined. Interestingly, NIK has been found to be upregulated in melanoma and is thought to contribute to pathogenesis through inhibition of cellular senescence (196, 197). Similar to breast cancer, melanoma cells have been shown to utilize the collective mode of cell invasion (101). Therefore, it will be important to investigate whether NIK-mediated collective invasion seen in glioma could be more universal mechanism controlling tumor cell invasion. Whether the follower cells are invading through tunnels created in the matrix (138) by the leader cells, or the follower cells recognize proinvasive factors produced by the leader cells, remains to be determined. Regardless, the ability of NIK to promote collective invasion in glioma underscores the

importance of targeting noncanonical NF-κB signaling, as this invasion mechanism could be a fundamental factor underlying glioma recurrence.

Critical to cell migration following integrin adhesion to matrix substrates is remodeling of the ECM by matrix proteases. In particular, integrins and the collagenase MT1-MMP are thought to cooperate to facilitate coordinated matrix proteolysis and cell invasion. MT1-MMP is capable of degrading a wide range of ECM and basement membrane proteins, such as collagen type I, II, and III, fibrin, fibronectin, vitronectin, and laminin (61, 68-70). Further, MT1-MMP has also been shown to complex with several integrin receptors, including αvβ3, α3β1, and α2β1, which form receptors for these matrix proteins (75, 81, 83). Here we provide evidence that MT1-MMP can form a complex with ITGA11, adding to a growing list of interactions which can facilitate and precisely direct coordinated cell adhesion, matrix proteolysis, and migration. Altogether, these studies provide a mechanism through which noncanonical NF-κB signaling promotes glioma cell invasion, providing further evidence of the pathogenicity of this signaling pathway.

CHAPTER IV

CONCLUSIONS AND FUTURE DIRECTIONS

CONCLUSIONS

The results in Chapter II demonstrate that NIK, a critical upstream regulator of noncanonical NF-κB signaling mediates glioma cell invasion into 3D type I collagen matrices. NIK expression also positively correlated with glioma cell invasiveness. As a possible mechanism through which NIK drives glioma cell invasion, we found NIK regulated the activity and phosphorylation of the collagen protease, MT1-MMP, though likely through indirect means. The formation of invasive pseudopodial protrusions and cell shape on collagen matrices were also controlled by NIK expression. NIK enhanced localization of activated MT1-MMP to pseudopodial structures in both glioma cells and MEFs. Importantly, NIK controlled these critical components of cell invasion independently of the canonical NF-κB pathway.

Staining of human patient glioma tumor sections demonstrated both NIK and phosphorylated MT1-MMP were co-expressed in glioma cells. Further, staining of glioma tumor xenografts revealed expression of phosphorylated MT1-MMP correlated with increased NIK expression. Finally, through examination of clinical databases, we found co-expression of NIK and MT1-MMP in human patient tumors was associated with poorer patient survival rates. These results help to explain how noncanonical NF-κB signaling, through NIK, promotes the invasiveness of glioma cells and suggest inhibiting this pathway therapeutically may have benefit for glioma patients.

Chapter III reveals a potential mechanism through which NIK could control glioma cell shape changes and recruitment and activation of MT1-MMP at pseudopodia, as well as promote invasion into collagen matrices. Initially, we determined that expression of the collagen-binding ITGA11subunit was correlated with more invasive glioma cell lines. Staining performed by The Human Protein Atlas demonstrated ITGA11, type I collagen, and MT1-MMP expression were upregulated in glioma tissue, compared to normal brain tissue. Modulation of NIK expression revealed NIK upregulation increased both the mRNA and protein expression of ITGA11, while NIK silencing conversely decreased *ITGA11* expression. Knockdown of ITGA11 in an invasive glioma cell line also attenuated invasion into 3D type I collagen matrices, indicating ITGA11 could be a key mediator of NIK-driven glioma cell invasion.

Interestingly, ITGA11 has been found to be a functional marker of leader cells in breast cancer, which promote collective cell invasion (44). As NIK controlled the expression of ITGA11 in glioma cells, we investigated whether NIK could initiate collective cell invasion of glioma cells. In co-culture invasion assays, NIK-expressing cells increased the invasion distance and density of non-invasive cells, demonstrating NIK enhances the formation of a leader cell phenotype in invasive cells and mediates the invasion of normally non-invasive cells.

Collectively, these studies provide further evidence that noncanonical NF-κB signaling promotes the invasiveness of glioma cells. NIK increases the expression of the integrin ITGA11 subunit, which forms a type I collagen binding integrin. ITGA11 can promote the adhesion of glioma cells to collagen matrices. Integrin adhesion to matrix

substrates is well known to initiate formation of pseudopodial structures (77, 78), which we have shown are driven by NIK expression. NIK also promotes the phosphorylation, activity, and recruitment of the collagenase MT1-MMP to invasive pseudopodial structures. Altogether these phenotypes provide a mechanism by which NIK can drive glioma cell invasion (Figure 29).

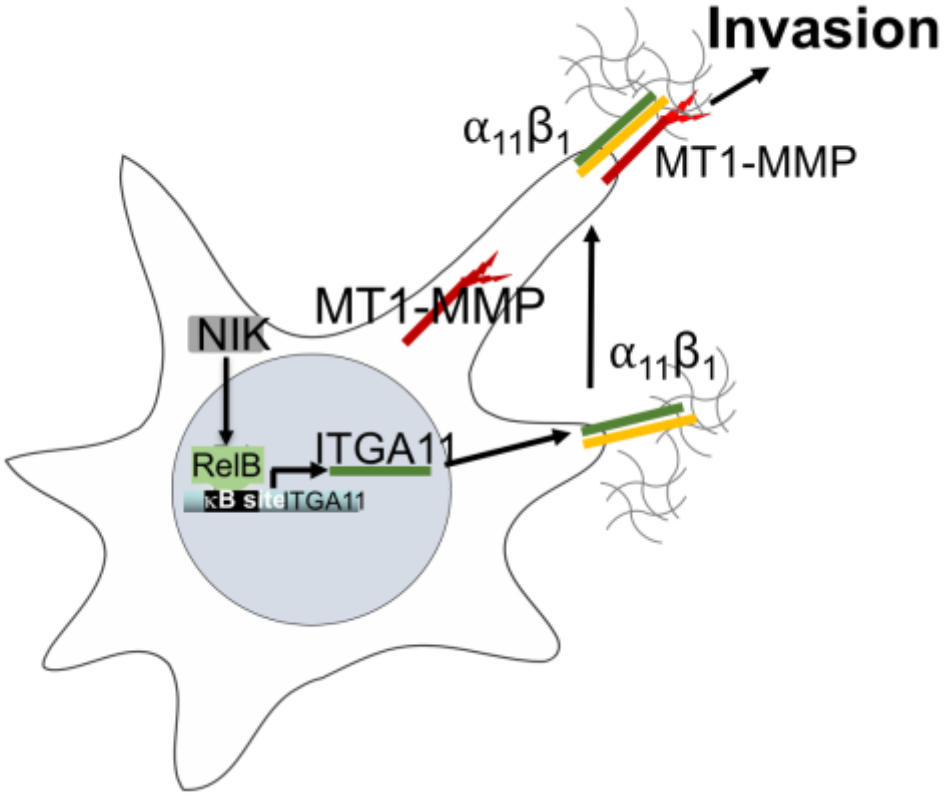

Figure 29. Mechanism of NIK-driven glioma cell invasion.

FUTURE DIRECTIONS

In these studies, we have found noncanonical NF-κB signaling, through stabilization of NIK, drives glioma cell invasion into 3D collagen matrices. NIK also regulates the mRNA and protein expression of ITGA11. Knockdown of ITGA11 decreases glioma cell adhesion to collagen in 2D and invasion into 3D collagen matrices. These results lend themselves to further investigation.

While mRNA expression of ITGA11 was controlled by NIK, whether ITGA11 is a transcriptional target of RelB, or if ITGA11 transcription is regulated by noncanonical NF-κB signaling by indirect means remains to be determined. Another important question is if ITGA11 activity is both necessary and sufficient for noncanonical NF-κB-driven glioma invasion. NIK is known to control several mechanisms which promote an invasive phenotype (29, 198); consequently, it is unlikely that ITGA11 would be sufficient to completely rescue invasion with the loss of NIK. However, even a partial rescue would highlight the importance of ITGA11 for glioma cell invasion. Knockdown of ITGA11 almost completely abolished U87 cell invasion; therefore, ITGA11 is expected to be necessary for NIK-induced glioma cell invasion.

In the setting of lung cancer, ITGA11 expression correlates with increasing tumor grade and poor prognosis in patients (41). While we have found ITGA11 expression is upregulated in glioma tissue compared to normal brain tissue, and its expression is increased in more invasive glioma cells, whether ITGA11 expression is correlated with higher grade tumors and poor patient outcomes is unknown. Additionally, ITGA11 expression reduces glioma cell adhesion to collagen and invasion into 3D collagen

matrices. Cells must adhere to their surroundings to degrade and migrate through the extracellular millieu. Integrins have been shown to be essential for these functions, as well as for promoting cell growth and survival; therefore, it would be intruging to determine how the attenuation of these behaviors *in vitro* would translate *in vivo* during orthotopic tumor xenograft experiments.

Further, as tumors are made up of a hetergeneous population of cells, an interesting question is where ITGA11 and NIK are expressed within the tumor mass. As NIK promotes an invasive phenotype, increased expression in the cells at the tumor border may occur. This would promote invasiveness at the tumor periphery, where cells are exposed to collagen, and moreover, as NIK enhances expression of ITGA11, this would further drive an invasive phenotype. These proteins have the potential to serve as markers of more invasive cells which could contribute to glioblastoma recurrence. Another possibility is the contribution of ITGA11 binding to collagen leading to a feed-forward loop through activation of NIK. Integrin signaling is known to enhance receptor tyrosine kinase activation, enhancing downstream signaling. Whether ITGA11 ligation to collagen promotes stabilization of NIK and downstream NF-κB signaling is unknown.

Another important area for potential investigation is targeting ITGA11 therapeutically. We have shown ITGA11 is not highly expressed in the normal brain, which corresponds to a lack of type I collagen deposition under normal conditions. Therefore, inhibiting ITGA11 could serve as an attractive therapy in the brain with the potential of specifically targeting only tumor cells. ITGA11 is a transmembrane protein,

with domains exposed on either side of the cell membrane, perhaps leading it to be a more "druggable" target.

During glioma cell invasion assays, we found NIK promoted collective invasion, allowing normally non-invasive cells to migrate into the collagen matrix behind leader cells. Several questions remain to be answered with regard to how NIK and ITGA11 drive this type of invasion. The cells expressing NIK could solely act to degrade the matrix in an MMP-dependent manner, forming a tunnel for non-invasive cells to migrate through, in a MMP-independent manner. Alternatively, NIK and ITGA11 expressing cells could release pro-invasive factors, which promote the normally non-invasive cells to follow.

ITGA11 expression has been shown to increase with increasing tumor grade in lung cancer (41) and control the invasiveness of leader cells in breast cancer (44). The data here show that ITGA11 expression also positively correlates with invasiveness in osteosarcoma and melanoma. While increased NIK expression has been linked to lung and melanoma cancer (26, 196, 197), whether noncanonical NF-κB signaling is elevated in the setting of these cancers to control ITGA11 expression and invasion is unknown. If so, it could point a more universal mechanism of tumor cell invasion, further underscoring the need to develop therapeutics against noncanonical NF-κB signaling and its targets.

REFERENCES

1. Ostrom QT, Bauchet L, Davis FG, Deltour I, Fisher JL, Langer CE, et al. The epidemiology of glioma in adults: a "state of the science" review. Neuro Oncol. 2014;16(7):896-913.

2. Louis DN, Ohgaki H, Wiestler OD, Cavenee WK, Burger PC, Jouvet A, et al. The 2007 WHO classification of tumours of the central nervous system. Acta Neuropathol. 2007;114(2):97-109.

3. Sanai NA-B, A.; Berger, M.S. Neural stem cells and the origin of gliomas. New England Journal of Medicine. 2005;353(8):811-22.

4. Stiles CD, Rowitch DH. Glioma stem cells: a midterm exam. Neuron. 2008;58(6):832-46.

5. Stupp R, Mason WP, van den Bent MJ, Weller M, Fisher B, Taphoorn MJ, et al. Radiotherapy plus concomitant and adjuvant temozolomide for glioblastoma. N Engl J Med. 2005;352(10):987-96.

6. Zhang JS, M.F.; Bradshaw, T.D. Temozolomide: mechanisms of action, repair and resistance. Current Molecular Pharmacology. 2012;5(1):102-14.

7. Stupp R, Hegi ME, Mason WP, van den Bent MJ, Taphoorn MJ, Janzer RC, et al. Effects of radiotherapy with concomitant and adjuvant temozolomide versus radiotherapy alone on survival in glioblastoma in a randomised phase III study: 5-year analysis of the EORTC-NCIC trial. Lancet Oncol. 2009;10(5):459-66.

8. Goodenberger ML, Jenkins RB. Genetics of adult glioma. Cancer Genet. 2012;205(12):613-21.

9. The Cancer Genome Atlas Research Network. Comprehensive genomic characterization defines human glioblastoma genes and core pathways. Nature. 2008;455(7216):1061-8.

10. Brennan CW, Verhaak RG, McKenna A, Campos B, Noushmehr H, Salama SR, et al. The somatic genomic landscape of glioblastoma. Cell. 2013;155(2):462-77.

11. Verhaak RG, Hoadley KA, Purdom E, Wang V, Qi Y, Wilkerson MD, et al. Integrated genomic analysis identifies clinically relevant subtypes of glioblastoma characterized by abnormalities in PDGFRA, IDH1, EGFR, and NF1. Cancer Cell. 2010;17(1):98-110.

12. Saitoh T, Nakayama M, Nakano H, Yagita H, Yamamoto N, Yamaoka S. TWEAK induces NF-kappaB2 p100 processing and long lasting NF-kappaB activation. J Biol Chem. 2003;278(38):36005-12.

13. Claudio EB, K.; Park, S.; Wang, H.; Siebenlist, U. BAFF-induced NEMO-independent processing of NF-kappa B2 in maturing B cells. Nature Immunology. 2002;3(10):958-65.

14. Dejardin E, Droin NM, Delhase M, Haas E, Cao Y, Makris C, et al. The lymphotoxin-beta receptor induces different patterns of gene expression via two NF-kappaB pathways. Immunity. 2002;17(4):525-35.

15. Novack DV, Yin L, Hagen-Stapleton A, Schreiber RD, Goeddel DV, Ross FP, et al. The IkappaB function of NF-kappaB2 p100 controls stimulated osteoclastogenesis. J Exp Med. 2003;198(5):771-81.

16. Munroe ME, Bishop GA. Role of tumor necrosis factor (TNF) receptor-associated factor 2 (TRAF2) in distinct and overlapping CD40 and TNF receptor 2/CD120b-mediated B lymphocyte activation. J Biol Chem. 2004;279(51):53222-31.

17. Jin J, Xiao Y, Chang JH, Yu J, Hu H, Starr R, et al. The kinase TBK1 controls IgA class switching by negatively regulating noncanonical NF-kappaB signaling. Nature Immunology. 2012;13(11):1101-9.

18. Razani B, Zarnegar B, Ytterberg AJ, Shiba T, Dempsey PW, Ware CF, et al. Negative feedback in noncanonical NF-kappaB signaling modulates NIK stability through IKKalpha-mediated phosphorylation. Science Signaling. 2010;3(123):ra41.

19. Sun SC. Controlling the fate of NIK: a central stage in noncanonical NF-kappaB signaling. Science Signaling. 2010;3(123):pe18.

20. Sun SC. Non-canonical NF-kappaB signaling pathway. Cell Research. 2011;21(1):71-85.

21. Perkins ND. The diverse and complex roles of NF-kappaB subunits in cancer. Nat Rev Cancer. 2012;12(2):121-32.

22. Senftleben U, Cao Y, Xiao G, Greten FR, Krahn G, Bonizzi G, et al. Activation by IKKalpha of a second, evolutionary conserved, NF-kappa B signaling pathway. Science. 2001;293(5534):1495-9.

23. Matsushima A, Kaisho T, Rennert PD, Nakano H, Kurosawa K, Uchida D, et al. Essential role of nuclear factor (NF)-kappaB-inducing kinase and inhibitor of kappaB (IkappaB) kinase alpha in NF-kappaB activation through lymphotoxin beta receptor, but not through tumor necrosis factor receptor I. J Exp Med. 2001;193(5):631-6.

24. Keats JJ, Fonseca R, Chesi M, Schop R, Baker A, Chng WJ, et al. Promiscuous mutations activate the noncanonical NF-kappaB pathway in multiple myeloma. Cancer Cell. 2007;12(2):131-44.

25. Pham LV, Fu L, Tamayo AT, Bueso-Ramos C, Drakos E, Vega F, et al. Constitutive BR3 receptor signaling in diffuse, large B-cell lymphomas stabilizes nuclear factor-kappaB-inducing kinase while activating both canonical and alternative nuclear factor-kappaB pathways. Blood. 2011;117(1):200-10.

26. Saitoh Y, Martinez Bruyn VJ, Uota S, Hasegawa A, Yamamoto N, Imoto I, et al. Overexpression of NF-kappaB inducing kinase underlies constitutive NF-kappaB activation in lung cancer cells. Lung Cancer. 2010;70(3):263-70.

27. Uno M, Saitoh Y, Mochida K, Tsuruyama E, Kiyono T, Imoto I, et al. NF-kappaB inducing kinase, a central signaling component of the non-canonical pathway of NF-kappaB, contributes to ovarian cancer progression. PLoS One. 2014;9(2):e88347.

28. Demchenko YN, Glebov OK, Zingone A, Keats JJ, Bergsagel PL, Kuehl WM. Classical and/or alternative NF-kappaB pathway activation in multiple myeloma. Blood. 2010;115(17):3541-52.

29. Lee DW, Ramakrishnan D, Valenta J, Parney IF, Bayless KJ, Sitcheran R. The NF-kappaB RelB protein is an oncogenic driver of mesenchymal glioma. PLoS One. s2013;8(2):e57489.

30. Cherry EM, Lee DW, Jung JU, Sitcheran R. Tumor necrosis factor-like weak inducer of apoptosis (TWEAK) promotes glioma cell invasion through induction of NF-

kappaB-inducing kinase (NIK) and noncanonical NF-kappaB signaling. Molecular Cancer. 2015;14(1):9.

31. Hynes RO. Integrins: versatility, modulation, and signaling in cell adhesion. Cell. 1992;69(1):11-25.

32. Ruoslahti E, Pierschbacher MD. New perspectives in cell adhesion: RGD and integrins. Science. 1987;238(4826):491-7.

33. Hood JD, Cheresh DA. Role of integrins in cell invasion and migration. Nat Rev Cancer. 2002;2(2):91-100.

34. Velling T, Kusche-Gullberg M, Sejersen T, Gullberg D. cDNA cloning and chromosomal localization of human alpha(11) integrin. A collagen-binding, I domain-containing, beta(1)-associated integrin alpha-chain present in muscle tissues. J Biol Chem. 1999;274(36):25735-42.

35. Zhang WM, Popova SN, Bergman C, Velling T, Gullberg MK, Gullberg D. Analysis of the human integrin alpha11 gene (ITGA11) and its promoter. Matrix Biol. 2002;21(6):513-23.

36. Popova SN, Barczyk M, Tiger CF, Beertsen W, Zigrino P, Aszodi A, et al. Alpha11 beta1 integrin-dependent regulation of periodontal ligament function in the erupting mouse incisor. Mol Cell Biol. 2007;27(12):4306-16.

37. Schulz JN, Zeltz C, Sorensen IW, Barczyk M, Carracedo S, Hallinger R, et al. Reduced granulation tissue and wound strength in the absence of alpha11beta1 integrin. J Invest Dermatol. 2015;135(5):1435-44.

38. Holmbeck K, Bianco P, Caterina J, Yamada S, Kromer M, Kuznetsov SA, et al. MT1-MMP-deficient mice develop dwarfism, osteopenia, arthritis, and connective tissue disease due to inadequate collagen turnover. Cell. 1999;99(1):81-92.

39. Beertsen W, Holmbeck K, Niehof A, Bianco P, Chrysovergis K, Birkedal-Hansen H, et al. On the role of MT1-MMP, a matrix metalloproteinase essential to collagen remodeling, in murine molar eruption and root growth. Eur J Oral Sci. 2002;110(6):445-51.

40. Wang KK, Liu N, Radulovich N, Wigle DA, Johnston MR, Shepherd FA, et al. Novel candidate tumor marker genes for lung adenocarcinoma. Oncogene. 2002;21(49):7598-604.

41. Chong IW, Chang MY, Chang HC, Yu YP, Sheu CC, Tsai JR, et al. Great potential of a panel of multiple hMTH1, SPD, ITGA11 and COL11A1 markers for diagnosis of patients with non-small cell lung cancer. Oncol Rep. 2006;16(5):981-8.

42. Navab R, Strumpf D, Bandarchi B, Zhu CQ, Pintilie M, Ramnarine VR, et al. Prognostic gene-expression signature of carcinoma-associated fibroblasts in non-small cell lung cancer. Proc Natl Acad Sci U S A. 2011;108(17):7160-5.

43. Navab R, Strumpf D, To C, Pasko E, Kim KS, Park CJ, et al. Integrin alpha11beta1 regulates cancer stromal stiffness and promotes tumorigenicity and metastasis in non-small cell lung cancer. Oncogene. 2016;35(15):1899-908.

44. Westcott JM, Prechtl AM, Maine EA, Dang TT, Esparza MA, Sun H, et al. An epigenetically distinct breast cancer cell subpopulation promotes collective invasion. J Clin Invest. 2015;125(5):1927-43.

45. Liotta LA, Stetler-stevenson WG. Tumor invasion and metastasis : An imbalance of positive and negative regulation. Cancer Research. 1991;51:5054s-9.

46. Itoh Y, Seiki M. MT1-MMP: a potent modifier of pericellular microenvironment. Journal of Cellular Physiology. 2006;206(1):1-8.

47. Nagase H, Woessner JF. Matrix metalloproteinases. The Journal of Biological Chemistry. 1999;274(31):21491-4.

48. Li X-y, Ota I, Yana I, Sabeh F, Weiss SJ. Molecular dissection of the structural machinery underlying the tissue-invasive activity of membrane type-1 matrix metalloproteinase. Molecular Biology of the Cell. 2008;19(August):3221-33.

49. Birkedal-Hansen H. Catabolism and turnover of collagens: collagenases. Methods in Enzymology. 1987;144:140-71.

50. Egeblad M, Werb Z. New functions for the matrix metalloproteinases in cancer progression. Nature Reviews Cancer. 2002;2(3):161-74.

51. Brooks PC, Stromblad S, Sanders LC, von Schalscha TL, Aimes RT, Stetler-Stevenson WG, et al. Localization of matrix metalloproteinase MMP-2 to the surface of invasive cells by interaction with integrin alpha v beta 3. Cell. 1996;85(5):683-93.

52. Lochter A, Galosy S, Muschler J, Freedman N, Werb Z, Bissell MJ. Matrix metalloproteinase stromelysin-1 triggers a cascade of molecular alterations that leads to stable epithelial-to-mesenchymal conversion and a premalignant phenotype in mammary epithelial cells. The Journal of Cell Biology. 1997;139(7):1861-72.

53. Sabeh F, Shimizu-Hirota R, Weiss SJ. Protease-dependent versus -independent cancer cell invasion programs: three-dimensional amoeboid movement revisited. The Journal of Cell Biology. 2009;185(1):11-9.

54. Sabeh F, Ota I, Holmbeck K, Birkedal-hansen H, Soloway P, Balbin M, et al. Tumor cell traffic through the extracellular matrix is controlled by the membrane-anchored collagenase MT1-MMP. The Journal of Cell Biology. 2004:769-81.

55. Hotary KB, Yana I, Sabeh F, Li X-Y, Holmbeck K, Birkedal-Hansen H, et al. Matrix metalloproteinases (MMPs) regulate fibrin-invasive activity via MT1-MMP-dependent and -independent processes. The Journal of Experimental Medicine. 2002;195(3):295-308.

56. Chun T-H, Sabeh F, Ota I, Murphy H, McDonagh KT, Holmbeck K, et al. MT1-MMP-dependent neovessel formation within the confines of the three-dimensional extracellular matrix. The Journal of Cell Biology. 2004;167(4):757-67.

57. Zhou Z, Apte SS, Soininen R, Cao R, Baaklini GY, Rauser RW, et al. Impaired endochondral ossification and angiogenesis in mice deficient in membrane-type matrix metalloproteinase I. Proceedings of the National Academy of Sciences of the United States of America. 2000;97(8):4052-7.

58. Pei D, Weiss SJ. Transmembrane-deletion mutants of the membrane-type matrix metalloproteinase-1 process progelatinase A and express intrinsic matrix-degrading activity. The Journal of Biological Chemistry. 1996;271(15):9135-40.

59. Yana I, Weiss SJ. Regulation of membrane type-1 matrix metalloproteinase activation by proprotein convertases. Molecular Biology of the Cell. 2000;11(July):2387-401.

60. Langlois S, Nyalendo C, Di Tomasso G, Labrecque L, Roghi C, Murphy G, et al. Membrane-type 1 matrix metalloproteinase stimulates cell migration through epidermal growth factor receptor transactivation. Molecular Cancer Research : MCR. 2007;5(6):569-83.

61. Nyalendo C, Michaud M, Beaulieu E, Roghi C, Murphy G, Gingras D, et al. Src-dependent phosphorylation of membrane type I matrix metalloproteinase on cytoplasmic tyrosine 573. The Journal of Biological Chemistry. 2007;282(21):15690-9.

62. Gingras D, Michaud M, Di Tomasso G, Béliveau E, Nyalendo C, Béliveau R. Sphingosine-1-phosphate induces the association of membrane-type 1 matrix metalloproteinase with p130Cas in endothelial cells. FEBS Letters. 2008;582(3):399-404.

63. Remacle AG, Chekanov AV, Golubkov VS, Savinov AY, Rozanov DV, Strongin AY. O-Glycosylation regulates autolysis of cellular membrane type-1 matrix metalloproteinase (MT1-MMP). The Journal of Biological Chemistry. 2006;281(25):16897-905.

64. Lehti K, Valtanen H, Wickström SA, Lohi J, Keski-Oja J. Regulation of membrane-type-1 matrix metalloproteinase activity by its cytoplasmic domain. The Journal of Biological Chemistry. 2000;275(20):15006-13.

65. Remacle AG, Rozanov DV, Baciu PC, Chekanov AV, Golubkov VS, Strongin AY. The transmembrane domain is essential for the microtubular trafficking of membrane type-1 matrix metalloproteinase (MT1-MMP). Journal of Cell Science. 2005;118:4975-84.

66. Yana I, Sagara H, Takaki S, Takatsu K, Nakamura K, Nakao K, et al. Crosstalk between neovessels and mural cells directs the site-specific expression of MT1-MMP to endothelial tip cells. Journal of Cell Science. 2007;120(Pt 9):1607-14.

67. Sternlicht MD, Werb Z. How matrix metalloproteinases regulate cell behavior. Annual Review of Cell and Developmental Biology. 2001;17:463-516.

68. Koshikawa N, Minegishi T, Sharabi A, Quaranta V, Seiki M. Membrane-type matrix metalloproteinase-1 (MT1-MMP) is a processing enzyme for human laminin gamma 2 chain. The Journal of Biological Chemistry. 2005;280(1):88-93.

69. Ohuchi E, Imai K, Fujii Y, Sato H, Seiki M, Okada Y. Membrane type 1 matrix metalloproteinase digests interstitial collagens and other extracellular matrix macromolecules. The Journal of Biological Chemistry. 1997;272(4):2446-51.

70. Sato H, Takino T, Miyamori H. Roles of membrane-type matrix metalloproteinase-1 in tumor invasion and metastasis. Cancer Science. 2005;96(4):212-7.

71. Montgomery AMP, Reisfeld RA, Cheresh DA. Integrin alphavbeta3 rescues melanoma cells from apoptosis in three-dimensional dermal collagen. Proceedings of the National Academy of Sciences of the United States of America. 1994;91(September):8856-60.

72. Davis GE. Affinity of integrins for damaged extracellular matrix: alpha v beta 3 binds to denatured collagen type I through RGD sites. Biochemical and Biophysical Research Communications. 1992;182(3):1025-31.

73. Deryugina EI, Ratnikov BI, Postnova TI, Rozanov DV, Strongin AY. Processing of integrin alpha(v) subunit by membrane type 1 matrix metalloproteinase stimulates migration of breast carcinoma cells on vitronectin and enhances tyrosine phosphorylation of focal adhesion kinase. The Journal of Biological Chemistry. 2002;277(12):9749-56.

74. Soldi R, Mitola S, Strasly M, Defilippi P, Tarone G, Bussolino F. Role of alphavbeta3 integrin in the activation of vascular endothelial growth factor receptor-2. The EMBO Journal. 1999;18(4):882-92.

75. Sacharidou A, Koh W, Stratman AN, Mayo AM, Fisher KE, Davis GE. Endothelial lumen signaling complexes control 3D matrix-specific tubulogenesis through interdependent Cdc42- and MT1-MMP-mediated events. Blood. 2010;115(25):5259-69.

76. Stetler-Stevenson WG, Aznavoorian S, Liotta LA. Tumor cell interactions with the extracellular matrix during invasion and metastasis. Annu Rev Cell Biol. 1993;9:541-73.

77. Lauffenburger DA, Horwitz AF. Cell migration: a physically integrated molecular process. Cell. 1996;84(3):359-69.

78. Sanz-Moreno V, Marshall CJ. The plasticity of cytoskeletal dynamics underlying neoplastic cell migration. Curr Opin Cell Biol. 2010;22(5):690-6.

79. Artym VV, Zhang Y, Seillier-Moiseiwitsch F, Yamada KM, Mueller SC. Dynamic interactions of cortactin and membrane type 1 matrix metalloproteinase at invadopodia: defining the stages of invadopodia formation and function. Cancer Research. 2006;66(6):3034-43.

80. Clark ES, Whigham AS, Yarbrough WG, Weaver AM. Cortactin is an essential regulator of matrix metalloproteinase secretion and extracellular matrix degradation in invadopodia. Cancer Res. 2007;67(9):4227-35.

81. Galvez BG, Matias-Roman S, Yanez-Mo M, Sanchez-Madrid F, Arroyo AG. ECM regulates MT1-MMP localization with beta1 or alphavbeta3 integrins at distinct cell compartments modulating its internalization and activity on human endothelial cells. J Cell Biol. 2002;159(3):509-21.

82. Bravo-Cordero JJ, Marrero-Diaz R, Megias D, Genis L, Garcia-Grande A, Garcia MA, et al. MT1-MMP proinvasive activity is regulated by a novel Rab8-dependent exocytic pathway. EMBO J. 2007;26(6):1499-510.

83. Deryugina EI, Ratnikov BI, Postnova TI, Rozanov DV, Strongin AY. Processing of integrin alpha(v) subunit by membrane type 1 matrix metalloproteinase stimulates migration of breast carcinoma cells on vitronectin and enhances tyrosine phosphorylation of focal adhesion kinase. J Biol Chem. 2002;277(12):9749-56.

84. Schenk S, Quaranta V. Tales from the crypt[ic] sites of the extracellular matrix. Trends Cell Biol. 2003;13(7):366-75.

85. Davis GE, Bayless KJ, Davis MJ, Meininger GA. Regulation of tissue injury responses by the exposure of matricryptic sites within extracellular matrix molecules. Am J Pathol. 2000;156(5):1489-98.

86. Tatti O, Vehvilainen P, Lehti K, Keski-Oja J. MT1-MMP releases latent TGF-beta1 from endothelial cell extracellular matrix via proteolytic processing of LTBP-1. Exp Cell Res. 2008;314(13):2501-14.

87. Fisher KE, Sacharidou A, Stratman AN, Mayo AM, Fisher SB, Mahan RD, et al. MT1-MMP- and Cdc42-dependent signaling co-regulate cell invasion and tunnel formation in 3D collagen matrices. J Cell Sci. 2009;122(Pt 24):4558-69.

88. Schmidt CE, Horwitz AF, Lauffenburger DA, Sheetz MP. Integrin-cytoskeletal interactions in migrating fibroblasts are dynamic, asymmetric, and regulated. J Cell Biol. 1993;123(4):977-91.

89. Shiraha H, Glading A, Gupta K, Wells A. IP-10 inhibits epidermal growth factor-induced motility by decreasing epidermal growth factor receptor-mediated calpain activity. J Cell Biol. 1999;146(1):243-54.

90. Guirguis R, Margulies I, Taraboletti G, Schiffmann E, Liotta L. Cytokine-induced pseudopodial protrusion is coupled to tumour cell migration. Nature. 1987;329(6136):261-3.

91. Klemke RL. Trespassing cancer cells: 'fingerprinting' invasive protrusions reveals metastatic culprits. Current Opinion in Cell Biology. 2012;24(5):662-9.

92. Beaty BT, Sharma VP, Bravo-Cordero JJ, Simpson MA, Eddy RJ, Koleske AJ, et al. Beta1 integrin regulates Arg to promote invadopodial maturation and matrix degradation. Mol Biol Cell. 2013;24(11):1661-75, S1-11.

93. Shankar J, Messenberg A, Chan J, Underhill TM, Foster LJ, Nabi IR. Pseudopodial actin dynamics control epithelial-mesenchymal transition in metastatic cancer cells. Cancer Res. 2010;70(9):3780-90.

94. Le Clainche C, Carlier MF. Regulation of actin assembly associated with protrusion and adhesion in cell migration. Physiol Rev. 2008;88(2):489-513.

95. Yamaguchi H, Condeelis J. Regulation of the actin cytoskeleton in cancer cell migration and invasion. Biochim Biophys Acta. 2007;1773(5):642-52.

96. Friedl P, Alexander S. Cancer invasion and the microenvironment: plasticity and reciprocity. Cell. 2011;147(5):992-1009.

97. Rorth P. Fellow travellers: emergent properties of collective cell migration. EMBO Rep. 2012;13(11):984-91.

98. Yu X, Zech T, McDonald L, Gonzalez EG, Li A, Macpherson I, et al. N-WASP coordinates the delivery and F-actin-mediated capture of MT1-MMP at invasive pseudopods. The Journal of Cell Biology. 2012;199(3):527-44.

99. Wolf K, Wu YI, Liu Y, Geiger J, Tam E, Overall C, et al. Multi-step pericellular proteolysis controls the transition from individual to collective cancer cell invasion. Nature Cell Biology. 2007;9(8):893-904.

100. Nguyen-Ngoc KV, Cheung KJ, Brenot A, Shamir ER, Gray RS, Hines WC, et al. ECM microenvironment regulates collective migration and local dissemination in

normal and malignant mammary epithelium. Proc Natl Acad Sci U S A. 2012;109(39):E2595-604.

101. Hegerfeldt Y, Tusch M, Brocker EB, Friedl P. Collective cell movement in primary melanoma explants: plasticity of cell-cell interaction, beta1-integrin function, and migration strategies. Cancer Research. 2002;62(7):2125-30.

102. Nabeshima K, Inoue T, Shimao Y, Okada Y, Itoh Y, Seiki M, et al. Front-cell-specific expression of membrane-type 1 matrix metalloproteinase and gelatinase A during cohort migration of colon carcinoma cells induced by hepatocyte growth factor/scatter factor. Cancer Research. 2000;60(13):3364-9.

103. Serres E, Debarbieux F, Stanchi F, Maggiorella L, Grall D, Turchi L, et al. Fibronectin expression in glioblastomas promotes cell cohesion, collective invasion of basement membrane in vitro and orthotopic tumor growth in mice. Oncogene. 2014;33(26):3451-62.

104. McLennan R, Schumacher LJ, Morrison JA, Teddy JM, Ridenour DA, Box AC, et al. Neural crest migration is driven by a few trailblazer cells with a unique molecular signature narrowly confined to the invasive front. Development. 2015;142(11):2014-25.

105. McLennan R, Schumacher LJ, Morrison JA, Teddy JM, Ridenour DA, Box AC, et al. VEGF signals induce trailblazer cell identity that drives neural crest migration. Dev Biol. 2015;407(1):12-25.

106. Burghardt RC, Burghardt JR, Taylor JD, 2nd, Reeder AT, Nguen BT, Spencer TE, et al. Enhanced focal adhesion assembly reflects increased mechanosensation and

mechanotransduction at maternal-conceptus interface and uterine wall during ovine pregnancy. Reproduction. 2009;137(3):567-82.

107. Huijbers IJ, Iravani M, Popov S, Robertson D, Al-Sarraj S, Jones C, et al. A role for fibrillar collagen deposition and the collagen internalization receptor endo180 in glioma invasion. PLoS One. 2010;5(3):e9808.

108. Wolf K, Te Lindert M, Krause M, Alexander S, Te Riet J, Willis AL, et al. Physical limits of cell migration: control by ECM space and nuclear deformation and tuning by proteolysis and traction force. The Journal of Cell Biology. 2013;201(7):1069-84.

109. Lee PF, Bai Y, Smith RL, Bayless KJ, Yeh AT. Angiogenic responses are enhanced in mechanically and microscopically characterized, microbial transglutaminase crosslinked collagen matrices with increased stiffness. Acta Biomater. 2013;9(7):7178-90.

110. Puliyappadamba VT, Hatanpaa KJ, Chakraborty S, Habib AA. The role of NF-κB in the pathogenesis of glioma. Molecular & Cellular Oncology. 2014;1(3):e963478.

111. Hayden MS, Ghosh S. NF-kappaB, the first quarter-century: remarkable progress and outstanding questions. Genes & development. 2012;26(3):203-34.

112. Riehmer V, Gietzelt J, Beyer U, Hentschel B, Westphal M, Schackert G, et al. Genomic profiling reveals distinctive molecular relapse patterns in IDH1/2 wild-type glioblastoma. Genes Chromosomes Cancer. 2014;53(7):589-605.

113. Murphy DA, Courtneidge SA. The 'ins' and 'outs' of podosomes and invadopodia: characteristics, formation and function. Nat Rev Mol Cell Biol. 2011;12(7):413-26.

114. Wolf K, Friedl P. Mapping proteolytic cancer cell-extracellular matrix interfaces. Clinical & Experimental Metastasis. 2009;26(4):289-98.

115. Gilles C, Polette M, Piette J, Munaut C, Thompson EW, Birembaut P, et al. High level of MT-MMP expression is associated with invasiveness of cervical cancer cells. International Journal of Cancer, Journal International du Cancer. 1996;65(2):209-13.

116. Polette M, Nawrocki B, Gilles C, Sato H, Seiki M, Tournier JM, et al. MT-MMP expression and localisation in human lung and breast cancers. Virchows Archiv: An International Journal of Pathology. 1996;428(1):29-35.

117. Nomura H, Sato H, Seiki M, Mai M, Okada Y. Expression of membrane-type matrix metalloproteinase in human gastric carcinomas. Cancer Research. 1995;55(15):3263-6.

118. Yamamoto M, Mohanam S, Sawaya R, Fuller GN, Seiki M, Sato H, et al. Differential expression of membrane-type matrix metalloproteinase and its correlation with gelatinase A activation in human malignant brain tumors in vivo and in vitro. Cancer Research. 1996;56(2):384-92.

119. Yana I, Weiss SJ. Regulation of membrane type-1 matrix metalloproteinase activation by proprotein convertases. Molecular Biology of the Cell. 2000;11(7):2387-401.

120. Remacle AG, Rozanov DV, Fugere M, Day R, Strongin AY. Furin regulates the intracellular activation and the uptake rate of cell surface-associated MT1-MMP. Oncogene. 2006;25(41):5648-55.

121. Nyalendo C, Michaud M, Beaulieu E, Roghi C, Murphy G, Gingras D, et al. Src-dependent phosphorylation of membrane type I matrix metalloproteinase on cytoplasmic tyrosine 573: role in endothelial and tumor cell migration. The Journal of Biological Chemistry. 2007;282(21):15690-9.

122. Gingras D, Michaud M, Di Tomasso G, Beliveau E, Nyalendo C, Beliveau R. Sphingosine-1-phosphate induces the association of membrane-type 1 matrix metalloproteinase with p130Cas in endothelial cells. FEBS Letters. 2008;582(3):399-404.

123. Itoh Y. Membrane-type matrix metalloproteinases: Their functions and regulations. Matrix Biology: Journal of the International Society for Matrix Biology. 2015;44-46:207-23.

124. Boukerche H, Su ZZ, Emdad L, Sarkar D, Fisher PB. MDA-9/Syntenin regulates the metastatic phenotype in human melanoma cells by activating nuclear factor-kappaB. Cancer Research. 2007;67(4):1812-22.

125. Annabi B, Laflamme C, Sina A, Lachambre MP, Beliveau R. A MT1-MMP/NF-kappaB signaling axis as a checkpoint controller of COX-2 expression in CD133+ U87 glioblastoma cells. Journal of Neuroinflammation. 2009;6:8.

126. Fritz RD, Radziwill G. CNK1 promotes invasion of cancer cells through NF-kappaB-dependent signaling. Molecular Cancer Research. 2010;8(3):395-406.

127. Bayless KJ, Kwak HI, Su SC. Investigating endothelial invasion and sprouting behavior in three-dimensional collagen matrices. Nature Protocols. 2009;4(12):1888-98.

128. Kelly JJ, Stechishin O, Chojnacki A, Lun X, Sun B, Senger DL, et al. Proliferation of human glioblastoma stem cells occurs independently of exogenous mitogens. Stem Cells. 2009;27(8):1722-33.

129. Kwak HI, Kang H, Dave JM, Mendoza EA, Su SC, Maxwell SA, et al. Calpain-mediated vimentin cleavage occurs upstream of MT1-MMP membrane translocation to facilitate endothelial sprout initiation. Angiogenesis. 2012;15(2):287-303.

130. Bayless KJ, Davis GE. Sphingosine-1-phosphate markedly induces matrix metalloproteinase and integrin-dependent human endothelial cell invasion and lumen formation in three-dimensional collagen and fibrin matrices. Biochemical and Biophysical Research Communications. 2003;312(4):903-13.

131. Gao J, Aksoy BA, Dogrusoz U, Dresdner G, Gross B, Sumer SO, et al. Integrative analysis of complex cancer genomics and clinical profiles using the cBioPortal. Science Signaling. 2013;6(269):pl1.

132. Cerami E, Gao J, Dogrusoz U, Gross BE, Sumer SO, Aksoy BA, et al. The cBio cancer genomics portal: an open platform for exploring multidimensional cancer genomics data. Cancer Discovery. 2012;2(5):401-4.

133. Wright SP. Adjusted p-values for simultaneous inference. Biometrics. 1992;48(4):1005-13.

134. Yin Z, Sadok A, Sailem H, McCarthy A, Xia X, Li F, et al. A screen for morphological complexity identifies regulators of switch-like transitions between discrete cell shapes. Nature Cell Biology. 2013;15(7):860-71.

135. Hiraoka N, Allen E, Apel IJ, Gyetko MR, Weiss SJ. Matrix metalloproteinases regulate neovascularization by acting as pericellular fibrinolysins. Cell. 1998;95(3):365-77.

136. Sato H, Takino T, Okada Y, Cao J, Shinagawa A, Yamamoto E, et al. A matrix metalloproteinase expressed on the surface of invasive tumour cells. Nature. 1994;370(6484):61-5.

137. Lehti K, Valtanen H, Wickstrom SA, Lohi J, Keski-Oja J. Regulation of membrane-type-1 matrix metalloproteinase activity by its cytoplasmic domain. The Journal of Biological Chemistry. 2000;275(20):15006-13.

138. Fisher KE, Pop A, Koh W, Anthis NJ, Saunders WB, Davis GE. Tumor cell invasion of collagen matrices requires coordinate lipid agonist-induced G-protein and membrane-type matrix metalloproteinase-1-dependent signaling. Molecular Cancer. 2006;5:69.

139. Thu YM, Richmond A. NF-kappaB inducing kinase: a key regulator in the immune system and in cancer. Cytokine & Growth Factor Reviews. 2010;21(4):213-26.

140. Zarnegar B, Yamazaki S, He JQ, Cheng G. Control of canonical NF-kappaB activation through the NIK-IKK complex pathway. Proc Natl Acad Sci U S A. 2008;105(9):3503-8.

141. Sakurai H, Chiba H, Miyoshi H, Sugita T, Toriumi W. IkappaB kinases phosphorylate NF-kappaB p65 subunit on serine 536 in the transactivation domain. The Journal of Biological Chemistry. 1999;274(43):30353-6.

142. Yin L, Wu L, Wesche H, Arthur CD, White JM, Goeddel DV, et al. Defective lymphotoxin-beta receptor-induced NF-kappaB transcriptional activity in NIK-deficient mice. Science. 2001;291(5511):2162-5.

143. Varghese F, Bukhari AB, Malhotra R, De A. IHC Profiler: an open source plugin for the quantitative evaluation and automated scoring of immunohistochemistry images of human tissue samples. PLoS One. 2014;9(5):e96801.

144. Annunziata CM, Davis RE, Demchenko Y, Bellamy W, Gabrea A, Zhan F, et al. Frequent engagement of the classical and alternative NF-kappaB pathways by diverse genetic abnormalities in multiple myeloma. Cancer Cell. 2007;12(2):115-30.

145. Odqvist L, Sanchez-Beato M, Montes-Moreno S, Martin-Sanchez E, Pajares R, Sanchez-Verde L, et al. NIK controls classical and alternative NF-kappaB activation and is necessary for the survival of human T-cell lymphoma cells. Clin Cancer Res. 2013;19(9):2319-30.

146. Ben-Neriah Y, Karin M. Inflammation meets cancer, with NF-kappaB as the matchmaker. Nature Immunology. 2011;12(8):715-23.

147. Moss NM, Wu YI, Liu Y, Munshi HG, Stack MS. Modulation of the membrane type 1 matrix metalloproteinase cytoplasmic tail enhances tumor cell invasion and proliferation in three-dimensional collagen matrices. The Journal of Biological Chemistry. 2009;284(30):19791-9.

148. Azevedo H, Moreira-Filho CA. Topological robustness analysis of protein interaction networks reveals key targets for overcoming chemotherapy resistance in glioma. Scientific Reports. 2015;5:16830.

149. Ridley AJ. Life at the leading edge. Cell. 2011;145(7):1012-22.

150. Nurnberg A, Kitzing T, Grosse R. Nucleating actin for invasion. Nature Reviews Cancer. 2011;11(3):177-87.

151. Sero JE, Sailem HZ, Ardy RC, Almuttaqi H, Zhang T, Bakal C. Cell shape and the microenvironment regulate nuclear translocation of NF-kappaB in breast epithelial and tumor cells. Molecular Systems Biology. 2015;11(1):790.

152. Gray GK, McFarland BC, Nozell SE, Benveniste EN. NF-kappaB and STAT3 in glioblastoma: therapeutic targets coming of age. Expert Review of Neurotherapeutics. 2014;14(11):1293-306.

153. Didonato JA, Mercurio F, Karin M. NF-κB and the link between inflammation and cancer. Immunol Rev. 2012;246(1):379-400.

154. Xia Y, Shen S, Verma IM. NF-κB, an active player in human cancers. Cancer Immunology Research. 2014;2(9):823-30.

155. Stupp R, Pavlidis N, Jelic S. ESMO minimum clinical recommendations for diagnosis, treatment and follow-up of malignant glioma. Annals of Oncology: Official Journal of the European Society for Medical Oncology / ESMO. 2005;16 Suppl 1:i64-5.

156. Phillips HS, Kharbanda S, Chen R, Forrest WF, Soriano RH, Wu TD, et al. Molecular subclasses of high-grade glioma predict prognosis, delineate a pattern of disease progression, and resemble stages in neurogenesis. Cancer Cell. 2006;9(3):157-73.

157. Duran CL, Lee DW, Jung JU, Ravi S, Pogue CB, Toussaint LG, et al. NIK regulates MT1-MMP activity and promotes glioma cell invasion independently of the canonical NF-kappaB pathway. Oncogenesis. 2016;5(6):e231.

158. Bellail AC, Hunter SB, Brat DJ, Tan C, Van Meir EG. Microregional extracellular matrix heterogeneity in brain modulates glioma cell invasion. Int J Biochem Cell Biol. 2004;36(6):1046-69.

159. Chintala SK, Sawaya R, Gokaslan ZL, Fuller G, Rao JS. Immunohistochemical localization of extracellular matrix proteins in human glioma, both in vivo and in vitro. Cancer Lett. 1996;101(1):107-14.

160. Sweeney SM, Orgel JP, Fertala A, McAuliffe JD, Turner KR, Di Lullo GA, et al. Candidate cell and matrix interaction domains on the collagen fibril, the predominant protein of vertebrates. The Journal of Biological Chemistry. 2008;283(30):21187-97.

161. Leitinger B. Transmembrane collagen receptors. Annu Rev Cell Dev Biol. 2011;27:265-90.

162. Humphries MJ. Integrin structure. Biochem Soc Trans. 2000;28(4):311-39.

163. Calderwood DA, Shattil SJ, Ginsberg MH. Integrins and actin filaments: reciprocal regulation of cell adhesion and signaling. The Journal of Biological Chemistry. 2000;275(30):22607-10.

164. Calle Y, Burns S, Thrasher AJ, Jones GE. The leukocyte podosome. European Journal of Cell Biology. 2006;85(3-4):151-7.

165. Adams JC. Regulation of protrusive and contractile cell-matrix contacts. J Cell Sci. 2002;115(Pt 2):257-65.

166. Geiger B, Bershadsky A, Pankov R, Yamada KM. Transmembrane crosstalk between the extracellular matrix--cytoskeleton crosstalk. Nat Rev Mol Cell Biol. 2001;2(11):793-805.

167. Yu CH, Rafiq NB, Krishnasamy A, Hartman KL, Jones GE, Bershadsky AD, et al. Integrin-matrix clusters form podosome-like adhesions in the absence of traction forces. Cell Reports. 2013;5(5):1456-68.

168. Galvez BG, Matias-Roman S, Yanez-Mo M, Vicente-Manzanares M, Sanchez-Madrid F, Arroyo AG. Caveolae are a novel pathway for membrane-type 1 matrix metalloproteinase traffic in human endothelial cells. Molecular Biology of the Cell. 2004;15(2):678-87.

169. Takino T, Watanabe Y, Matsui M, Miyamori H, Kudo T, Seiki M, et al. Membrane-type 1 matrix metalloproteinase modulates focal adhesion stability and cell migration. Exp Cell Res. 2006;312(8):1381-9.

170. Desgrosellier JS, Cheresh DA. Integrins in cancer: biological implications and therapeutic opportunities. Nature Reviews Cancer. 2010;10(1):9-22.

171. Bello L, Francolini M, Marthyn P, Zhang J, Carroll RS, Nikas DC, et al. Alpha(v)beta3 and alpha(v)beta5 integrin expression in glioma periphery. Neurosurgery. 2001;49(2):380-9.

172. Knight CG, Morton LF, Peachey AR, Tuckwell DS, Farndale RW, Barnes MJ. The collagen-binding A-domains of integrins alpha(1)beta(1) and alpha(2)beta(1) recognize the same specific amino acid sequence, GFOGER, in native (triple-helical) collagens. The Journal of Biological Chemistry. 2000;275(1):35-40.

173. Bayless KJ, Davis GE, Meininger GA. Isolation and biological properties of osteopontin from bovine milk. Protein Expr Purif. 1997;9(3):309-14.

174. Lee N, Smolarz AJ, Olson S, David O, Reiser J, Kutner R, et al. A potential role for Dkk-1 in the pathogenesis of osteosarcoma predicts novel diagnostic and treatment strategies. Br J Cancer. 2007;97(11):1552-9.

175. Dave JM, Abbey CA, Duran CL, Seo H, Johnson GA, Bayless KJ. Hic-5 mediates the initiation of endothelial sprouting by regulating a key surface metalloproteinase. J Cell Sci. 2016;129(4):743-56.

176. Lee PF, Yeh AT, Bayless KJ. Nonlinear optical microscopy reveals invading endothelial cells anisotropically alter three-dimensional collagen matrices. Exp Cell Res. 2009;315(3):396-410.

177. Uhlen M, Fagerberg L, Hallstrom BM, Lindskog C, Oksvold P, Mardinoglu A, et al. Proteomics. Tissue-based map of the human proteome. Science. 2015;347(6220):1260419.

178. Dave JM, Kang H, Abbey CA, Maxwell SA, Bayless KJ. Proteomic profiling of endothelial invasion revealed receptor for activated C kinase 1 (RACK1) complexed with vimentin to regulate focal adhesion kinase (FAK). The Journal of Biological Chemistry. 2013;288(42):30720-33.

179. Takino T. Regulation of cell motility by MT1-MMP. Seikagaku. 2006;78(12):1159-63.

180. Selbekk T, Brekken R, Solheim O, Lydersen S, Hernes TA, Unsgaard G. Tissue motion and strain in the human brain assessed by intraoperative ultrasound in glioma patients. Ultrasound Med Biol. 2010;36(1):2-10.

181. Chakraborty A, Bamber JC, Dorward NL. Slip elastography: a novel method for visualising and characterizing adherence between two surfaces in contact. Ultrasonics. 2012;52(3):364-76.

182. Ishihara S, Yasuda M, Harada I, Mizutani T, Kawabata K, Haga H. Substrate stiffness regulates temporary NF-kappaB activation via actomyosin contractions. Exp Cell Res. 2013;319(19):2916-27.

183. Miroshnikova YA, Mouw JK, Barnes JM, Pickup MW, Lakins JN, Kim Y, et al. Tissue mechanics promote IDH1-dependent HIF1alpha-tenascin C feedback to regulate glioblastoma aggression. Nature Cell Biology. 2016;18(12):1336-45.

184. Gritsenko PG, Ilina O, Friedl P. Interstitial guidance of cancer invasion. J Pathol. 2012;226(2):185-99.

185. Lefranc F, Brotchi J, Kiss R. Possible future issues in the treatment of glioblastomas: special emphasis on cell migration and the resistance of migrating glioblastoma cells to apoptosis. J Clin Oncol. 2005;23(10):2411-22.

186. Ulrich TA, de Juan Pardo EM, Kumar S. The mechanical rigidity of the extracellular matrix regulates the structure, motility, and proliferation of glioma cells. Cancer Research. 2009;69(10):4167-74.

187. Kaufman LJ, Brangwynne CP, Kasza KE, Filippidi E, Gordon VD, Deisboeck TS, et al. Glioma expansion in collagen I matrices: analyzing collagen concentration-dependent growth and motility patterns. Biophys J. 2005;89(1):635-50.

188. Rao SS, Bentil S, DeJesus J, Larison J, Hissong A, Dupaix R, et al. Inherent interfacial mechanical gradients in 3D hydrogels influence tumor cell behaviors. PLoS One. 2012;7(4):e35852.

189. Provenzano PP, Inman DR, Eliceiri KW, Knittel JG, Yan L, Rueden CT, et al. Collagen density promotes mammary tumor initiation and progression. BMC Med. 2008;6:11.

190. Provenzano PP, Inman DR, Eliceiri KW, Keely PJ. Matrix density-induced mechanoregulation of breast cell phenotype, signaling and gene expression through a FAK-ERK linkage. Oncogene. 2009;28(49):4326-43.

191. Guo YP, Martin LJ, Hanna W, Banerjee D, Miller N, Fishell E, et al. Growth factors and stromal matrix proteins associated with mammographic densities. Cancer Epidemiol Biomarkers Prev. 2001;10(3):243-8.

192. Boyd NF, Dite GS, Stone J, Gunasekara A, English DR, McCredie MR, et al. Heritability of mammographic density, a risk factor for breast cancer. N Engl J Med. 2002;347(12):886-94.

193. Boyd NF, Guo H, Martin LJ, Sun L, Stone J, Fishell E, et al. Mammographic density and the risk and detection of breast cancer. N Engl J Med. 2007;356(3):227-36.

194. McCormack VA, dos Santos Silva I. Breast density and parenchymal patterns as markers of breast cancer risk: a meta-analysis. Cancer Epidemiol Biomarkers Prev. 2006;15(6):1159-69.

195. Levental KR, Yu H, Kass L, Lakins JN, Egeblad M, Erler JT, et al. Matrix crosslinking forces tumor progression by enhancing integrin signaling. Cell. 2009;139(5):891-906.

196. De Donatis GM, Pape EL, Pierron A, Cheli Y, Hofman V, Hofman P, et al. NF-kB2 induces senescence bypass in melanoma via a direct transcriptional activation of EZH2. Oncogene. 2016;35(21):2735-45.

197. Thu YM, Su Y, Yang J, Splittgerber R, Na S, Boyd A, et al. NF-kappaB inducing kinase (NIK) modulates melanoma tumorigenesis by regulating expression of pro-survival factors through the beta-catenin pathway. Oncogene. 2012;31(20):2580-92.

198. Jung JU, Ravi S, Lee DW, McFadden K, Kamradt ML, Toussaint LG, et al. NIK/MAP3K14 regulates mitochondrial dynamics and trafficking to promote cell invasion. Curr Biol. 2016;26(24):3288-302.